Fall 2016

Channel Sediment And Mining-Lead Storage In Flat River Creek, Old Lead Belt, Missouri

Ralph Joseph Hill

CHANNEL SEDIMENT AND MINING-LEAD STORAGE IN FLAT RIVER CREEK, OLD LEAD BELT, MISSOURI

A Masters Thesis

Presented to

The Graduate College of

Missouri State University

In Partial Fulfillment

Of the Requirements for the Degree

Master of Science, Geospatial Sciences in Geography and Geology

By

Ralph Joseph Hill

December 2016

CHANNEL SEDIMENT AND MINING-LEAD STORAGE IN FLAT RIVER CREEK, OLD LEAD BELT, MISSOURI

Geography, Geology, and Planning

Missouri State University, December 2016

Master of Science

Ralph Joseph Hill

ABSTRACT

Historical mining for lead (Pb) in the Old Lead Belt District introduced large volumes of tailings into nearby streams resulting in the large-scale contamination of channel bed and bar deposits in Big River which drains the southeastern Missouri Ozarks. Tailings pile sites have been remediated so that present contamination sources to the river are primarily from the remobilization of Pb stored in channel and floodplain deposits. This study examined the channel geomorphology and sediment geochemistry of Flat River Creek (FRC), a major tributary to the Big River which drains an area that includes three of the six major mines in the District. The goal was to determine the volume of contaminated sediment stored within the channel in bed, active bar, and stable bar deposits assuming the associated stored Pb could be a source of future contamination. Channel sediment contamination >1,000 ppm Pb occurs in the lower 9.5 km of FRC with concentrations spiking below mine locations and decreasing in reaches where tributaries from non-mining areas enter and dilute the mining sediment. Zn concentrations are elevated immediately downstream from the Elvins mine and decrease downstream. Approximately 170,000 m^3 of contaminated channel deposits are stored in FRC with 42 % in the lower segment below the most downstream tailings pile. About 24 % of contaminated sediment is stored in channel bed deposits, 41 % in active bar deposits, and 35 % in stable bar deposits. Overall, 133 Mg of Pb and 93 Mg of Zn from mining sources are stored in FRC. Therefore, reworked channel deposits will provide a long-term source of metal contamination Big River as well as FRC.

KEYWORDS: lead, mining, contamination, sediment, Missouri

This abstract is approved as to form and content

_____

Robert T. Pavlowsky, PhD
Chairperson, Advisory Committee
Missouri State University

CHANNEL SEDIMENT AND MINING-LEAD STORAGE IN FLAT RIVER CREEK, OLD LEAD BELT, MISSOURI

By

Ralph Joseph Hill

A Masters Thesis
Submitted to the Graduate College
Of Missouri State University
In Partial Fulfillment of the Requirements
For the Degree of Master of Science, Geospatial Sciences in Geography and Geology

December 2016

Approved:

_____
Robert T. Pavlowsky, PhD

_____
Jun Luo, PhD

_____
Toby J. Dogwiler, PhD

_____
Julie Masterson, PhD: Dean, Graduate College

ACKNOWLEDGEMENTS

I have several individuals I would like to thank for their support throughout this entire process. I would like to extend a heartfelt thank you to David Spears, Virginia State Geologist, and William Lassetter, Virginia State Economic Geologist for their letters of recommendation and support. I would not be here without their support and guidance leading up to my decision to apply to Missouri State University.

Thank you to the United States Fish and Wildlife Service and United States Environmental Protection Agency for helping to partially support my thesis project. Thank you to all of the staff of the Ozarks Environmental and Water Resources Institute and especially Marc Owen for his technical help, ideas, patience, and input throughout my entire process.

I am also very grateful for the volunteers who helped with field sampling, especially Felix Corrodi, Allison Keppel, Laura Speir, Karen Zelzer, Lisa Andes, Megan Hente, Matthew Thies, and Nickolas Bradley. A special thank you also goes to Drs. Dan Hanes and Aaron Pearson, from St. Louis University who helped collect bar core samples. I also want to thank my thesis committee for their help, including Dr. Pavlowsky as my chair for his endless support and guidance over the two years and committee members Dr. Jun Luo and Dr. Toby Dogwiler.

Finally, my deepest love to my parents Ralph E. Hill and Joanne Hill for their constant love and support. I certainly would not be who I am and where I am today without you.

TABLE OF CONTENTS

LIST OF TABLES

LIST OF FIGURES

INTRODUCTION

Rivers are fundamentally important for the transport and redistribution of sediment on the Earth's surface (Miller, 1997). Schumm (1977) conceptualized a river system consisting of a steeper, upland zone of erosion where runoff and sediment originate, a central zone of balanced transport within which water and sediment inputs generally equal outputs, and a lower gradient, downstream zone with frequent deposition in floodplains or deltas (Figure 1). Thus, sediment transport can be viewed as a series of steps within and between each of the three zones with relatively long periods of sediment storage (no movement) in bed, bar, and floodplain deposits (Engelund and Hansen, 1967; Magilligan, 1985).

The processes and patterns of sediment storage within a channel network are spatially and temporally complex (Walling, 1983). Coarse sediment, including gravel, cobble, and boulder particles >2 mm in diameter, tends to be stored in colluvial deposits at the base of hill-slopes along the river valley and on the channel bed. Compared to coarse sediments, fine-grained sediment particles, including sand, silt, and clay <2 mm in diameter, are transported more often and dispersed more widely with primary storages in channel bar, levee, and floodplain deposits. Channel bed storage is usually temporary since it can be easily mobilized during periods of higher flow, even if such flow does not cause sediment deposition in the floodplain (Walling et al., 1998). Geomorphic adjustments of channel systems to geologic, climatic, and land use/cover changes may result in increased storage of fine-grained sediment over time periods ranging from decades to millennia (Trimble and Lund, 1982; Walling et al., 2003).

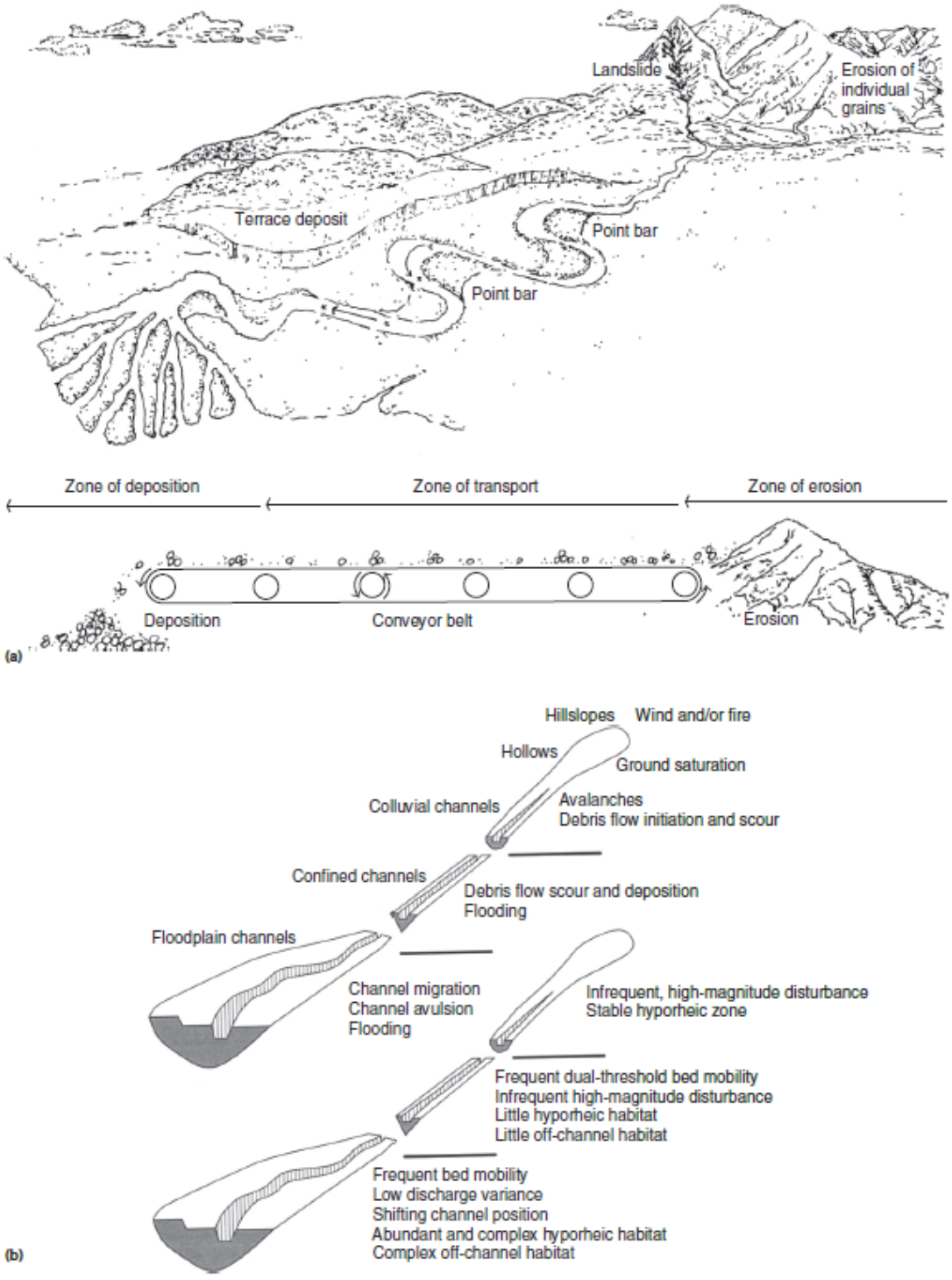

Figure 1. Conceptual model of zones of erosion, transport and deposition after Schumm 1977 in Buffington and Montgomery (2013).

Land managers are becoming increasingly interested in the geomorphic responses of stream channels due to erosion and sedimentation in watersheds (Trimble and Lund, 1982; Dennis et al., 2009; Gran et al. 2009). They often need to know where sediment will be deposited, how long it will be stored there, and how it will be remobilized (Reid and Dunne, 1996). A sediment budget is often used to conceptualize the linkages between sediment storage and transport in a watershed (Figure 2). Efforts to quantify a sediment budget often include estimates of the sources and volumes of sediment stored and transported in a watershed, where and when sediment is transported, and how much eventually exits from the watershed (Reid and Dunne, 1996; Trimble, 1999; Gran et al., 2009) (Figure 2). Sediment budget techniques are useful for evaluating a variety of sediment yield and contamination problems. For example, contaminated sediments produced by past mining activities can be stored in floodplains for long periods, become remobilized later, and cause present-day pollution in rivers (Lecce and Pavlowsky, 1997; 2014).

Conceptual models of sediment budgets recognize the importance of sediment connectivity and the pathways and storages involved when sediment is distributed down hillslopes, into channels, and along channel networks (Wohl, 2014). Sediment moves through channel networks to become deposited within lower elevation bed and bar deposits and higher elevation bench and floodplain deposits. As rivers migrate laterally across the lowlands they create a complex topography of terraces, floodplain back-swamps, and channels using sediment delivered from upstream areas (Stout and Belmont, 2014; Wohl, 2014). Sediment storage within a river system can be divided among

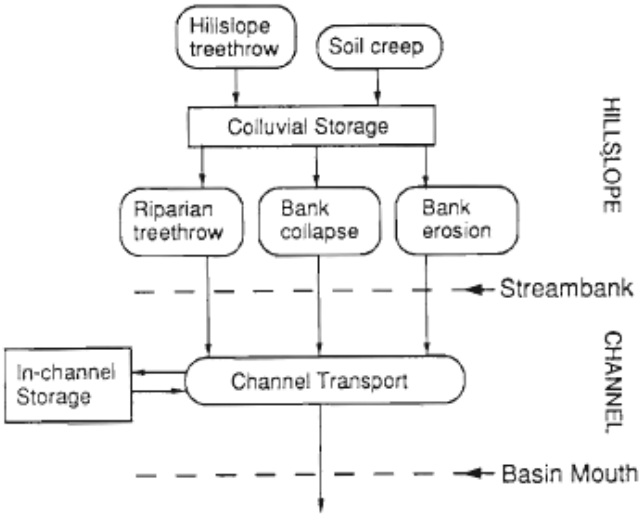

Figure 2. Generalized flowchart of sediment storage in a watershed (Reid and Dunne, 1996).

different deposits, with each having unique characteristics relating to sediment transport and sediment budgets.

Channel Sediment Deposits

In general, channel storage can be classified as bed, active bar, and stable bar deposits (Walling et al, 1998, 2003). Channel bed deposits are typically composed of coarse gravel and cobble with void spaces filled with fine sediment. The channel bed can be further divided in three units: glides, where flow shallows and spreads out at the tail-end of a pool prior to crossing a riffle crest; riffles, where the bed steepens locally, becomes more coarse in texture, and flows down toward the next pool; and pools, which form a deeper and wider section where bed slope and low flow velocity decreases (Panfil and Jacobson, 2001) (Figure 3). Channel bed (and bar) deposits may develop a coarser "armored" surface layer formed by fluvial scour and winnowing of finer sediments

Figure 3. Coarse channel bed deposit from Flat River Creek at R-km 0.35.

during the falling stages of a flood (Montgomery and Buffington, 1997). While bed sediment tends to be coarse, fine-grained sedimentation can occur in channel pools and glides when flow velocity decreases during the falling limb of a flood and settling is induced. It is assumed that fine-grained sediments within bed deposits are relatively easily to mobilize during higher discharges and represent a sediment source readily available for transport (Lewin and Macklin, 1987).

Active bar deposits are higher elevation sediment bodies compared to the bed that are typically exposed above the water line during low flow conditions, composed of sand and gravel, and have little vegetation cover (Figure 4). Bar features tend to form coarser heads (upstream end) and gradually fine in texture downstream toward the tail (Lewin and Macklin, 1987, Panfil and Jacobson, 2001). Channel bars occur at reach locations of

Figure 4. Active bar deposit from Flat River Creek at R-km 5.05.

flow separation in the channel such as in point bars along the inside of channel bends or where transport capacity drops such as center bars in over-widened channels. Bar surfaces are typically light-colored with sediment characteristics easily observed indicating reworking of the bar surface by flood events throughout the year. Patches of woody shrubs or small trees may occur on active bar surfaces as long on the bar surface reflects recent bed load transport. Active bars adjust to passing floods as sediments are deposited and eroded by variable flows. However, the whole bar is not usually remobilized by a single flood and bar deposits may contain material representing transport trends from a year to more than a decade ago, depending on geomorphic history and specific bar location.

In this study, the term “shadow” bar is used to describe relatively small (less than a few square meters), fine-grained deposits on active bar surfaces formed in localized flow separation zones behind larger obstructions such as boulders, tree roots, and logs, and anthropogenic materials such as bridge piers and construction wastes. As faster moving flows pass these obstacles, the flow velocity drops to almost zero on the downstream side and deposition occurs. It is generally assumed that active bar deposits represent sediment storages readily available for remobilization during floods over timescales of several years. However, shadow bar deposits probably respond to individual floods and therefore are interpreted to reflect sediment properties of the most recent sediment transport events.

Stable bars form along the margins of the channel or in protected areas surrounded by active bar deposits where fine-grained deposition can occur on upper bar surfaces, often in association with increased vegetation cover. They form at elevations typically lower than adjacent floodplains, but higher than nearby active bars (Figure 5). Stable bars can develop from active bar deposits where flow energy has decreased over time, relatively uniform vegetation growth has occurred, and fine sediment has been deposited over the top bar surface to a depth of approximately 5 cm. Some stable bars are in the process of forming new floodplains by vertical deposition and these young floodplain features are sometimes called benches or shelves (Owen et al., 2011). It is assumed that stable bars represent sediment storage over periods of decades or longer and can remove available sediment from transport by the river for relatively long periods.

Figure 5. Stable bar deposit from Flat River Creek at R-km 7.55.

Floodplain deposits typically represent the largest volume of stored sediment in alluvial river systems and are often the primary focus of studies on longer-term sediment transport and contamination trends in watersheds (Leece and Pavlowsky, 2014). While in-channel bed and bar storage may compose a smaller fraction of total alluvial storage, they are important deposits that indicate sediment in transit and available for dispersal downstream as the river temporally adjusts to climate and land use factors (Knighton, 1998). Further, the mobility and quality of channel sediment directly affects habitat quality for aquatic life and effectiveness of stream restoration projects (Gale et al., 2004, Roberts et al, 2009).

Mine-waste Contamination in Rivers

Sediment transport and storage are natural processes that can complicate studies of contamination in fluvial systems. Historical base-metal mining activities have been responsible for contaminating river systems throughout the world (Miller, 1997). These mining operations typically extract metal-bearing sulfide ores from underground mines and produce relatively large volumes of contaminated mineral wastes across a range of particle sizes including waste rock, tailings, and ultrafine (rock flour) particles. Milling operations may use both gravity and flotation methods to separate ore from the host rock. Gravity mills grind ore into coarse sand and fine gravel sizes for separation using shaking tables and water sorting by density (Macklin et al., 2006). Ore separation by flotation techniques use chemical treatment of sand-size feed to "float" and concentrate sulfide-bearing grains (Macklin et al., 2006). In addition, flotation employ a range of organic compounds that produce effluent that is highly toxic and, if improperly discharged, can have catastrophic and long-lasting effects on freshwater ecosystems (Macklin et al., 2006).

The milling process is not entirely efficient and the mineral wastes or tailings produced typically contain high concentrations of metals at levels of environmental concern in soil and sediment (Gale et al., 2004; Bussiere, 2007). Gravity milling releases coarser tailings to local streams predominantly in the fine gravel or 2-16 mm size range. Flotation milling produces tailings in the fine to medium sand or 0.1-0.3 mm size range. Further, fine-grained "slimes" are created as rock flour particles less than 0.06 mm in diameter during ore crushing and grinding circuits. During historical mining, milling wastes were poorly contained and tailings of all sizes were typically discharged to local

rivers to become incorporated into channel and floodplain deposits (Bradley, 1989). Overall, tailings are composed of fine-grained particles created during the mining process that do not have economic value, but contain residual metal concentrations at levels that can be a major source of contamination in fluvial systems.

Mining operations often contaminate river systems with tailings sediments and high concentrations of metals for long distances >100 km (Macklin et al., 2006). Metal concentrations (i.e., parts per million (ppm)) in the fine sediments of the channel bed generally decrease exponentially with distance from the source (Miller, 1997; Walling et al. 2003). Metal storage mass (i.e., kilograms or megagrams) in bed deposits is generally greatest in the middle and lower reaches of the rivers where channel width increases downstream and sediment deposition is more likely to occur in bar deposits (Wohl, 2014). Overall, sediment transport is unevenly distributed throughout a river system and the deposition rate (i.e., kilograms per kilometer or square meter) of sediment and associated contaminants increases in places where stream power decreases, channel widens, or sediment is deposited on the floodplain (Graf, 1997).

Macklin et al. (2006) provides a summary of recent literature on sediment-associated metal dispersion in rivers affected by mining actives, specifically the response and recovery of river systems following the failures of tailings dams. They conclude the long-term effects of mine tailings-spills have on river systems are a function of four factors: quality of sediment, quantity of sediment, the amount of time contaminates were discharged into water bodies, and effectiveness of cleanup efforts. A case study was reported about a tailings dam failure at Aznalcolar, Spain which dumped high concentrations of Pb, Zn, copper, arsenic into the river and contaminated several hundred

kilometers of river. Another case study focused on a tailings dam failure into Rio Pilaya in Bolivia which had significant effects on local biology and wildlife downstream. Again, several hundreds of kilometers of river were contaminated and the greatest concentrations of contaminated sediment were closest to the mining source.

Miller (1997) stated that fluvial processes are fundamentally important to the transport and redistribution of heavy metals at the Earth's surface. Lewin and Macklin (1987) discuss the mechanics behind mining waste dispersal and define the fluvial processes as either "passive dispersal" or "active transformation." Passive dispersal is characterized by the transportation of the mining waste sediments along with the natural sediment load of the system (Lewin and Macklin, 1987; Miller, 1997). Metal rich sediments may accumulate temporarily within channels, or be spread out across the floodplains. Active transformation is a change in the river morphology because of a geomorphic response to the large volumes of added mine waste sediment. If mining sediment inputs are excessive, active transformation may induce a metamorphosis of the entire sedimentary structure and floodplain morphology of the river system (James, 1989).

In-channel deposits and floodplains act as both sinks and sources of mine waste in fluvial systems (Lecce and Pavlowsky, 1997, 2001, 2014). During mining periods, more than forty percent of tailings introduced into a fluvial system may become stored in floodplain deposits (Lecce and Pavlowsky, 1997). Floodplain and channel deposits are reworked intermittently by erosion, therefore reintroducing these contaminants into the fluvial system in time (Lecce and Pavlowsky, 1997, 2001; Graf 1997, Walling et al. 2003, Lecce et al., 2011). This reintroduction of contaminants causes problems for

agencies attempting to assess changes of upstream pollution sources on downstream water quality. Therefore, understanding contaminated sediment storage in a river can have benefits for understanding the sedimentology and sediment transport regime of a river, but also the long-term risk in contaminated rivers.

Mine-waste Contamination in Southeast Missouri

Big River drains the majority of the Old Lead Belt, Missouri (Figure 6). Past and ongoing releases of chat and fine tailings to the river have resulted in the large-scale contamination of channel sediment and floodplain deposits with toxic levels of Pb along 145 km of the Big River from Leadwood to its confluence with the Meramec River (Roberts et al., 2009; Pavlowsky et al., 2010). Section 303(d) of the Clean Water Act requires the states to identify streams and lakes that do not meet water quality standards. The Missouri 2008 303(d) List identifies over 89 km of the Big River, as well as 16 km of its tributaries, as impaired due to Pb, Zn, and calcium (Ca) derived from mining sediments (MDNR, 2008).

Lead and Zn contamination in Big River was caused by historical mining in the Old Lead Belt and the release of large volumes of tailings sediments to the river and its major tributaries from six major mines which were global producers of Pb from 1864 to 1972 (Seeger, 2008). These tailings contain elevated levels of Pb, Zn, and other heavy metals that have harmful effects on wildlife (Besser et al., 2008; Gale et al., 2004; EPA, 2012) and humans (Gulson et al., 1994) when they contaminate fluvial systems.

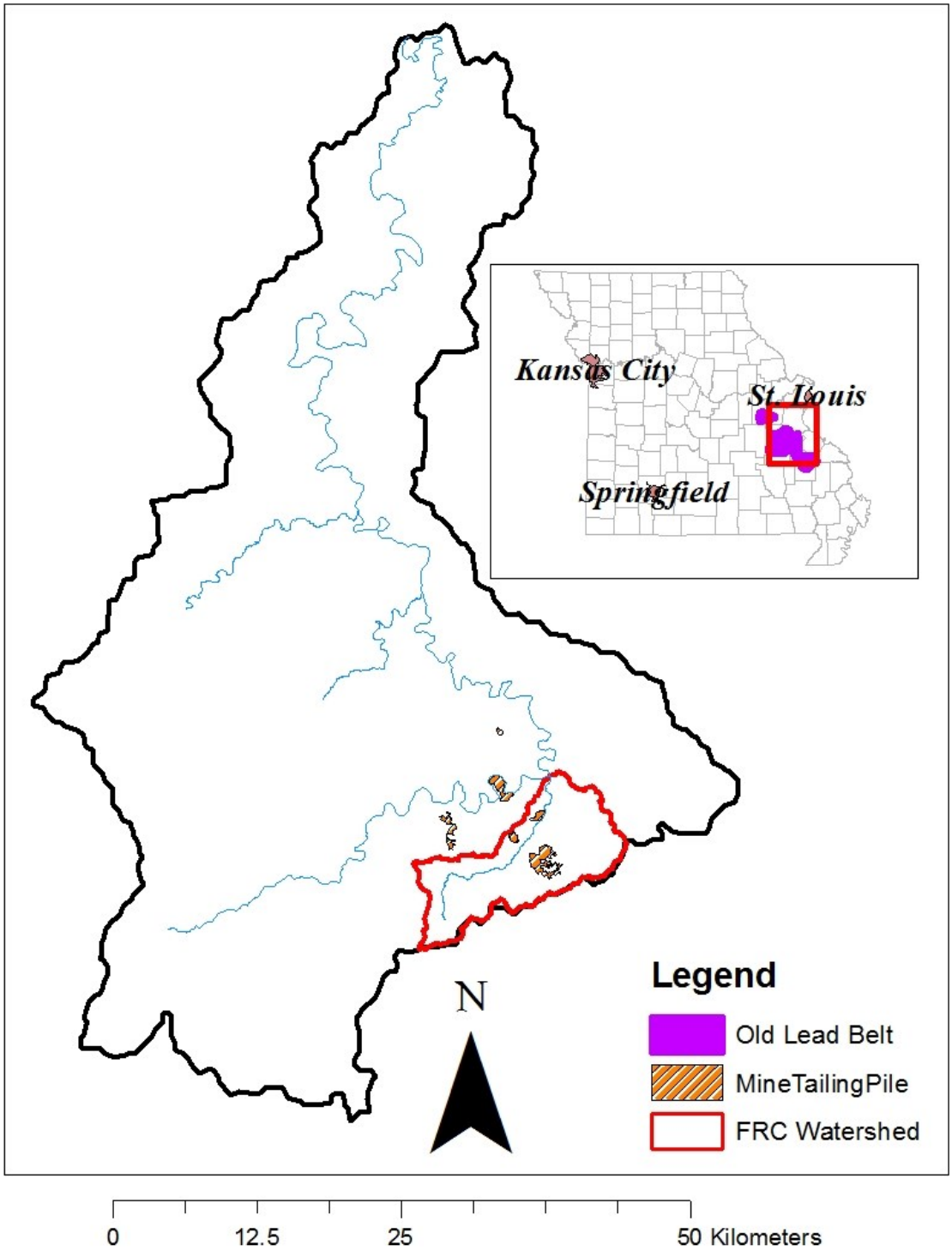

Figure 6. Big River and Flat River Creek Watershed, Old Lead Belt, Missouri.

Contaminated sediment above 128 ppm Pb and 459 ppm Zn are a danger to fish and mussel populations (MacDonald et al., 2000). High blood-lead levels in children are a health risk posed by tailings contamination in Big River (Gulson, et al., 1994). In general, fine-sized tailings released to Big River are capable of downstream transport during flood events and also interacting with channel and floodplain storages over various timescales (Engelund and Hanson, 1967; Evans and Davies, 1993; Pavlowsky et al., 2010).

The effect of tailings contamination on the main stem of Big River has been studied, however, our understanding of the extent of sediment interactions with channel deposits and the spatial extent of contamination within tributary watersheds, particularly where mining activities were intensive, is not well understood. Previous studies quantify the concentrations and storage of contaminated sediment stored in Big River (Roberts et al. 2009; Pavlowsky et al. 2010). Earlier studies by Smith and Schumacher (1991, 1993), and Gale et al. (2004) also addressed the state of the contamination, however little attention has been given to the extent of Pb and sediment storage in its most heavily mined tributary, Flat River Creek (FRC), and how it has affected contaminated sediment delivery and storage in Big River below the FRC confluence. FRC is a major tributary to the Big River and contains three of the six major tailing piles which were active from 1895 to 1972. Newfields (2007) reported the area and volume of combined chat and tailings in each of the major tailings piles (Table 1). All three piles have been stabilized and remediated so future sediment Pb sources are related to release from storage.

While previous studies in the Old Lead Belt focus primarily on the Big River, some sediment sampling did occur in FRC. Smith and Schumacher (1991) found that Pb

Table 1. Description of Tailings Piles, after Newfields (2007) in Pavlowsky et al. 2010.

Pile	Area (km^2)	Tailings Volume (m^3)	Avg. Pb (ppm)	Avg. Zn (ppm)
Federal	4.7	3,973,000	885	293
Elvins/Rivermines	0.6	7,946,000	4,440	5,541
National	0.6	4,890,000	3,661	417

and Zn concentrations in bed sediment of FRC increase downstream from the confluence of Harris Branch (Smith and Schumacher, 1991).

Later work by Smith and Schumacher (1993) noted the stream bed downstream of the National Pile was composed entirely of sandy mill tailings and the channel was unstable. They reported Pb concentrations in bed sediments in the stream segment between the Elvins/Rivermines Pile tributary (R-km 7.6) to Shaw Branch (R-km 6.3) draining the Federal Pile ranged from 2,050 ppm to 3,140 ppm. Smith and Schumacher (1993) found the highest bed sediment Pb concentration of the study at a location upstream of the National pile at 10,100 ppm. Bed sediments downstream of the National Pile contained Pb concentrations ranging from 1,000 ppm to 7,200 ppm. They also noted the concentrations of Pb and Zn increase as particle size decreases. Longitudinally, Smith and Schumacher (1993) determined that Pb concentrations in bed sediment increase in the downstream direction in FRC.

More recently, Roberts et al. (2009) found heavy metal concentrations in sediment samples from the Big River increase downstream of the confluence with FRC, further justifying the need for continued scientific investigation of the effect that contaminated sediment input from FRC has on Big River metal trends below the

confluence (Figure 7). Additionally, Gale et al. (2004) evaluated metal contamination in sediments at four sites along FRC located just below Shaw Branch, upstream and downstream of the National Tailings Pile, and at a control site approximately one kilometer above Harris Branch. Gale et al. (2004) also observed an increasing trend in Pb concentrations downstream and a peak in Zn concentrations below the Elvins/Rivermines confluence and then a downstream decreasing trend in Zn concentrations. They concluded that historical mining activities continue to significantly impact sediment and fish health in the Big River and FRC. Figure 8 summarizes the Pb concentrations by R-km in FRC from previous studies.

The ability of Big River to recover from long-term mining contamination depends on the amount of stored contaminated sediment available for release to the stream from FRC as well as the time it takes to remove contaminants from present-day storage in Big River itself by transport, solution, dilution, sediment burial, or mitigation efforts. However, this information is not yet available for FRC. Pavlowsky et al. (2010) only reported contaminated storage volumes in FRC for one reach located below the St. Joe Bridge crossing (R-km 3.9) using seven cross-sections as having average unit storage of 590 m^3 / 100 m, maximum unit storage of 1,142 m^3 / 100 m, and 16 percent of the total contaminated sediment in active and stable bar storage. Unit storage is a unit of measurement summarizing a volume of sediment per unit distance. Unit storage allows easy comparison since sediment storage varies with different sized rivers.

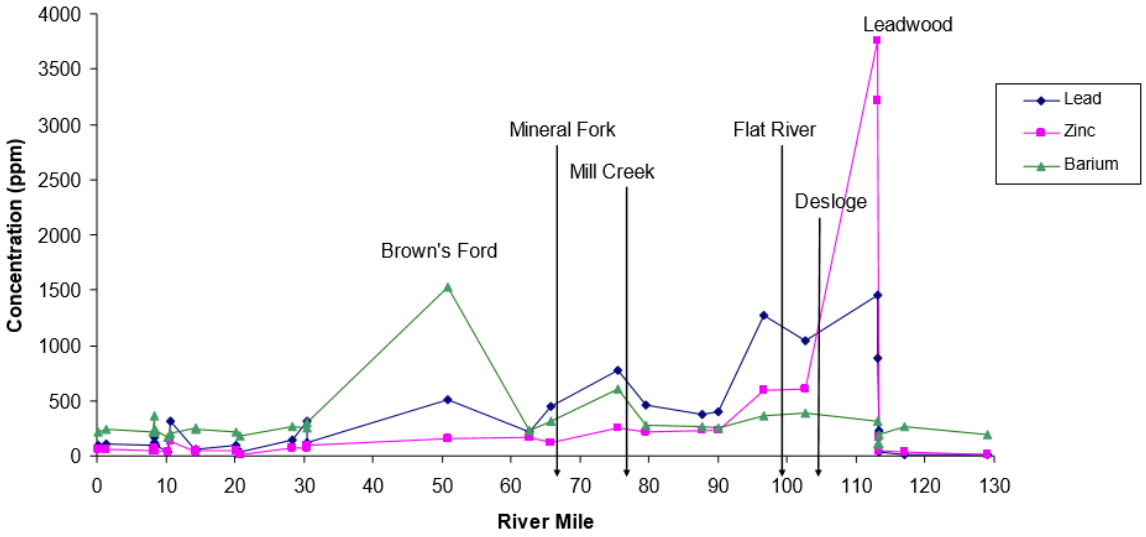

Figure 7. Heavy metal concentrations in sediments from the Big River (Roberts et al. 2009). Pb concentrations noticeably increase downstream of the Flat River Creek and Big River confluence.

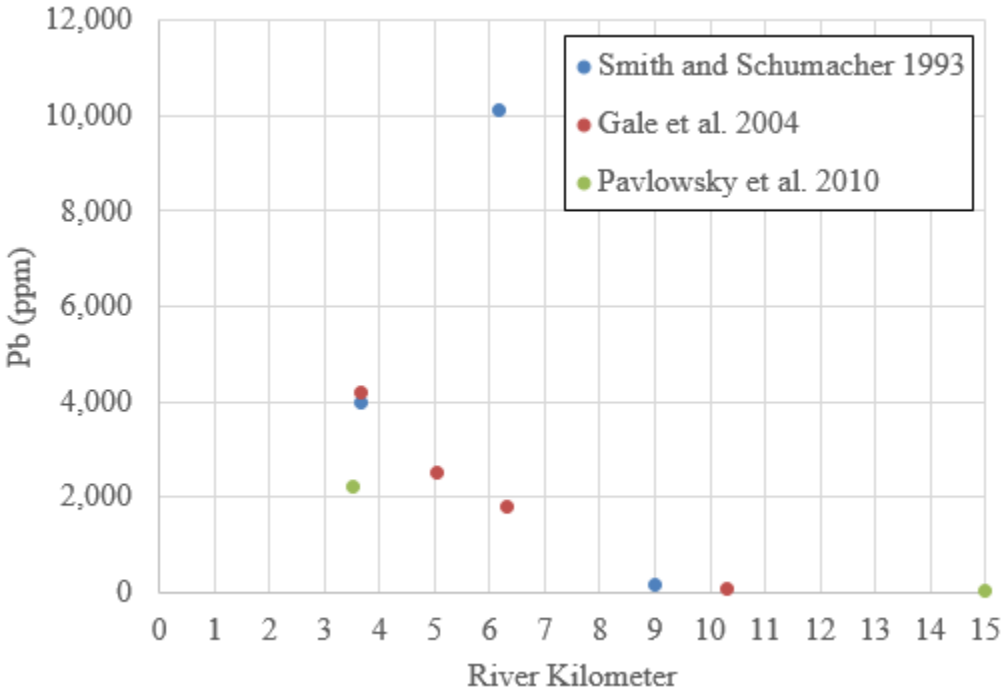

Figure 8. Pb concentrations in previous studies in Flat River Creek.

Research Questions and Objectives

Many studies use sediment budget approaches to determine the volume of contaminated sediment stored in the river system. Volumetric calculations require width, depth, and length of the sediment deposit obtained from field sampling or remote sensing methods such as Dennis et al. (2009) in the River Swale and Gunnerside Beck in Yorkshire, United Kingdom. The bulk density of the most abundant rock formation in the catchment, sandstone in this case, was multiplied by the sediment volume to determine a mass (Mg) of sediment, and the sediment mass was multiplied by metal concentration to determine the mass of contaminated sediment storage. It is estimated that approximately half of the metal-contaminated sediment was removed from the system by natural fluvial process and would take nearly 5,000 years to be completely removed naturally. Metal concentrations actually increase in the downstream direction from source because of the additional input from other contaminated watersheds and concentrations finally begin to decline 75 km downstream from source. Dennis et al. (2009) also determined nearly 44 percent of Pb in the system has been removed by natural processes transporting contaminated sediment downstream or by storing in the floodplain over the century since the cessation of mining operations.

Graf (1997) focused on understanding the spatial distribution of radioactive plutonium in fluvial sediment in the Los Alamos Canyon system, California. Graf (1997) used field methods to map the canyon system for geomorphic information at each location, including width, depth, and length of each deposit. Aerial photos were also used to verify many of the features. The sediment storages evaluated included channel bed, floodplains, point bars, and mid-channel bars and were the most common features

storing sediment (Graf, 1997). Plutonium concentrations were observed to decrease in a downstream direction from the source when considering the entire canyon system. However, on a segment or reach scale, concentrations did not decline smoothly in the downstream direction, but were spatially variable and linked to the stream power driving transport, and the hydraulic resistance acting against it.

The purpose of this study is to determine the spatial distribution and volume of contaminated sediment in FRC. There are few studies in the Old Lead Belt and in the Ozarks in general that focus on river sediment storage. Current remediation efforts in the Big River are focused on Big River below the FRC confluence. However, the effectiveness of these management efforts to reduce Pb contamination problems rely on quantifying the role that FRC will play in releasing Pb from storage and transporting it to Big River. This research project will quantify the sediment volume and mass of Pb stored in FRC. Even though the TMDL for Big River, FRC, and Shaw Branch has been completed, an unknown amount of contaminated sediment remains in channel deposits and bar deposits in FRC.

Research questions to be addressed include:

1) **What are the characteristics and spatial distribution of sediments, alluvial deposits, and channel form of FRC?** Understanding the sediment characteristics and distribution will explain where and why sediment is deposited and the geomorphic factors controlling them.

2) **How much and where is contaminated sediment and Pb stored in FRC?** Pb storages will be assessed for bed, active bar, and stable bar deposits. Understanding the locations and quantities of contaminated deposits are important for local land and remediation managers. Such locations can be monitored for future contamination effects or completely removed.

3) **Is stored in-channel mining sediment in FRC an important source of contamination to the Big River now and in the future?** Previous studies have shown Pb concentrations in the main stem of the Big River spike

downstream of the FRC confluence. This study will provide information to investigate concerns of FRC being a major contributor of contamination based on available sediment volumes and metal masses for transport to Big River.

Channel sediment in FRC is expected to reflect the characteristics of tailings materials produced by the flotation and gravity milling processes used in the Old Lead Belt covering the range of particle sizes associated with fine sediment in general (Smith and Schumacher, 1991; Pavlowsky et al., 2010) It is anticipated that channel sediment storage will be highest in places where channel slope decreases, channel width increases, unstable channel conditions enhance bar storage, and where channelization has not occurred (Graf, 1997). Channel reaches immediately downstream of mine tailing tributaries should contain the highest amount of contamination (Miller, 1997; Walling et al. 2003). However, the overall effect of the downstream transport of tailings and higher contaminated sediment storage rate along the lower gradient segments of FRC may increase Pb concentrations and storage volumes in the lower third of the channel system, below the influence of Elvins and Federal mine source points. Existing studies on the Big River have demonstrated that Pb levels increase significantly below the Big River and FRC confluence. However, it is not clear to what degree these surface sediment concentrations relate to overall source supply and storage of Pb in FRC. Even though the tailings piles have been sealed as part of Superfund plans and TMDL completion, there is still the potential for FRC to be a major source of contamination to the Big River. Besides the threat to Big River, sediment Pb concentrations in FRC well above probable effects concentration (PEC) thresholds at 128 ppm Pb and 459 ppm Zn are of concern too (MacDonald et al., 2000). Understanding the extent of present-day contamination is

important to local community leaders, remediation efforts, and land managers concerned with the water quality and ecology of FRC.

STUDY AREA

Regional Location

FRC is located within the Big River Watershed in southeast Missouri, approximately 60 miles south of St. Louis. The town of Flat River was merged with the surrounding towns of Elvins, Esther, and Rivermines in January 1994 to create the current town of Park Hills with a population of approximately 8,760 from the 2010 census (U.S. Census Bureau, 2010). Mineral mining attracted the earliest settlers to the region and was the driving force of population and economic growth during the 1800s and 1900s (McGraw, 1936) (Figure 9). Numerous mining companies were established and operated in Flat River from the 1850s until the last mine closed in 1972.

The Big River Watershed is located in the Salem Plateau of the Ozark Highlands and drain the majority of the Old Lead Belt. The Big River drains approximately 2,500 km^2 before it enters the Meramec River in Eureka, Missouri (Roberts et al. 2009). The FRC watershed is located entirely within the southeastern portion of the Big River Watershed in St. Francois County, Missouri.

Missouri is one of the top five state exporters of Pb and Zn in the United States and the World (Seeger, 2008). The Old Lead Belt exported over 8.5 million tons of lead metal during the 1900s (Wharton, 1975). By the 1920s, the majority of mines in the FRC watershed belonged to the St. Joseph Lead Company. Three of the six major tailings piles in the Old Lead Belt are located within the FRC watershed.

This study focuses on the lower 9.5 kilometers of FRC below the intersection of the Route 32 bridge crossing. This study area encompasses the town of Park Hill,

formally Flat River. The three major tailings piles of Federal, National, and Elvins/Rivermines are located within the study area (Figure 10). Field maps, channel profile characteristics, and sediment samples are all spatially-linked by river kilometer locations (R-km #), where R-km 0 is the confluence of FRC on Big River and R-km distance increase upstream from there. The most upstream tributary with mining influence is Harris Branch, which drains the south margin of the Federal Pile and enters FRC at R-km 9.1. The Elvins/Rivermines tailing pile tributary enters at R-km 7.6. The National Tailings Pile enters at R-km 5.05 and R-km 3.65. The FRC watershed is 123 km² in area and the main channel is 20.7 km long with headings in the St. Francois Mountains.

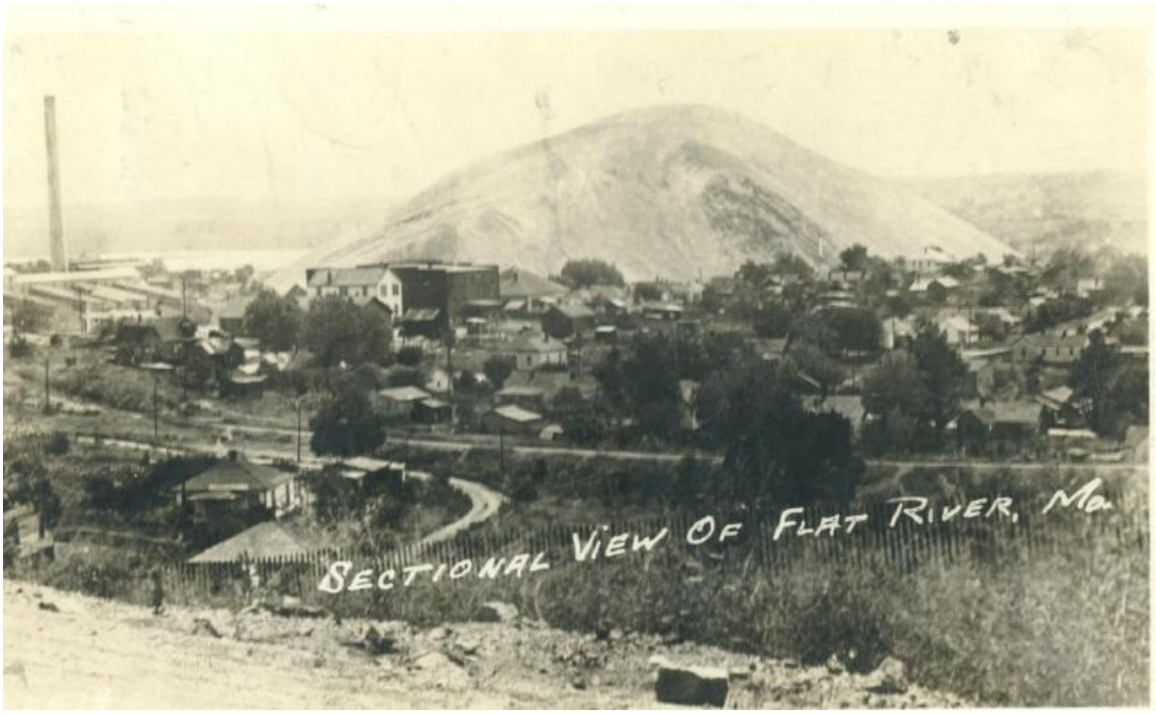

Figure 9. National Pile view from Flat River circa 1912.

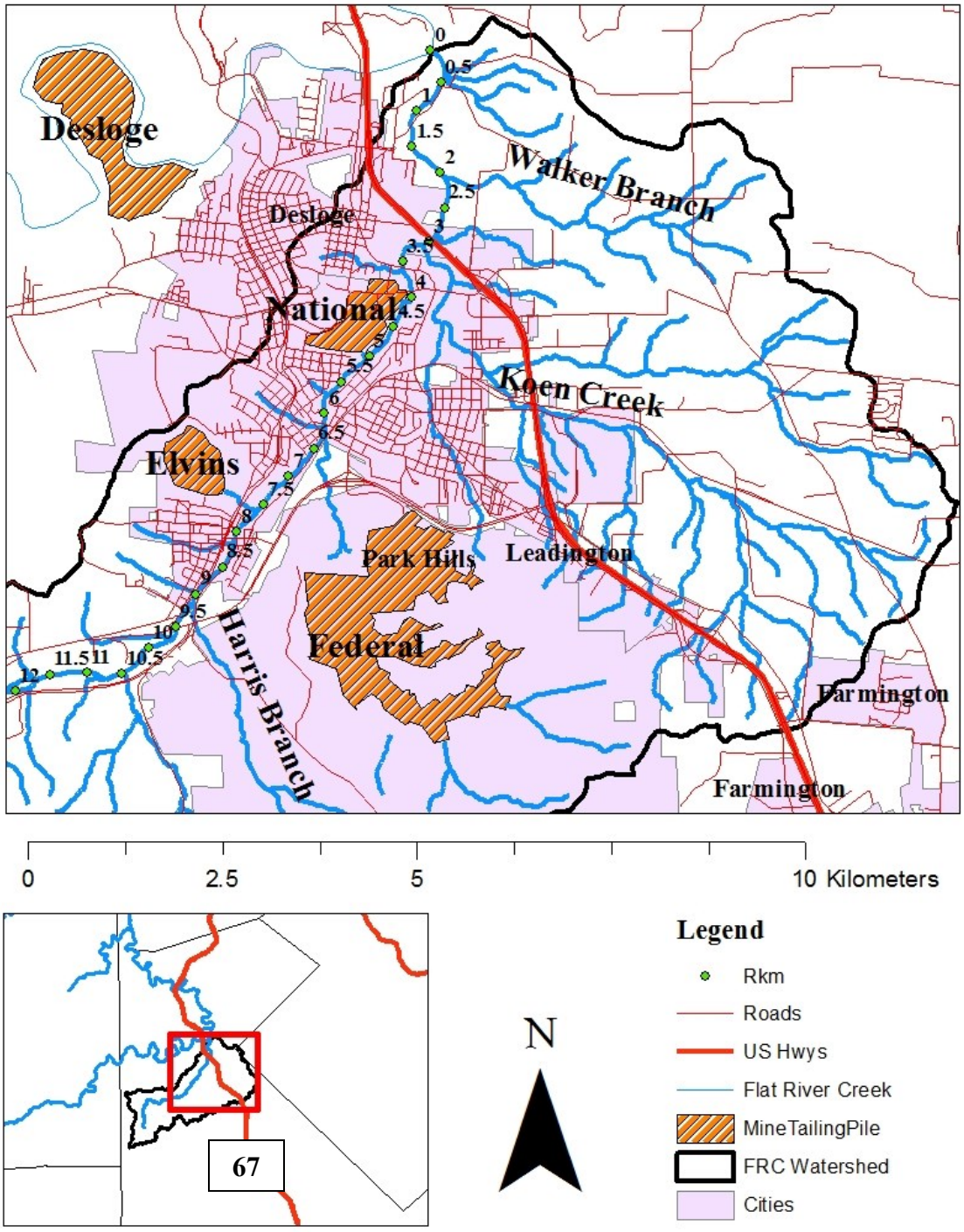

Figure 10. General map of Flat River Creek study site in Park Hills.

The mineral deposits mined in Southeast Missouri are Mississippi Valley Type (MVT) deposits. The first of these deposits were discovered in the Mississippi Valley and are found all over the world. The MVT in Southeast Missouri are metal-sulfide deposits hosed in Paleozoic dolostone, limestone, and to a lesser extent sandstone. Common trace elements found in MVT are Pb, Zn, arsenic, cadmium, cobalt, copper, and nickel. The primary metal-sulfide minerals in these deposits are galena (PbS), sphalerite (ZnS), and pyrite-marcasite (FeS_2) (Seeger, 2008). The MVT deposits are found in exposed Precambrian rocks of the St. Francois Mountains. The ore deposits are primarily found in the Cambrian age Bonne Terre Dolomite Formation and is typically 375 to 400 feet thick and found between 200 and 1000 feet deep. The Bonne Terre Formation extends into the underlying Lamotte Sandstone and overlying Davis Formation (Buckley, 1908).

There are two primary geologic units in the FRC watershed study area (Figure 11). The Elvins Group (Ceb) includes three units: the Derby-Doe Run Dolomite composed of alternating thin dolomite, siltstone, and shale; the Davis Formation composed of glauconitic shale with fine - grained sandstone, limestone, and dolomite; and Bonne Terre Dolomite composed of dolomite, dolomitic limestone, and limestone. The Eminence and Potosi Dolomite (Cep) where the Eminence Dolomite is dolomite with some druse - coated chert, and the Potosi Dolmite which is dolomite with abundance of druse - coated chert (Stoeser et al., 2007).

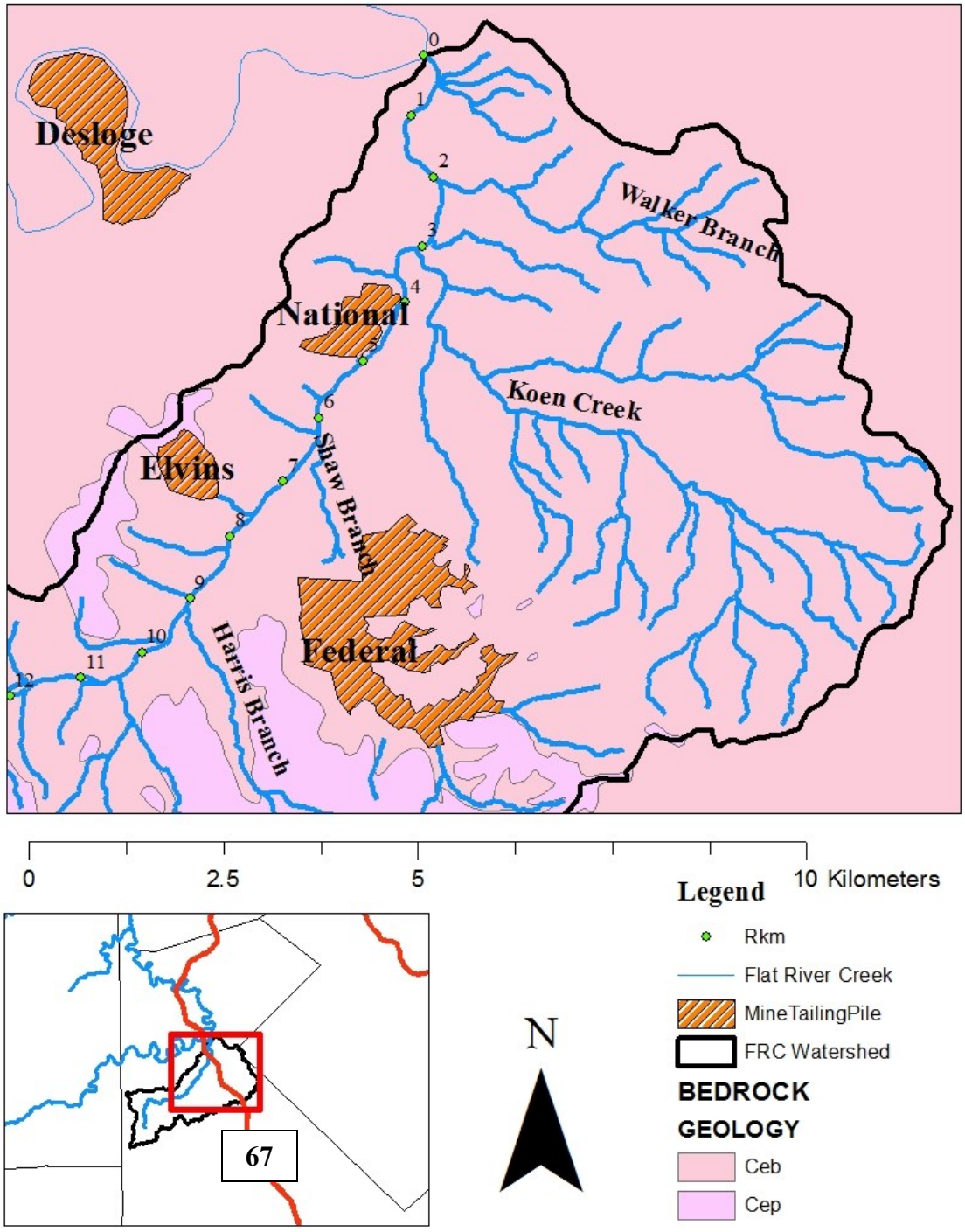

Figure 11. Geologic map of the Flat River Creek watershed.

The weathering of carbonate rocks produces variable thicknesses of residuum. Lower sloped areas accumulated thick-clayey residuum rich in chert gravel and cobbles up to 6 m to 7 m in thickness. Steeper sloping areas have thin clay-rich soils or no soils at all. The weathering of the carbonate rocks creates karst drainage on the upland and precipitation that does not evaporate infiltrates into the subsurface karst systems and emerges in springs along valley bottoms (Jacobson and Prim, 1997). Surface runoff is restricted to unusually intense rainfall events and many upland streams are dry year round (Jacobson and Primm, 1997).

A U.S. Geological Survey stream gauge was installed in FRC at the St. Joe Drive Bridge for Smith and Schumacher (1991; 1993) but was discontinued after the study completion. Smith and Schumacher (1993) reported the median discharge in 1988 was 0.21 cubic meters per second and the mean annual discharge was 0.29 cubic meters per second. This study calculated the average active channel width for the first 9.5 km of FRC is 23 m, the average wetted channel depth is 0.5 m, and water surface channel slope is 0.0036. The present study focuses on sediment storage and discharge and velocity measurements were not collected.

Southeastern Missouri has continental climate affected by the prevailing east-moving storm systems, Gulf Coast moisture sources from the south, and occasional continental polar from the north (Jacobsen and Primm, 1997). Southeastern Missouri is in a moist continental climate region. The average annual temperature is 55 °F ranging from an average of 32 °F in January to 77 °F in July. The annual rainfall in the region averages about 40 inches with the wettest period in the spring months (Jacobson and Pugh, 1992).

The growth of the town of Flat River coincides with the discovery and subsequent mining of Pb, first discovered in 1721 by French explorers. Settlement of the Ozark Highlands began in the early 1800s and the town of Flat River was established between 1805 and 1810 named after the local stream also named Flat River. In 1893, the Doe Run Lead Company reported finding a 23 ft thick layer of pure galena from one of their exploratory drills (Ste Gen. Herald, 1893). During the 1890s, many settlers migrated to the Ozarks for jobs in the mineral mining industry (Seeger, 2008, Smith and Schumacher, 1993). In 1902, the Federal Lead Company announced the construction of 1,000 new residences around the town of Flat River that would bring in roughly 20,000 persons for work in the mining district (St. Francois Herald, 1902) and circa 26 March, 1917, the town of Flat River was incorporated (Lead Belt News, 1917).

Mining History

The St. Joseph Lead Company, commonly referred to as St. Joe, was the dominant company in the Old Lead Belt and Flat River from 1864 to 1972. During the first 70 years of production, as many as 15 small companies operated in the area and were eventually all purchased and absorbed by St. Joe (Smith and Schumacher, 1993). Pb was the primary mineral mined with minor deposits of Zn found in the Federal Mine in Flat River (Seeger, 2008). The last Pb producing mine in the Old Lead Belt closed in 1972 and the Viburnum Trend became the current primary Pb producing sub-district in Missouri.

Tailings from mining operations were stored in the Federal, National, and Elvins/Rivermines Tailings Piles. The Federal Mine was owned by the Federal Lead

Company and mining operations began in 1902. During its first year of production, it produced 4,320 tons of concentrates. The company acquired several smaller companies and owned 16,000 acres of land, all located in St. Francois and Washington Counties. The Federal Lead Company had ten mines operating during 1907 and two mills processing a combined daily capacity of 3,200 tons (Buckley, 1908). From 1894 to 1906, nearly six million dollars of concentrate were produced and 55 acres of ground were mined. All tailings produced during early mining operations by the Federal Lead Company, and subsequently by St. Joe after its purchase in the early 1910s, were deposited in the Federal Pile. Shaw Branch drains this tailing pile and flows into FRC. Currently the Federal Tailings Pile covers approximately 4.7 km^2.

The National Tailings Pile is owned by the Doe Run Lead Company. The Doe Run Lead Company was organized in 1887 and in 1890 purchased land in the Flat River area. In 1907, Doe Run Lead Company purchased several small companies including Columbia Lead and Union Lead Company bringing its total holdings to 5,000 acres. By the end of 1907, Doe Run Lead Company produced 231,000 tons of concentrate valued over ten million dollars, from 50 acres of mined ground (Buckley, 1908). The Doe Run Lead Company was also purchased by St. Joe in the early 1910s and all tailings produced in the area are stored in the National Tailings Pile. Studies by Smith and Schumacher (1993) report that in 1983 there was a large slime pond near the National Tailings Pile and slimes are known to contain extremely high amounts of Pb. Currently the National Pile is approximately covers 0.6 km^2.

The Elvins/Rivermines pile is centrally located in the Old Lead Belt. In 1891, the Doe Run Lead Company began mining operations and subsequently began acquiring

properties belonging to the smaller mining operations. By 1909, the Doe Run Lead Company controlled 6,548 acres in the Flat River area with a total of seven mining shafts, and by 1911 had consolidated its mill operations at Elvins to a 1,500 to 2,000 tons per day mining plant. The mill operations by Doe Run in the Elvins/Rivermines area ceased in 1934 and the property was acquired by the St. Joe Minerals Corporation in 1936 (Buckly, 1908). The Elvins pile covers 0.6 km^2.

Present-day Land Use

The FRC Watershed (Figure 12) is covered by 49 percent forest and woodland, 27 percent grassland, 18 percent urban impervious surfaces, 4 percent barren, 1 percent cropland, and 1 percent open water (MDNR, 2007). The Elvins, Federal, and National tailings piles cover 3 percent of the total area of the FRC Watershed. There are 70 mines in the FRC watershed. There are 34 underground lead mines, 14 surface lead mines, 1 surface copper mine, and 21 surface mines classified as limestone quarries. All mines are past producers as all mining operations in the area ceased in 1972.

In 2008, a Total Maximum Daily Load (TMDL) was approved for Big River, FRC, and Shaw Branch (a tributary of FRC) in Jefferson, St. Francois, and Washington Counties, Missouri. It identified 8 km of stream length affected by Zn "pollutant" specifically from the Elvins/Rivermines tailing pile and 8 km of stream length of Pb and Non-Volatile Suspended Solids (NVSS) "pollutants" from the Old Lead Belt abandoned mine lands. It also identifies 3 km of stream length affected by Pb and NVSS "pollutants" along Shaw Branch, which is a tributary of FRC (MDNR, 2007). The TMDL gave FRC a priority ranking of "medium" for Zn and "high" for Pb and NVSS.

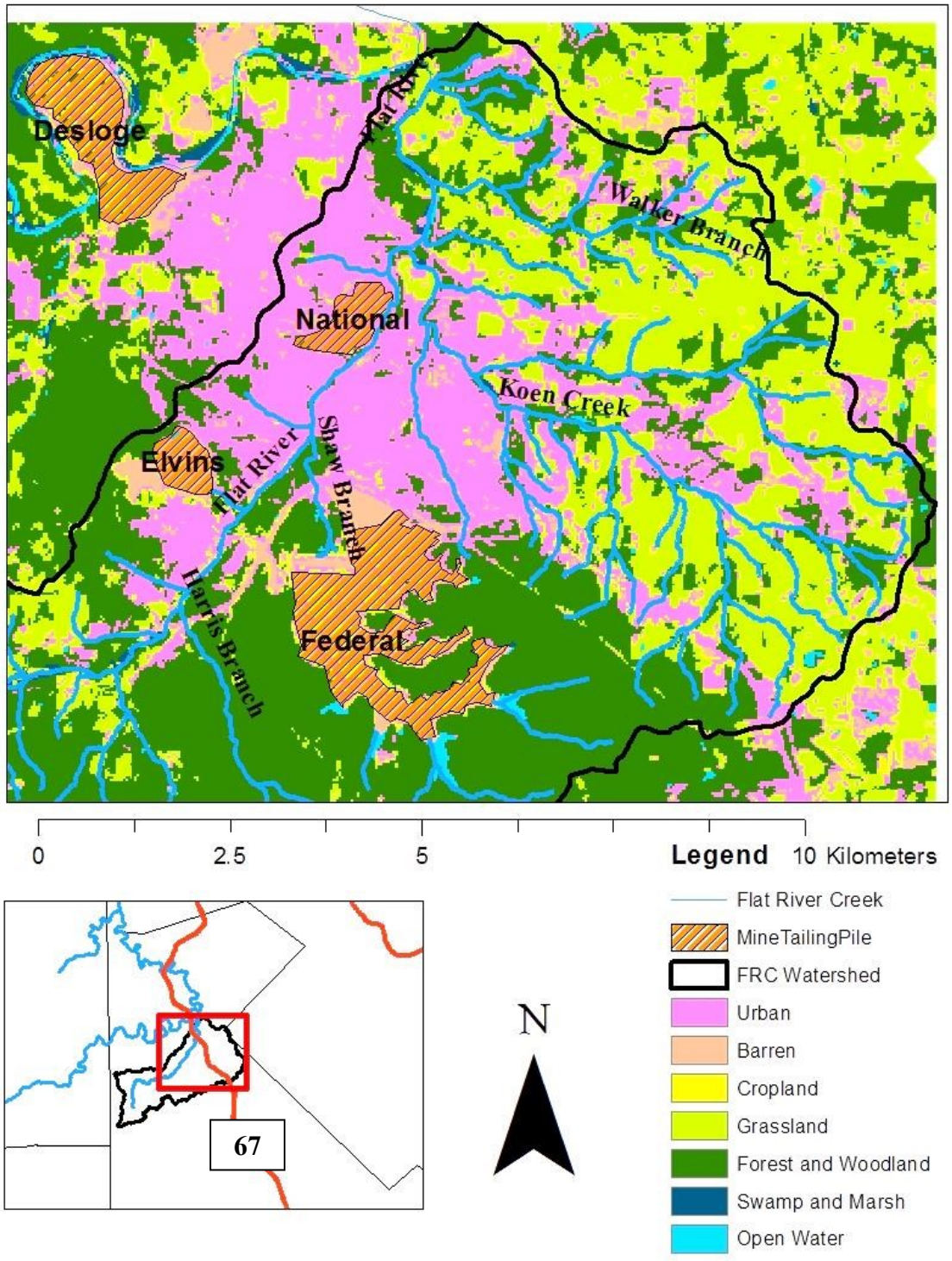

Figure 12. Land use land cover map of the Flat River Creek Watershed.

Shaw Branch was given a "medium" priority ranking for Pb and NVSSs. The TMDL lists the impaired uses as protection of aquatic life (warm-water fisheries) and human health protection (fish consumption).

The Elvins/Rivermines, Federal, and National Tailings piles were stabilized against wind and water erosion and mass movement. In 2010, FRC was delisted from the 303(d) list upon completion of its TMDL. Once stabilized, tailings no longer enter the waterways from the tailings piles and attention is focused on how much contaminated sediment is still in the river system (MDNR, 2007). There is still water runoff from storms that enter FRC at various locations and are areas of interest for their effect on channel morphology and sediment distribution.

A Superfund was established to address contamination caused by historical and recent metal mining across the Southeast Missouri Lead Mining District (MDNR, 2009). The Big River Mine Tailings Site is one of several sites designed as Superfund and covers approximately 285 km^2 within the Old Lead Belt, including the study area for the present study and all six major tailings piles in St. Francois County (MDNR, 2009; EPA, 2011). The TMDL recognizes the removal of contaminated sediment found from channel deposits and floodplains along Big River and FRC as a potential option for mitigation (MDNR, 2007). Additionally, in Spring 2015, Superfund contractors under the supervision of the Army Corp of Engineers and U.S. EPA installed a sediment trap structure on the Big River below the FRC and Big River confluence to collect mining-contaminated sediment for removal by dredging. Therefore, information regarding the volume and location of the contaminated deposits provided by this study will be useful to project managers as well as an amount of sediment potentially available to the Big River.

METHODS

The primary objective of this study is to quantify the volume of sediment and mass of Pb, Zn, and Ca stored in FRC and to understand how sedimentology, geomorphology, and mining activity affect its spatial distribution of contaminant storage. A combination of field, laboratory, and geospatial methods were used document the current geomorphology and channel profile. Field methods included the mapping of channel geometry including width and depth. Sediment samples were also collected and processed in the laboratory. Laboratory methods determined the metal concentrations and sedimentology, and were used to calculate the volume of contaminated sediment. Geospatial methods involving light detection and ranging (LiDAR) were used to model the channel planform to create a continuous dataset along the length of the study area. This chapter outlines the study design and methods used to create and analyze the data.

Sampling Approach

The calculation of a sediment volume requires information about the width, depth, and length of the depositional features. Width and depth are easily measured in the field; however most geomorphic assessment approaches are unable to account for every depositional feature in the river. Remote sensing techniques using LiDAR are able to capture width and length of features, but are unable to account for height of features below the waterline (Podhoranyi and Fedorcak, 2015). To account for all three components of sediment volume, a combination of field methods and geospatial remote sensing using LiDAR was implemented. The combination of these two techniques yields

sediment volume and similar techniques were used in Thoma et al. (2005). The availability and use of high-resolution LiDAR data has benefitted many studies involving fluvial geomorphology (Thoma et al., 2005, Vianello et al., 2009, Notebaert et al., 2009, Fisher et al. 2013).

The calculation of metal mass stored in sediment requires a volume of sediment, metal concentration, bulk density of the sediment, and the fraction of contaminated sediment, which in this study is the percent less than 2 mm size fraction. The sediment volume components of length, width, and depth are determined by using both field and remote sensing techniques. The metal concentration was determined using average concentrations by segments. The bulk density was obtained from the most abundantly deposited alluvial soils using the soil survey of St. Francois County. The percent less than 2 mm size fraction was determined from the laboratory analysis.

Field Methods

Field assessment activities for this project were divided into two components: geomorphic assessment of the channel bed, active bar, and stable bar deposits and sediment sampling of bed and bar deposits. The geomorphic assessment provides width and depth of channel features and their dimensions were used to calculate sediment volume. The sediment sampling revealed metal concentrations found in various channel and bar features.

Geomorphic Assessment. The following channel profile illustrates how features for a given cross-section are assessed: active channel width, total channel width, individual depositional feature width, left and right bankfull height, approximate depth of

fines, average channel depth, and maximum depth to refusal referenced from water level. Distances are measured with 100 m tapes. Depths from water level and height measurements are collected using stadia rods. Depth of fines and other depth to refusal measurements are collected using a sediment tile probe.

Each cross-sectional survey was collected roughly every 50 or 100 m depending on the geomorphology of the sample reach. The objective is to understand sediment storage and sites were selected based on presence of abundant sediment deposition in either the channel or bar deposits. Long reaches of exposed bedrock with little sediment storage were recorded in field notes but a cross-section was not taken.

Geomorphic assessment data were used to calculate sediment storage based on the following channel geometry (Figure 13):

1. Active channel storage = bed storage + active bar storage + stable bar storage.

2. Bed storage = Wetted channel width in meters (m) * (Depth (m) to refusal – average of 5 depths measured across channel).

3. Active and stable bar storage = Bar width (m) * (Depth (m) to refusal + bar height). Depth to refusal at each location will provide the maximum depth.

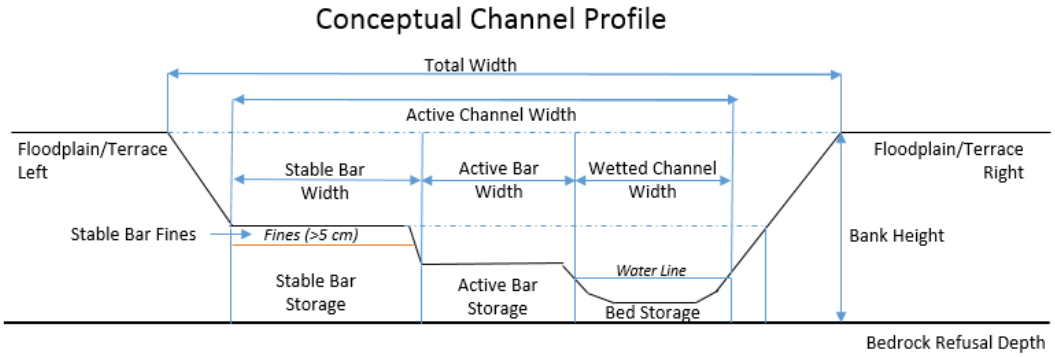

Figure 13. Channel morphological storage units conceptualized and designed for this study.

Sediment Sampling. Sediment sampling provided field samples of sediment from different locations along FRC. Samples were analyzed for geochemistry to reveal the presence or absence of Pb contamination. Sediment sampling was divided into three types: channel bed sediments, active bar sediments, and stable bar fines. Mining sediment is generally composed of fine-gravel and sand with varying amounts of silt and clay. Sediment particles in these size ranges are mobile and mixed by large floods and then re-deposited along the channel until they are stabilized by vegetation or river management practices (Lecce and Pavlowsky, 1997).

Channel bed sediment samples were collected from channel glide and in-filled pool units. Active bar and shadow bar samples are collected at a depth of 10 cm to 30 cm below the surface and were stored in labeled 1-quart or 1-gallon freezer bags. The 1-gallon freezer bags are used to ensure enough fine grained sediment would be present for laboratory analysis. Stable bar fines samples are collected from the head, middle, or tail end of the stable bar at a depth of 5 cm to 10 cm below the surface and are stored in labeled 1-quart freezer bags.

Bar Core Sampling. An assumption of this study is that Pb concentrations in the bar and bed samples collected from 0 – 30 cm depths are representative of average concentrations for the entire depth of the deposit. Bar core sampling provides metal concentration information with depth to verify this assumption. Knowledge of channel planform, specifically large bar deposits at least 1 m in height, are identified from the geomorphic assessment. Bar core sampling below the water table is difficult and to ensure the greatest depth possible for sample collection, large bars greater than 1 m in height are targeted.

Bar core sites were dug to at least 0.7 m depth where possible with shovels. Sites were at least 0.5 m to 1 m in width to prevent sediment from mixing as samples are collected. Samples were collected at 10 cm increments and stored in 1-quart freezer bags. Sites at bar tails were preferred to ensure enough fine grained sediment would be present for laboratory analysis. Bar core samples will be processed the same way as surface samples.

Upstream Sediment Collection. This study primarily focuses on the lower 9.5 km of FRC and the Harris Branch tributary is the uppermost known mining influence to FRC. Sediment samples from the bed and active bar deposits were collected upstream of known mining influence to determine Pb concentrations in sediment not affected by mining activites. Sample locations will be located near easy access points to county and public roads. A minimum of five samples spanning 0.5 km length at three different locations along FRC were collected similarly to surface samples.

Fieldwork for the geomorphic assessment was completed December 15 – 17, 2014. The lower 7.5 km of FRC were walked to fulfill the assessment. Sediment sampling was completed January 8 – 10, 2015. The lower 9.5 km of FRC were walked to collect sediment samples. The bar core sampling was completed August 4 – 5, 2015 and upstream sediment sampling was completed on September 17, 2015. There were 103 sediment samples collected from the first 9.5 kilometers of FRC and an additional 16 sediment samples collected upstream above mining influence to determine the background metal concentrations.

Laboratory Procedures

Laboratory methods involve preparation, physical analysis, and geochemical analysis of bed and bar sediments. Field samples were cataloged and verified with corresponding field notes. Field samples in plastic freezer bags were dried in an oven at 60° C, disaggregated with a mortar and pestle, weighed and put through a 32 mm and 2 mm size sieve set to isolate mining-related size-fractions for analysis. Sediments greater than 32 mm were weighed and discarded. The remaining sediment, greater than 2 mm, were weighed and saved in the sample freezer bag. Sediment less than 2 mm were weighed and placed in special metal free plastic X-ray fluorescence (XRF) bags, labelled with the sample number and "< 2mm fraction."

An X-Met3000TXS+ Handheld XRF Analyzer (OEWRI, 2011) was used to analyze sediments in the XRF bags for Pb, Zn, and Calcium (Ca) concentrations. For every 15^{th} to 20^{th} sample analyzed by the XRF, a laboratory duplicate and a known jasperoid standard were analyzed to determine the precision and accuracy of the XRF. Element standards were designed to produce strong x-ray signatures of elements of interest (MacDonald et al., 2000) and the jasperoid standard is the Pb standard. Accuracy was evaluated by using the standard deviation and relative percent difference of the jasperoid standard for each sample set. Precision was evaluated using the relative percent difference of the duplicate samples. Relative percent differences under fifteen percent were considered acceptable (OEWRI, 2011). Overall, the XRF device used in this study was statistically accurate and precise.

Additional quality assurance and quality control (QAQC) steps were taken for XRF measurements (Shefsky, 1997; EPA, 2007). XRF samples are routinely sent to

laboratories to be analyzed on atomic absorption spectrophotometers or inductively coupled plasma atomic emission spectrophotometers for additional QAQC. Random sediment samples of the <2 mm fraction were also selected and sent to an independent laboratory, ALS Chemistry, Nevada, to be evaluated via aqua regia to obtain a correction value that would be multiplied to the Pb, Zn, and Ca metal concentrations. This study focuses on the <2 mm fraction because sand, silt, and clay particles are the most mobile and metals tend to bind to fine sediments. Additionally, floatation separation techniques produce tailings <2 mm in size. Correction values obtained from previous studies focusing on the Big River around the Big River/FRC confluence were used. Pb concentrations were multiplied by 1.09, Zn by 1.27, and Ca concentrations by 0.73.

Geospatial Data Analysis

Geospatial databases and Geographical Information System (GIS) were used to organize and analyze field and laboratory data. A set of winter 2013 "leaf off" and summer 2014 "leaf on" aerial photographs with 1-meter resolution were obtained from Google Earth Pro and Missouri Spatial Data Information Service (MSDIS) respectively, and used as base maps.

Channel planform mapping involves the creation of polygon shapefiles classifying various stable and active bar features and in-channel sediment storage locations along FRC. These features are mapped based on rectified aerial photos and LiDAR data. LiDAR data was available for the entirety of FRC and channel planform is visible with the "hillshading" tool in GIS. Using the LiDAR data, a catalogue of in-channel depositional features is created and verified though field notes, geomorphic data,

GPS, and field pictures. Polyline shapefiles were created for the bank top and bank bottom on both left and right banks in GIS. Active and stable bar polylines were drawn and all polyline features were converted into polygon files creating individual polygons for each depositional feature. The polygon area for each features were calculated with GIS.

A 50 m buffer was created around the FRC centerline, since the maximum observed total channel width was 47.7 m. The 50 m buffer shapefile was divided into 100 m cells with the cell center point every half kilometer and was intersected with the channel planform polygon and feature area was calculated in each cell. This results in a detailed catalogue of channel planform data for every 100 m along FRC (Figure 14).

Segment Partitioning. Different components of the sediment storage and metal mass calculations are at different resolutions. Channel profile data and sediment sampling were collected irregularly at the reach scale. The channel planform technique based on the LiDAR data allows for data analysis at 100 m resolution. Accurately calculating sediment volume and metal mass requires data at a uniform resolution, the segment scale, in this study. All components of sediment storage and metal mass were calibrated to the segment scale.

FRC was partitioned into eleven segments to account for variations in distribution from mining and non-mining sources. Segment boundaries were created at major mine tributary or non-mining tributary confluences. Segment number, length, binding R-km, boundary justification, changes in drainage area (A_d), and land use are summarized in Table 2 and 3. The upstream and downstream boundary justification generally refers to the type of area they drain.

Sediment Storage Calculations. Total sediment storage is calculated by summing the volume of sediment found in the channel bed, active bar, and stable bar

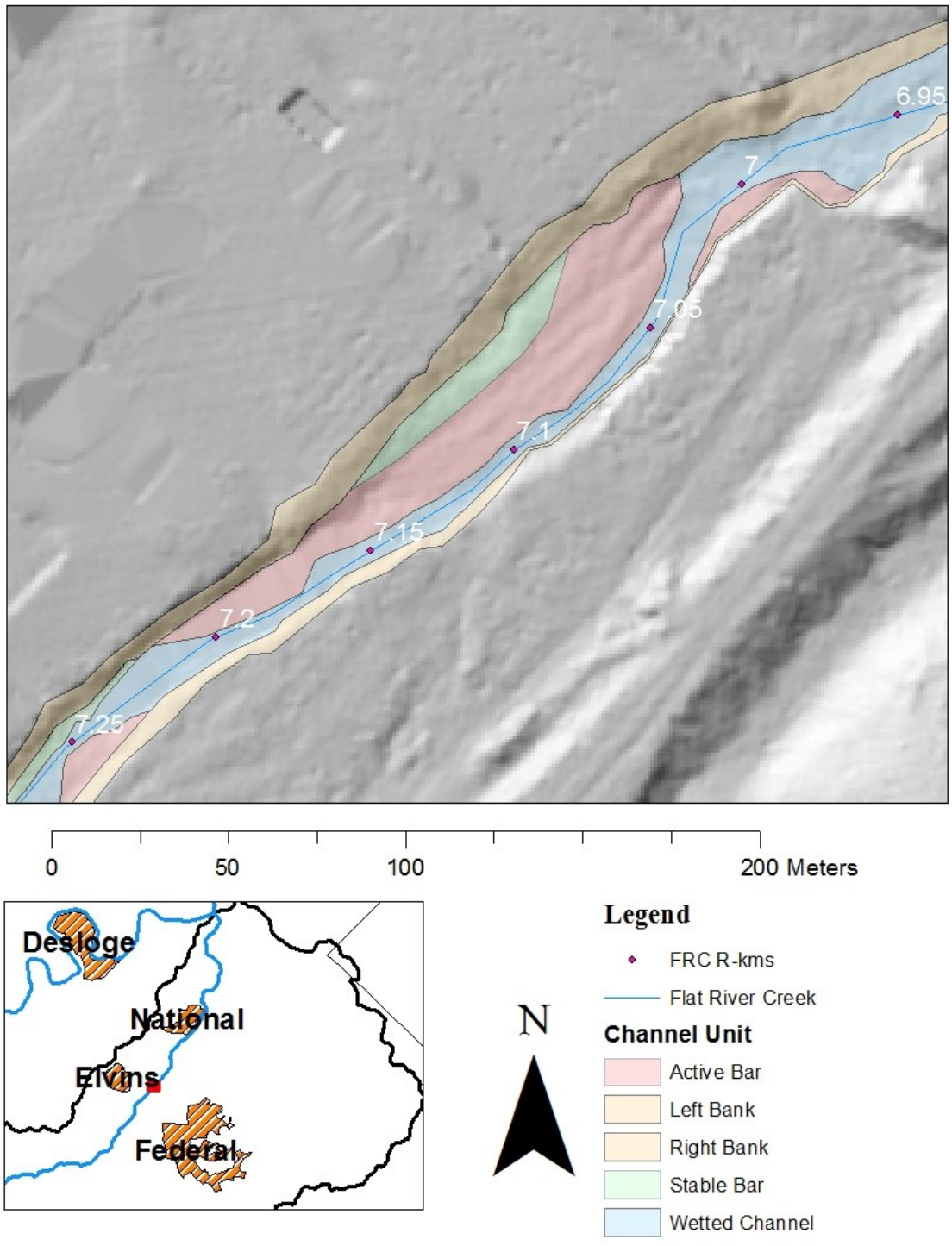

Figure 14. Example of channel planform derived from LiDAR hillshade**.**

Table 2. Summary of segment partitioning.

Segment	Length (km)	R-km Top	R-km Bottom	Boundary Justification Upstream	Boundary Justification Downstream
-	11.5	20.7	9.2	Non-mining segments	1st mining tributary at Harris Branch
1	1.05	9.2	8.15	Harris Branch	Non-mining tributary confluence
2	0.6	8.15	7.55	Non-mining area	Elvins tributary confluence
3	1.3	7.55	6.25	Elvins Pile	Shaw Branch
4	0.5	6.25	5.75	Federal Pile	Non-mining tributary confluence
5	0.7	5.75	5.05	Non-mining area	Upstream National Pile confluence
6	1.45	5.05	3.6	National Pile	Downstream National Pile confluence
7	0.55	3.6	3.05	National Pile	Koen Creek confluence
8	0.9	3.05	2.15	Koen Creek	Walker Branch confluence
9	0.9	2.15	1.25	Walker Branch	Outfall - Park Hills Mineral Belt WWTP
10	0.75	1.25	0.5	WWTP outfall	Unnamed tributaries
11	0.5	0.5	0	Unnamed tributaries	Big River confluence

Table 3. Summary of segment drainage area (A_d) and land use.

Segment	Cum. A_d (%)	A_d % Increase	Slope	Segment Land Use (%) Tailing Pile	Urban	Grassland	Forest
-	43	-	0.004	0	10	45	45
1	48	5	0.004	0	0	0	100
2	48.7	0.7	0.004	0	50	0	50
3	49.7	1	0.004	70	15	0	15
4	62.7	13	0.007	50	10	0	40
5	63	0.3	0.003	0	90	0	10
6	64.5	1.5	0.003	60	40	0	0
7	65.5	1	0.009	10	80	5	5
8	91.5	26	0.004	0	50	40	10
9	98	6.5	0.004	0	20	60	20
10	98.5	0.5	0.004	0	5	80	15
11	100	1.5	0.003	0	15	15	60

deposits in each segment in FRC. Calculating sediment volume requires the average length, average width, and average depth of sediment deposits. The length component is the segment length. The depth component is the average depth of sediment deposit features within the segment. Finally, widths of sediment deposit features extracted from the LiDAR derived cells are divided by 100 and averaged together by segment to obtain the width component.

Additional data processing was required for channel bed and the stable bar fines thickness. Channel bed thickness calculations in reaches with exposed bedrock were replaced with a thickness value of 0 m, indicating no channel bed storage. This adjustment was made before averaging the channel bed thickness. The stable bar fine thickness layer is assumed to contain higher concentrations of metals and must be addressed separately from the underlying "coarse" deposit. The fines thickness was subtracted from the total thickness and is referred to as stable bar fines fraction. The remaining thickness was used to calculate the rest of the stable bar sediment volume.

Metal Mass Calculations. Metal mass per segment for channel bed, active bar, stable bar "coarse", and stable bar fines is calculated by multiplying the sediment volume data, bulk density value, metal concentration data, and percent <2 mm sediment size together (Figure 15), similar to Thoma et al. (2005) and Dennis et al. (2009). Total metal mass is the sum of each metal mass per segment for each deposit type. Metal concentrations for channel bed, active, and stable bar deposits were averaged from samples collected from segments. Segment averages were used in order to minimize the effect of high concentration outliers that do not accurately represent the deposit. This same process was used for the percent <2 mm component.

A bulk density value of fine grained sediments depends on the composition of the sediment found there. The dominate soil type on alluvial soils of FRC are the Crider silt

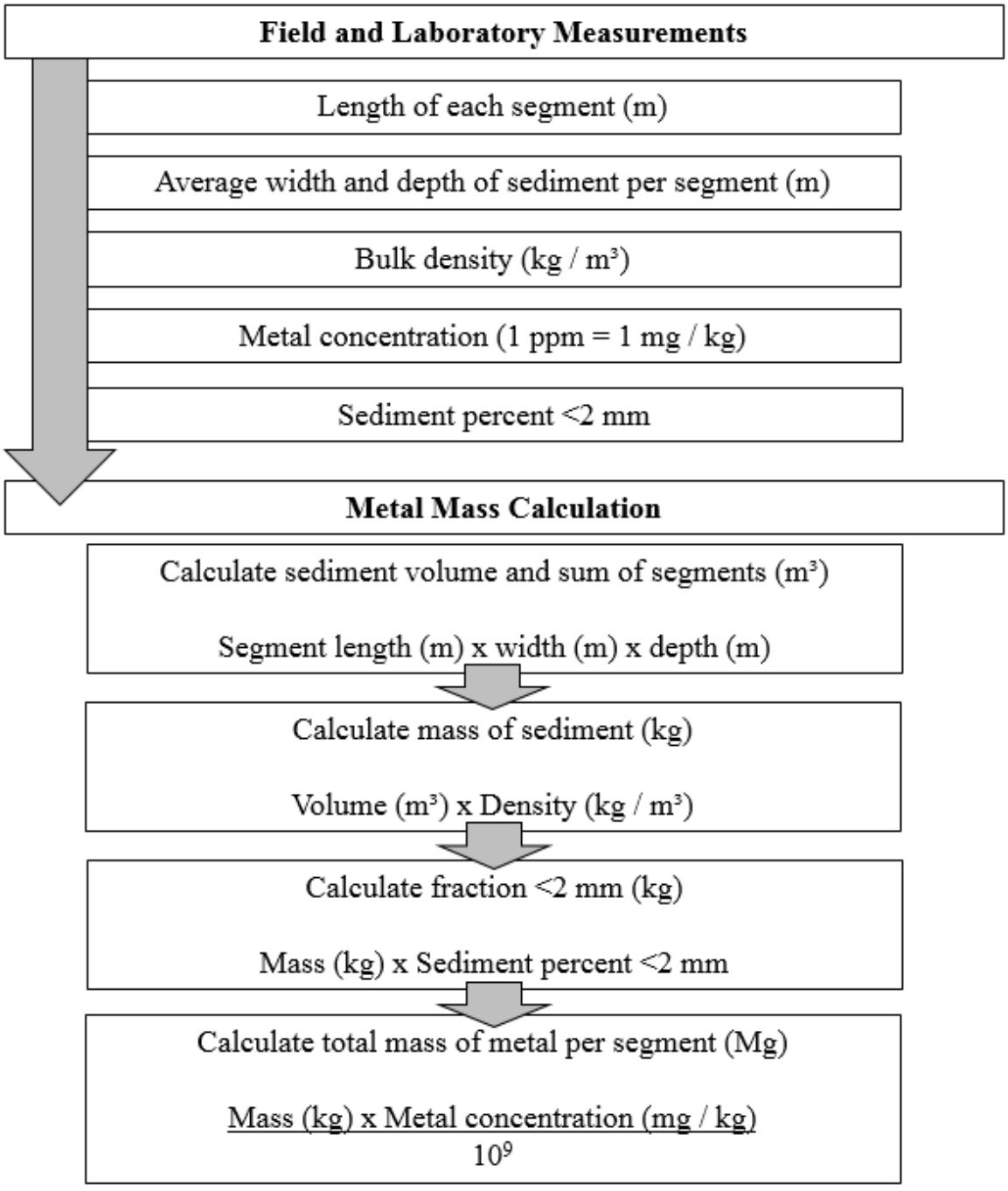

Figure 15. Flow chart of metal mass per segment calculation. Final metal mass per segment can be divided by segment length to obtain metal mass / 1 km. This mass per 1 km can be divided by 10 to obtain metal mass unit storage / 100 m.

loam and Caneyville silt loam soil series. Bulk density range from 1,200 – 1,550 kg / m^3 and 1,350 – 1,600 kg / m^3 respectively (Brown, 1981). An average bulk density value of 1,400 kg / m^3 is used for the metal mass calculations. This value may be considered low for channel bed material.

RESULTS AND DISCUSSION

This chapter describes variations of channel morphology, sediment storage, metal concentrations, and sediment geochemistry along the lower 9.5 kilometers of FRC. First, spatial trends in channel morphology are described including planform, slope, width, and depth. Second, storage analysis relates the type and volume of sediment deposits in FRC to controlling geomorphic and source/supply factors. Third, levels of metal concentrations in channel sediments are evaluated relative to toxic criteria and spatial trends. Final, metal storage analysis is used to calculate the volume and distribution of Pb, Zn, and Ca in contaminated sediment and identify factors that control metal storage patterns.

Channel Morphology Using LiDAR

Downstream variations in active channels, bed, and bar widths are used to quantify planform characteristics of FRC at 100 m increments based on the analysis of high resolution LiDAR data (Appendix A). Recall, active channel width is the sum of the channel bed, active bar, and stable bar width. Downstream trends in active channel width in FRC are influenced by increasing drainage area and by water and sediment inputs below major tributaries. Overall, active channel width trend can be grouped into four zones: increasing downstream from R-km 9 to 5.5, narrowing between R-km 5.0 and 3.2 along the National Pile, increasing again from R-km 3.2 to 1, and moderating below R-km 1.0 in the confluence zone (Figure 16-A).

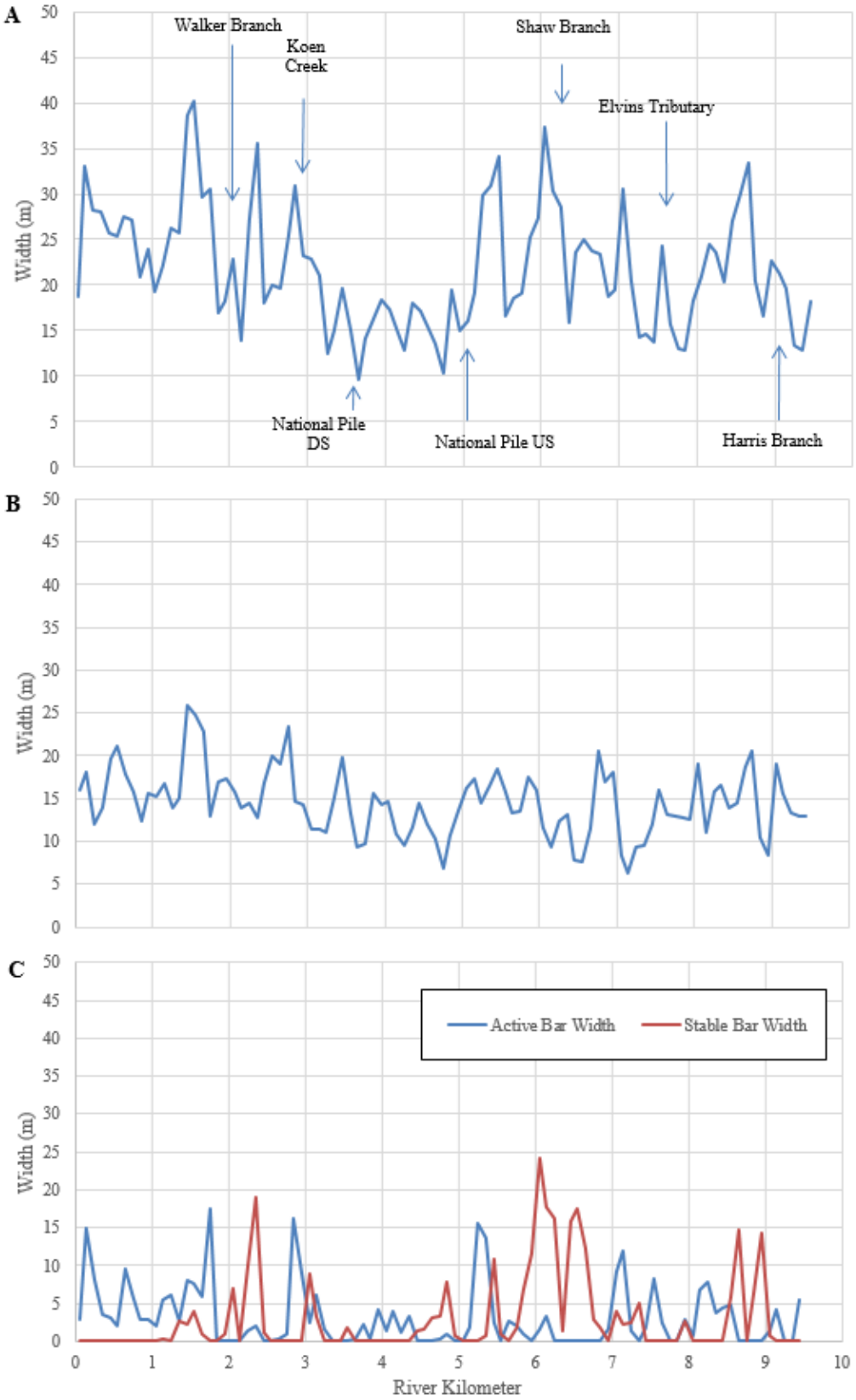

Figure 16. Width for: A- active channel, B- channel bed, and C- bars**.**

Active channel width locally increases downstream of major tributary confluences at Harris Branch, Elvins tributary, Shaw Branch, National Pile upstream and downstream tributaries, Koen Creek, and Walker Branch. Active channel width is very narrow between the National Pile upstream and downstream confluence at R-km 5.0 and 3.2, in the second zone. The narrow channel widths in this zone suggest human modifications to the channel, possibly in concert with remediation of the National Pile. In the third zone, active channel width increases dramatically from 15 m to 30 m (Figure 16-A). The widest section is approximately 500 m downstream of the Walker Branch confluence at R-km 1.5. It is 40 m wide with 25 m of it from channel bed width and the rest from active bars.

Channel bed width trends generally follow those of the same patterns of locally increased width as active channel widths increase. Bed widths range from 10 m to 20 m in zone one, increase from 9 m to 15 m in zone two, and range from 13 m to 25 m in zones three and four (Figure 16-B). This 25 m wide bed is located nearly 200 m downstream of the lower National Pile tributary.

The active and stable bar widths account for the large variation in active channel width (Figure 16-C) in the first zone. Bar widths in general are smaller than channel bed widths, except immediately downstream of major tributary confluences. Stable bar widths are greatest downstream of Shaw Branch, Koen Creek, and Walker Branch tributary confluences (Figure 16-C). Stable bar width is widest at approximately 24 m just downstream of Shaw Branch and the channel bed is only 13 m wide. Active and stable bar widths range between 2 and 7 m in this zone creating the overall narrow active channel. Overall, wider channel and bar widths are associated with tributary inputs.

Active and stable bar widths are generally greatest within 200 m upstream and downstream of major tributaries. Panfil and Jacobson (2001) reported wider active channels in Ozark streams tend to produce greater sediment accumulation in bar deposits.

LiDAR and Field Widths. The LiDAR derived data were compared to field measurements for ground-truthing purposes to evaluate active channel and bed widths acquired by remote-sensing methods (Figure 17 and 18). Overall, there is a positive trend between LiDAR derived width and field measurements with an R^2 of 0.48 for active channel width and 0.27 for channel bed width only. Some sources of variability between the two techniques come from variations in field conditions. Variations in water level at the time of data collection can cause problems accurately identifying the correct active channel width since LiDAR does not penetrate water (Podhoranyi and Fedorcak, 2015). High water levels could hide depositional features or even the base flow edges of the channel. Reaches with low sloping banks and wide active channels can be difficult to accurately identify boundaries. Furthermore, bar deposits near the channel banks, as interpreted by LiDAR evaluation could actually be benches above stable bar elevations and can be misclassified. Comparing the trendline to a 1:1 line shows that LiDAR techniques tend to under-predict wider active channel width. This may result from bank shaded by vegetation or lower bank angles. However, LiDAR over-predicts bed width for narrow channels possibly due to wider water width compared to the actual geomorphic bed with below.

To examine how LiDAR and field widths vary downstream, LiDAR based widths were divided by field widths for active channel and channel bed and plotted over R-km (Figure 19). Ratios for active width average about 1, indicating an overall similarity

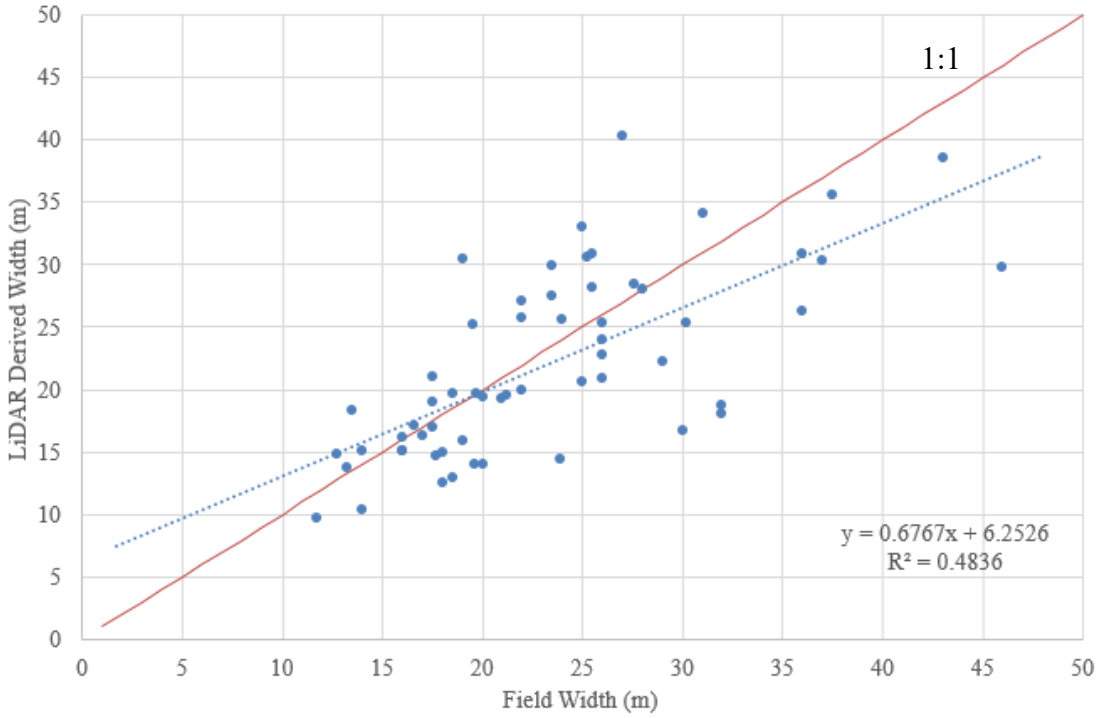

Figure 17. Comparison of LiDAR and field data for active channel width.

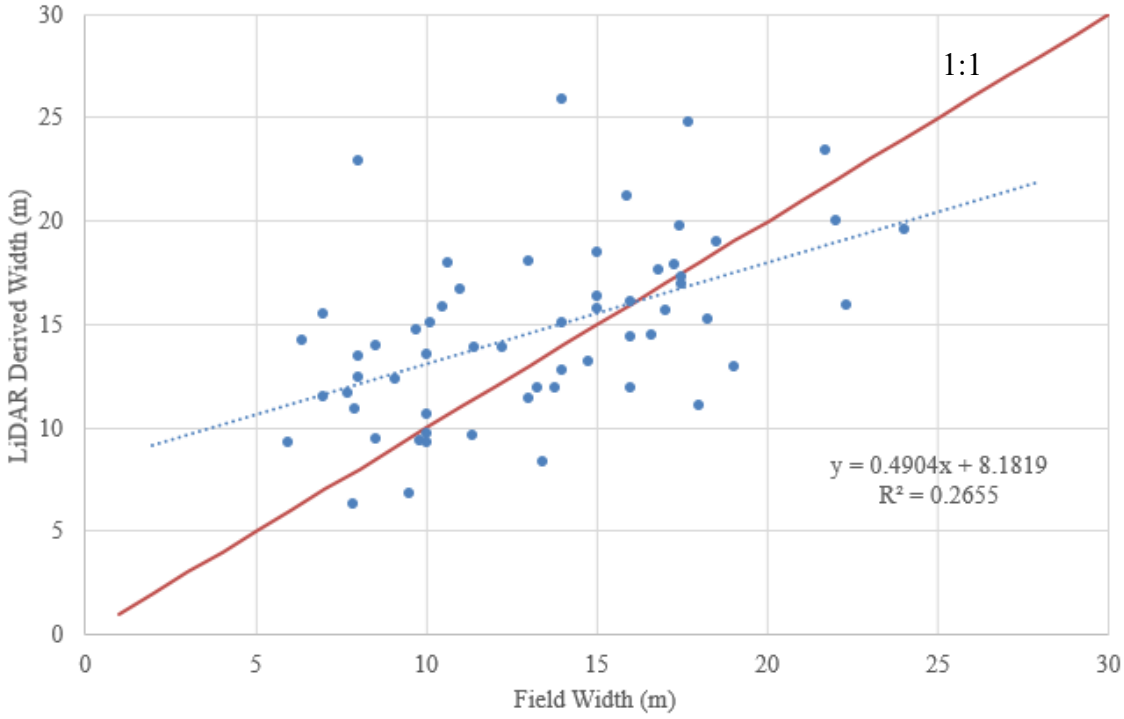

Figure 18. Comparison of LiDAR and field data channel bed width.

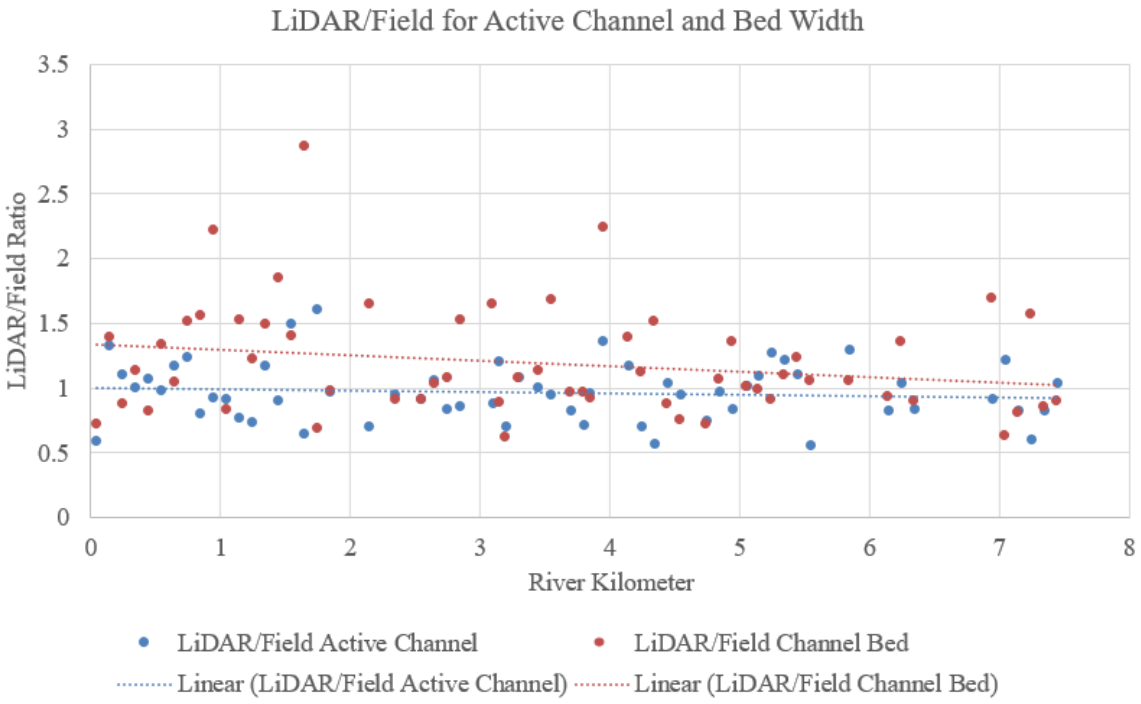

Figure 19. LiDAR/Field ratios for active channel and channel bed width**.**

between the two methods. However, bed width ratios average around 1.1 to 1.3, indicating that water surface widths are wider than active bed width.

Channel slope. High resolution LiDAR data were used to calculate the longitudinal profile and calculate the water surface slope for FRC (Figure 20). Elevations were extracted from the LiDAR every 25 m along the FRC centerline shapefile. LiDAR has limitations to hydraulic studies because of the inability of the near-IR beam to penetrate water surface (Notebaert et al. 2009; Podhoranyi and Fedorcak, 2015), therefore it was assumed the reading would be equivalent to water surface. The resulting longitudinal profile is smoothed out by removing elevations lower than the previous R-km measurement. FRC channel morphology in influenced by bedrock control. Long reaches of exposed bedrock have little sediment storage and are characterized as zones of transport (Owen et al. 2011). The bedrock prevents channel downcutting during periods

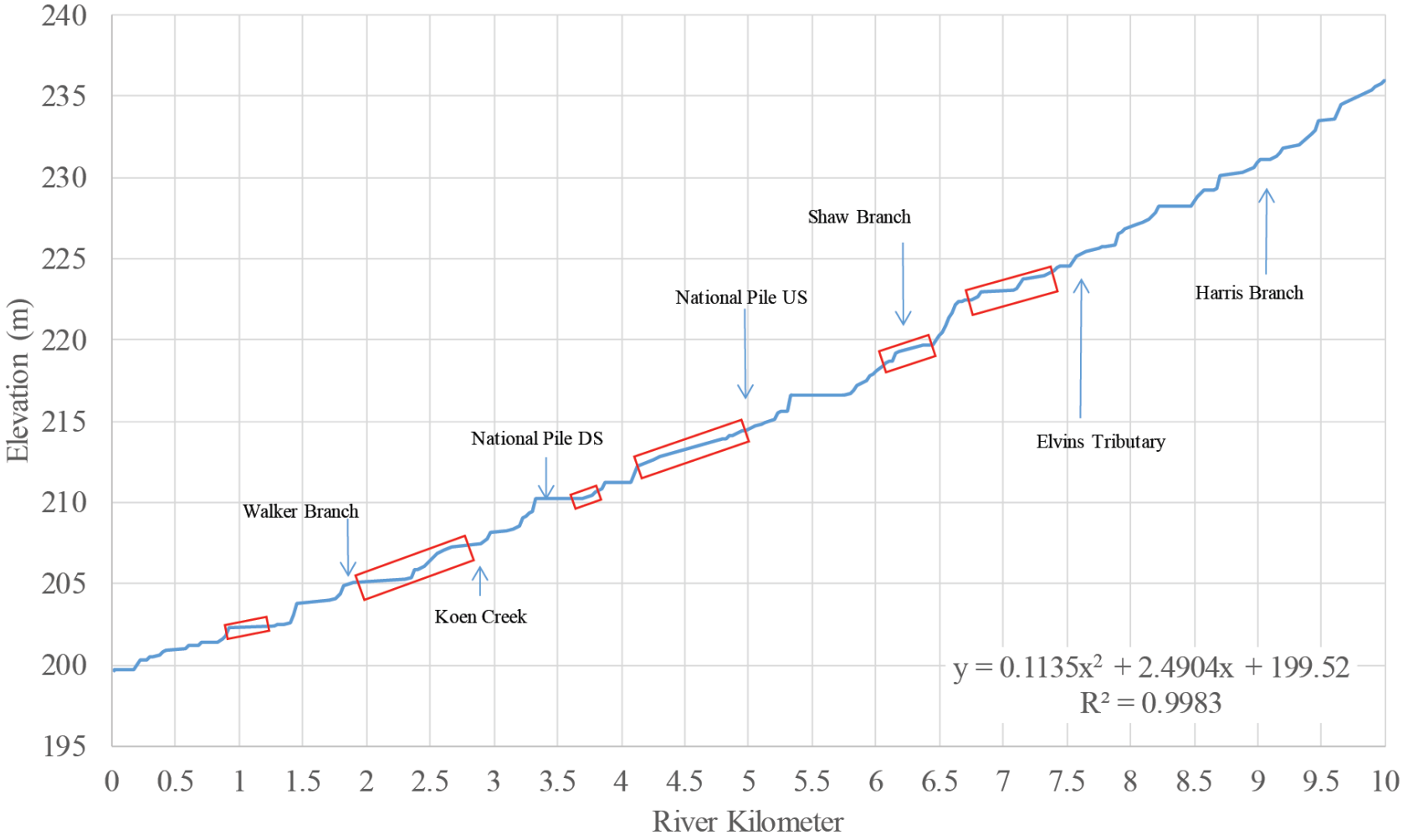

Figure 20. Longitudinal profile of Flat River Creek from LiDAR data. Bedrock dominated reaches are denoted in red.

of higher flow, resulting in a lateral dispersal of energy potentially causing channel widening. During the geomorphic assessment of FRC, reaches with bedrock control were noted. When calculating the average depth component for sediment volume, a 0 was manually entered for longer bedrock reaches to emphasis the effect of bedrock control on sediment storage.

Channel Sediment Storage by Segment

This section analyzes the trends and downstream distribution of sediment in FRC. The average width and depth of channel bed, active bar, and stable bar deposits were multiplied by the segment length to obtain their sediment volume per segment. Each feature was summed for the segment and segments were summed to obtain a total volume of sediment stored in FRC for the study area. Sediment storage was calculated for each segment (Appendix B).

Storage Width and Depth. Average channel bed widths in FRC range from 12 to 18 m by segment (Figure 21-A). Channel bed width generally increases downstream in segments 1 to 5, then becomes relatively narrow in segment 6 and 7, and then widens in segments 8 and 9, and then moderates in segments 10 and 11 creating four different zones, similar to the LiDAR width trends (Figure 21-A). The narrowest average channel bed widths are in segment 3, between the Elvins tributary and Shaw Branch, and segment 6, along the National Pile. The widest average width of 18 m is in segment 9 where Walker Branch flows into FRC.

Channel bed thickness averages generally ranges between 0.06 and 0.38 m among segments, and segment 4 has the smallest average thickness of 0.06 m because of long

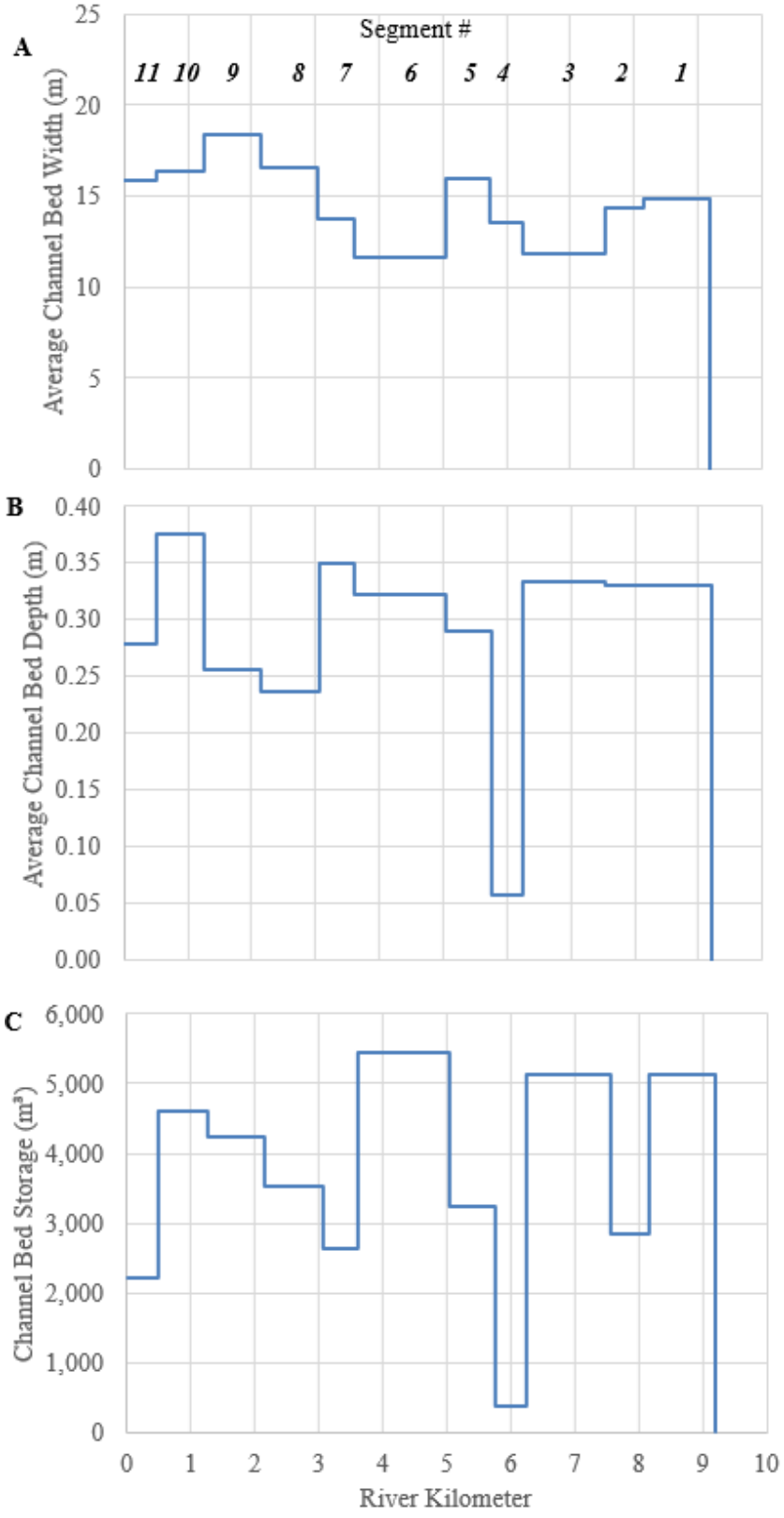

Figure 21. Dimensions for average channel bed: A- width, B- depth, and C- channel bed storage**.**

sections of exposed bedrock on the channel bed, creating a zone of transportation and little sediment deposition (Figure 21-B). Bed thicknesses measurements within a segment coefficient of variation values ranges from 42 to 173 percent (Appendix A). Recall, the average channel bed thickness is calculated by subtracting the average height of sediment found in the channel from the maximum probe depth. High variability can come from non-uniform sediment distribution in the bed sediment at a cross section, or relatively deep maximum probe depths potentially taken from in-filled pools where penetration is variable. Additionally, the low absolute value in thicknesses amplifies the percent variation. However, channel bed thicknesses range between 0.24 and 0.38 m across segments and therefore vary plus or minus 25 percent in general (Figure 21-B).

Average active bar widths by segment vary between 2.3 m and 10.8 m (Figure 22-A). They also follow the similar zone trends with channel bed widths, with an average width of 6 m in the first upstream zone, an overage of 2.5 m in the second zone, 8 m in the third zone, and 9 m in the fourth zone. The widest average active bar width is 10.8 m in segment 11, near the Big River confluence. Within a segment, active bar width coefficients of variation range between 38 and 104 percent.

Average active bar thickness ranges from 0.85 to 1.77 m (Figure 22-B). The thinnest active bars are located in segments 4, 5, 8, and 10, while the thickest are in segment 9. Segment 4 has only one active bar thickness calculation and is not a good indicator of average segment thickness due to small sample size. Coefficients of variation for active bar thicknesses range from 11 to 40 percent. The smallest variation is found in segment 9 and the largest variation is found in segment 11, at the Big River confluence where potential backwash when the Big River floods may cause thicker

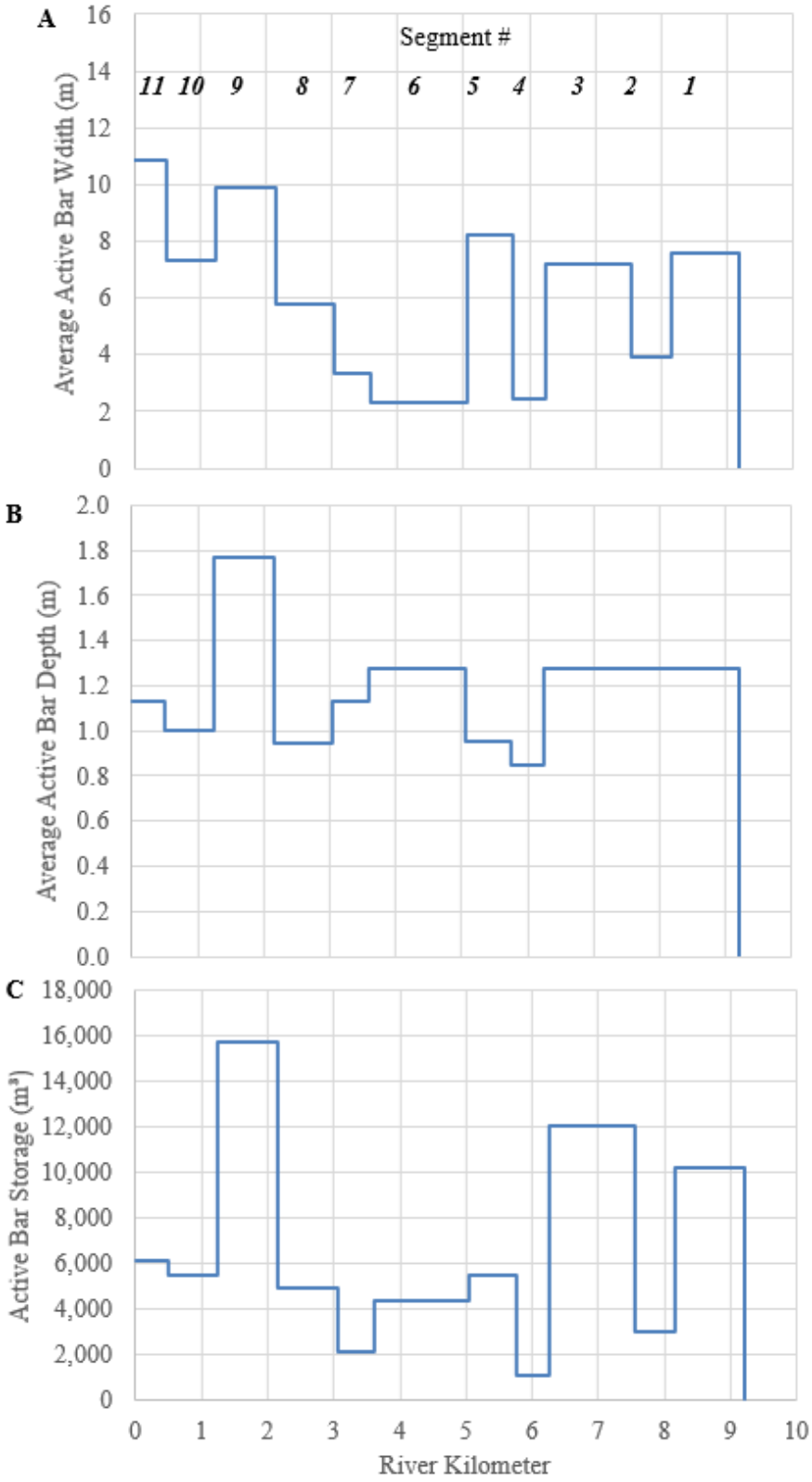

Figure 22. Dimensions for average active bar: A-width, B-depth, and C- active bar storage**.**

deposits. Sediment storage behavior is complex in confluence zones and potentially backwash from the Big River during high flow could explain the high variation in active bar thickness (Knighton, 1998; Wohl, 2014).

Average stable bar widths by segment vary between 4 m and 12 m (Figure 23-A). Segment 10 has one stable bar contribution with an average width of 0.19 m. This width is not representative of the entire segment and is probably the tail end of a stable bar that is centered in the most downstream cell found in the previous segment. Field observations also found very few stable bars in segment 10. Stable bars also exhibit the similar zone trend as channel bed and active bar widths. The average width in zone one is 7 m, zone two is 4 m, zone three is 6 m. The coefficient of variation for stable bar width range from 67 to 137 percent.

Average total stable bar thickness ranges between 0.68 m and 2.2 m (Figure 23-B). There are relatively thicker stable bars in segments 3 to 5 with an average thickness of 1.2 m. Segments 7 and 8 have only one calculation of thickness each, based on field data. Total stable bar thickness coefficients of variation range between 5 to 45 percent. Segment 3 has the largest coefficient of variation, and the average thickness was used for segments 1 and 2 for the thickness component for sediment volume.

The thickness of the fine-grained sediment layer forms the surface of stable bars. The fines thickness coefficient of variation ranges from 0 to 64 percent. Fines thicknesses have a very small range between 0.1 and 0.8 m among segments (Figure 23-B and C). Segment 3 has the highest coefficient of variation in fines with this entire range of fines thicknesses (Figure 23-B).

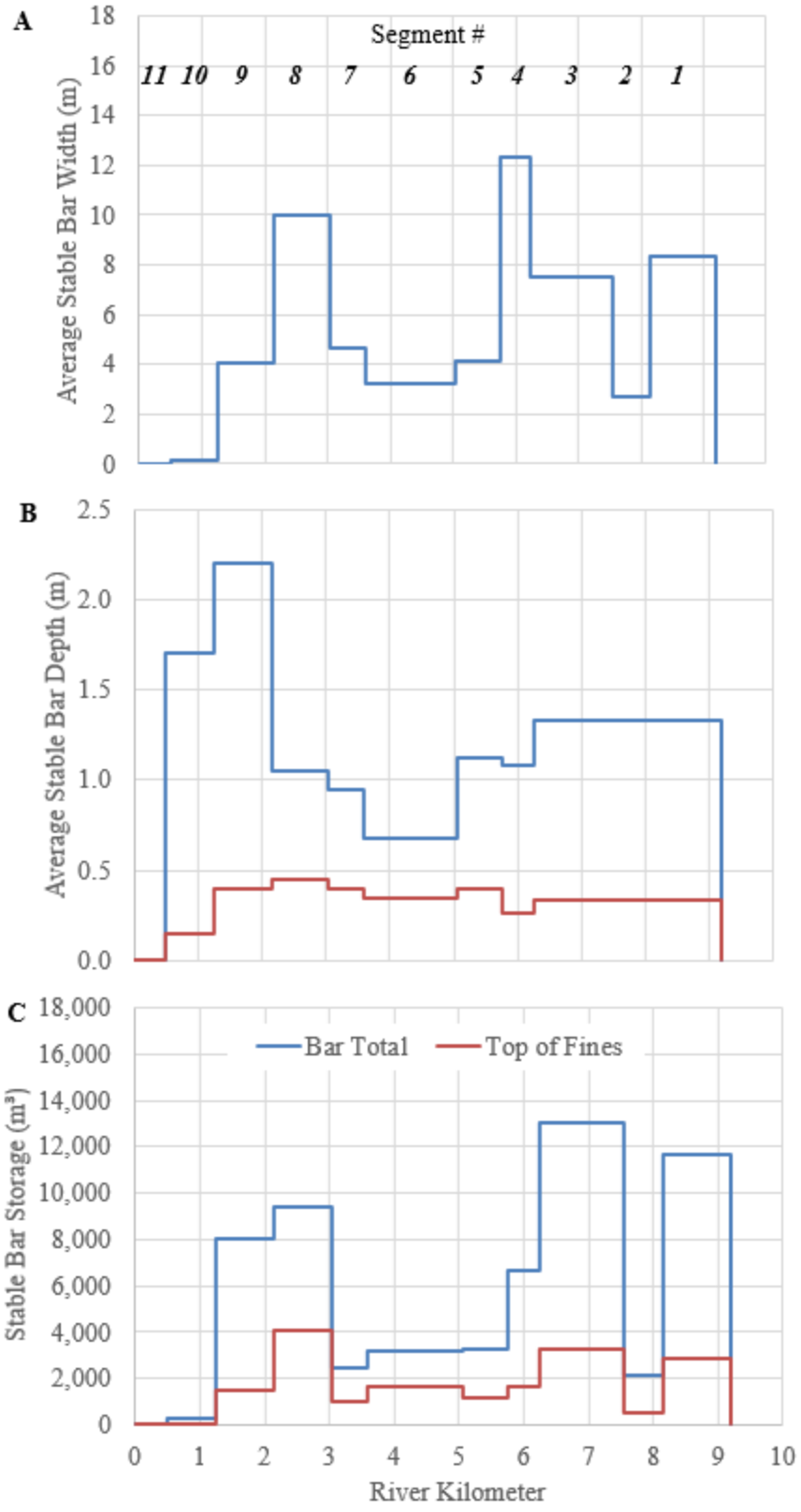

Figure 23. Dimensions for average stable bar: A- width, B- depth, C-stable bar storage.

Storage Volume. There is 170,000 m³ of sediment stored in channel deposits along FRC. Approximately 23 percent are channel bed deposits, 41 percent are active bar deposits, and 35 percent are stable bar deposits (Table 4). Segment total summarizes a volume of sediment stored per segment and the unit storage describes the storage rate per 100 m of river length. The red numbers in sediment storage (%) indicate segments with greater than the average storage for the deposit type (Table 4).

The greatest volume of sediment storage is found in segments 1, 3, and 9. Segment 1 contains sediment input from upstream non-mining sources. Recall the depth component of the storage calculation for segments 1 and 2 is the same as segment 3. Segment 3 contains 15 percent of total storage in active and stable bars. Active bar deposits have the greatest amount of sediment storage and is greatest in segment 9 (Figure 22-C). Sediment loads from Koen Creek and Walker Branch meet the lower channel slope of the FRC main stem and the decrease in velocity causes sediment deposition on the active bars. Segment 9 has 14 percent of total storage in active and stable bars.

Channel bed storage represents the smallest percent of total sediment storage in FRC. Fine-sediment stored in the channel bed is the most readily available to be transported. The greatest channel bed storage is in segment 6 (Figure 21-C) alongside of the National Pile. This segment has a large percent of exposed bedrock, which would indicate low channel bed storage. However, field data (Appendix B) shows the upper half of this segment is primarily exposed bedrock, while the bottom half contains some of the thickest channel bed deposits in FRC. This observation suggests that bedrock control is more influential on sediment storage on the reach scale rather than the segment scale.

Table 4. Percent of total storage by deposit, and sediment storage by total and unit. Red numbers indicate segments with greater than average storage.

	Sediment Storage (%)					Sediment Storage	
Segment	Channel Bed	Active Bar	Stable Bar Total	Segment Total (%)	Stable Bar Fines Only (%)	Total (m^3)	Unit (m^3 / 100 m)
1	**3.0**	**6.0**	**6.9**	**15.9**	**1.7**	27,020	2,573
2	1.7	1.8	1.3	4.7	0.3	8,010	1,335
3	**3.0**	**7.1**	**7.7**	**17.8**	**1.9**	30,174	2,321
4	0.2	0.6	**3.9**	4.8	**1.0**	8,095	1,619
5	1.9	3.2	1.9	7.1	0.7	11,998	1,714
6	**3.2**	2.5	1.9	7.6	**1.0**	12,972	895
7	1.5	1.2	1.4	4.2	0.6	7,157	1,301
8	2.1	2.9	**5.6**	**10.5**	**2.4**	17,861	1,985
9	**2.5**	**9.2**	**4.7**	**16.4**	0.9	27,925	3,103
10	**2.7**	3.2	0.1	6.1	0.0	10,359	1,381
11	1.3	3.6	0.0	4.9	0.0	8,338	1,668
Average:	2.1	3.8	3.2	9.1	0.9		
Sum:	23.2	41.4	35.4	100	10	169,909	

The distribution of total sediment storage is greatest in the upper mining segments 1 to 3 and downstream non-mining segments 8 to 11 and is the lowest in segments 4 to 7 (Figure 24-B). Comparing the average unit storage between these three sections confirms this distribution (Figure 24-A). There is a greater amount of average unit sediment storage in the upstream mining segments 1 to 3 at approximately 2000 m^3 / 100 m. Average unit storage in segments 4 to 7 is approximately 1400 m^3 / 100 m. Average unit storage for the downstream non-mining segments is approximately 1900 m^3 / 100 m.

Fine Sediment Trends. This study evaluates metal storage for only the <2 mm sediment fraction. Therefore, the volume of <2 mm sediment in each deposit and segment must be determined. The error bars project the ninety-five percent confidence interval, where sufficient sample size allow (i.e. $n \geq 2$). Segments where sample size was

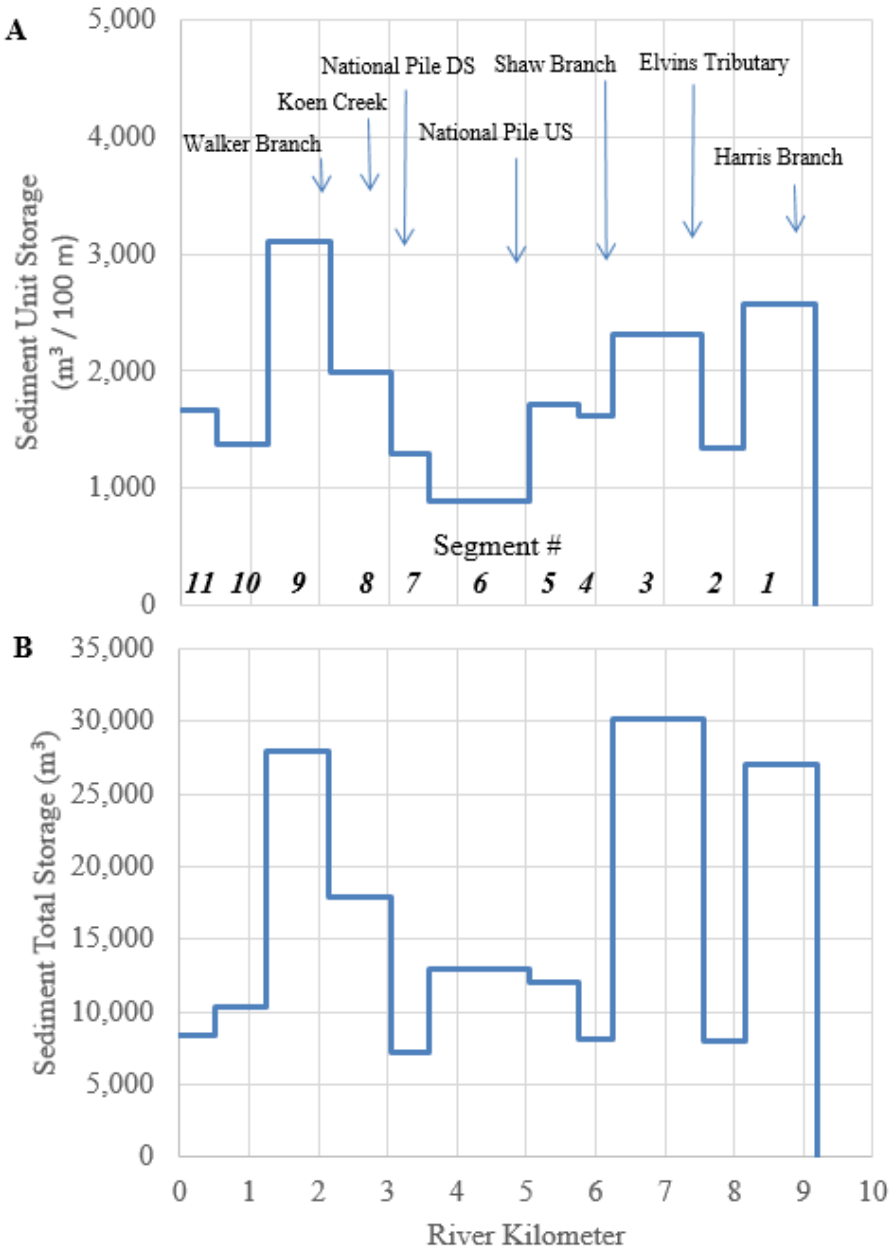

Figure 24. Sediment storage by: A-unit storage and B- total storage by segment.

insufficient (i.e. n = 1) error bars were not included, since a single value was used to select the average segment value. For segments containing no sediment sampling, the average value for the segments upstream and downstream were used for storage calculation, but are not plotted in figures.

Channel bed sediment is relatively coarse in the upstream mining reaches in segments 1, 2, and 3 (Figure 25). This sediment load comes primarily from the non-mining influence above the study area. Segment 4 appears to be affected by fine sediment input from Shaw Branch. The next relatively fine sediment input is in segment 8 (Figure 26) where Koen Creek supplies sediment from its relatively large drainage area. Channel bed sediment approximately thirty percent fines from Koen Creek to the Big River confluence.

Bars remain relatively fine in the mining segments. Active bars shows coarser sediment sizes in segment 3 below the Elvins tributary (Figure 26). Similarly, bars receive large amounts of fine sediment in segment 4 from Shaw Branch and gradually coarsen through segments 5, 6, and 7, until an influx of fine sediment from Koen Creek in segment at for the active and stable bars. Sediment mixes and gradually coarsens from 80 percent fines in segment 8 to 40 percent fines downstream towards the Big River confluence in segments 10 and 11 for all deposits.

Fine Sediment Storage. The calculated sediment volume for each sediment deposit per segment was multiplied by its corresponding segment percent <2 mm fraction (Figure 27). There is a total of 93,800 m^3 of fine sediment stored in FRC, which is approximately half of total sediment stored (Appendix C). There is 44 percent fine sediment stored in active bar deposits, 42 percent stored in stable bar deposits and 14 percent in channel bed deposits (Table 5). The storage patterns within a segment and longitudinally between segments are very similar to total sediment storage (Figure 24-B and 27-B). Fine sediment less than 2 mm in diameter is very easily entrained under high flow conditions and the decreasing trend could reflect the continued downstream

transport of fines as various tributaries contribute sediment and water to the FRC main stem (Graf, 1997; Knighton, 1998; Wohl 2014).

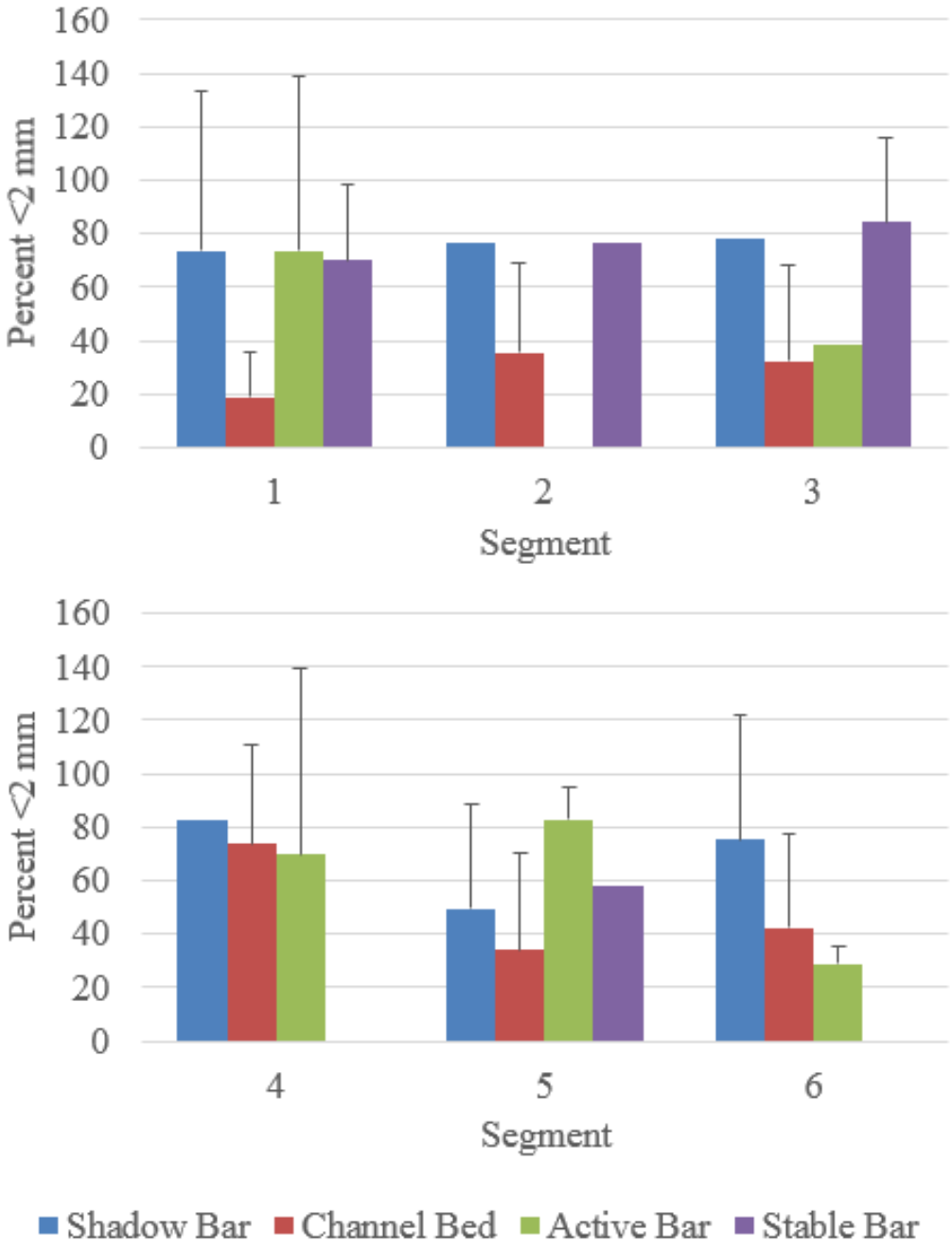

Figure 25. Percent less than 2 mm in channel bed, active bar, stable bar, and shadow bars in segments 1-6. Error bars represent 95th confidence interval. Lack of error bars denote n = 1.

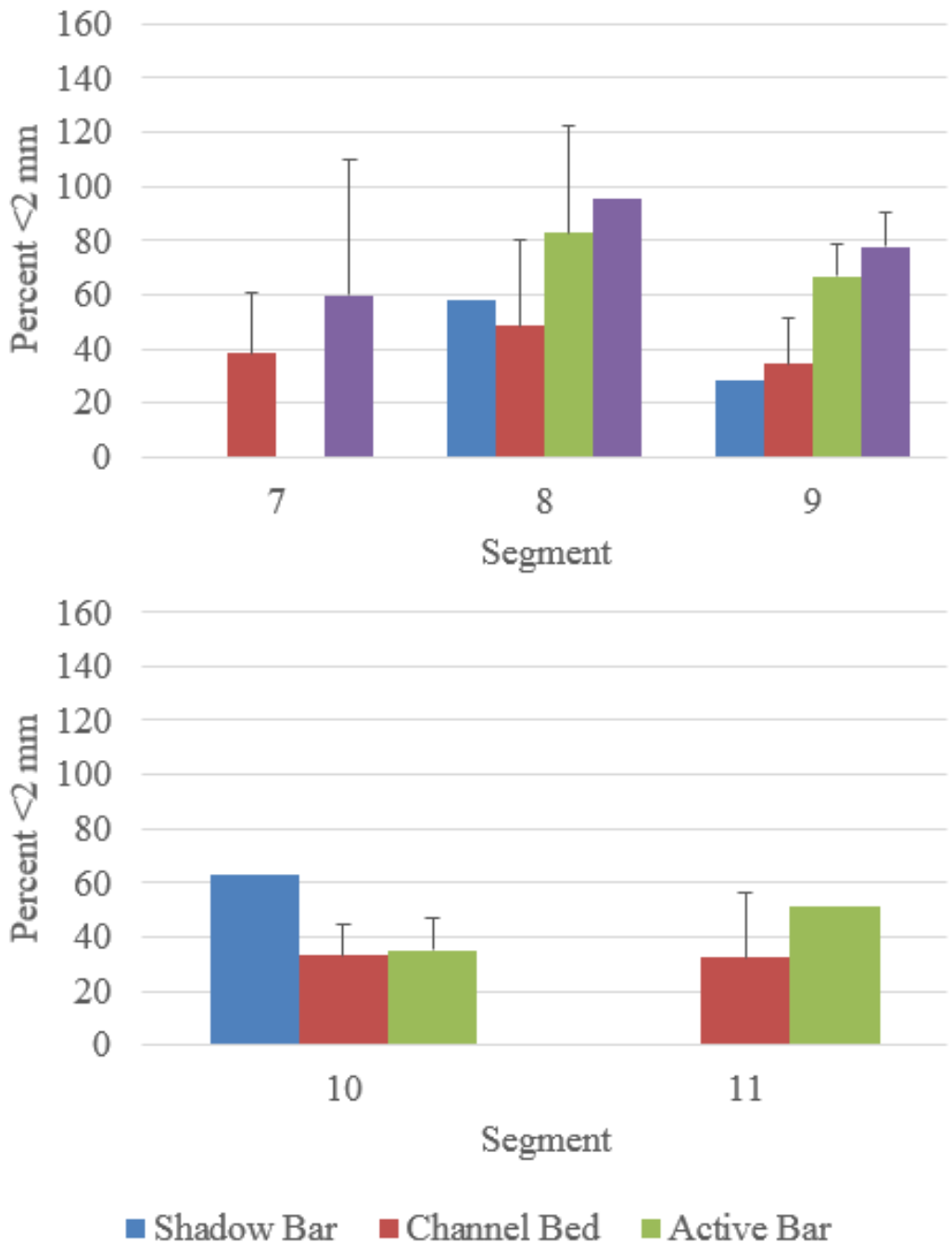

Figure 26. Percent less than 2 mm in channel bed, active bar, stable bar, and shadow bars in segments 7-11. Error bars represent 95th confidence interval. Lack of error bars denote n = 1.

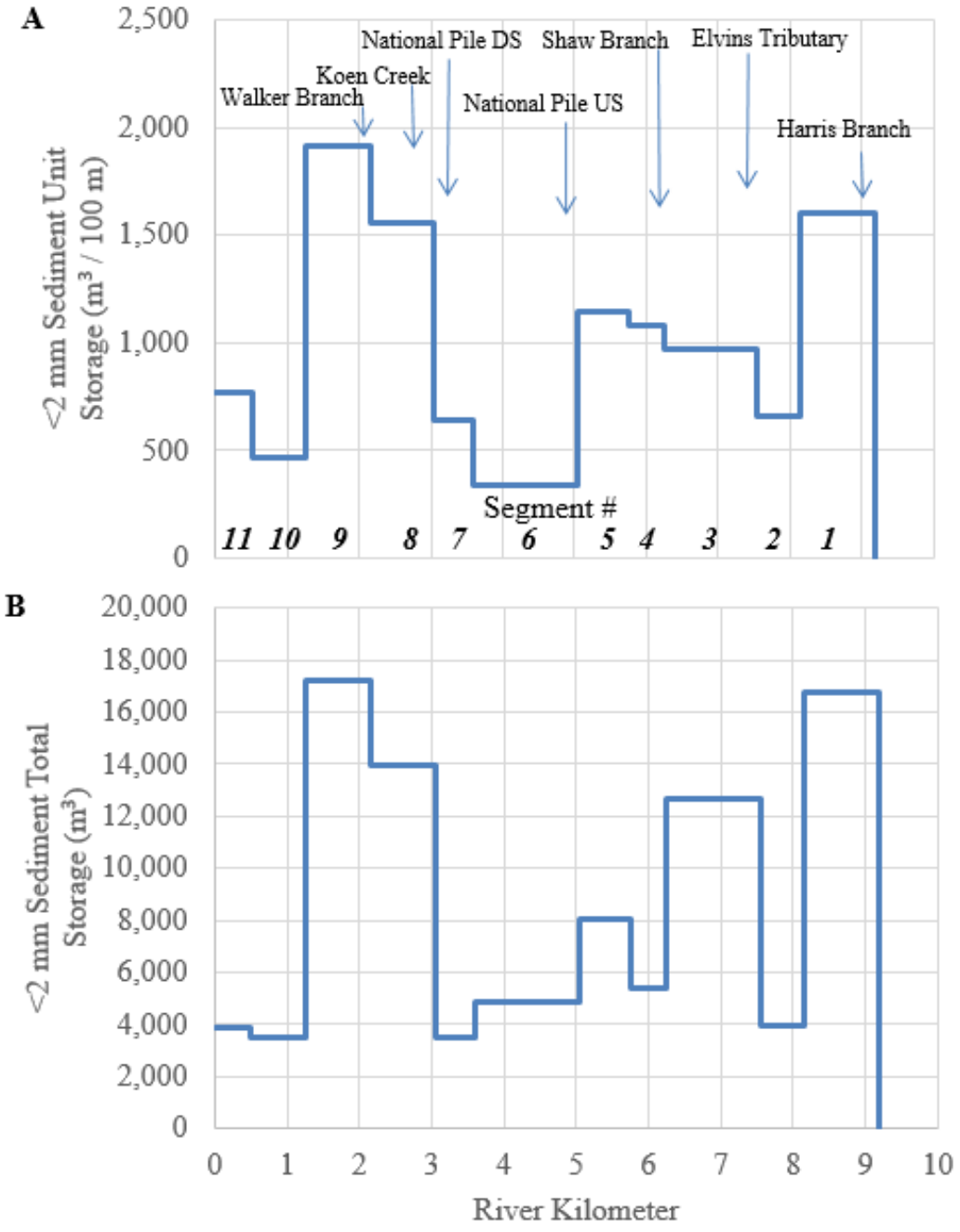

Figure 27. Sediment storage by A-unit storage and B- total storage by segment in the fine <2 mm fraction.

Table 5. Fine sediment percent of total storage by deposit and sediment storage unit. Red numbers indicate segments with greater than average storage.

	Fine Sediment Storage (%)					Sediment Storage	
Segment	Channel Bed	Active Bar	Stable Bar Total	Segment Total (%)	Stable Bar Fines Only (%)	Total (m^3)	Unit (m^3 / 100 m)
1	1.0	**8.0**	**9.0**	**17.9**	**2.1**	16,784	1599
2	1.1	1.8	1.4	4.2	0.4	3,948	658
3	**1.7**	**4.9**	**6.9**	**13.5**	**2.9**	12,644	973
4	0.3	0.8	**4.7**	5.8	1.0	5,404	1081
5	1.1	**4.9**	2.6	8.6	0.7	8,038	1148
6	**2.4**	1.3	1.5	5.2	1.0	4,891	337
7	1.1	1.2	1.5	3.8	0.6	3,530	642
8	**1.8**	**4.3**	**8.8**	**14.9**	**4.1**	13,971	1552
9	**1.5**	**11.1**	**5.8**	**18.4**	1.2	17,237	1915
10	**1.6**	2.1	0.1	3.7	0.0	3,496	466
11	0.8	3.3	0.0	4.1	0.0	3,843	769
Average:	1.3	4.0	3.8	9.1	1.3		
Sum:	14.4	43.5	42.1	100	14	93,787	

Metal Storage by Segment

This section evaluates metal concentrations, their downstream variations, background levels, and variations of metal concentrations with depth in bar deposits. Sediment geochemistry data is known to have a lognormal distribution (Ahrens, 1954; Reimann and Filzmoser, 2000; Singer, 2013). The geometric mean of metal concentrations was used to determine average Pb and Zn storage in each deposit type by segment.

Metal Concentrations. Any location that is mineralogically abundant will have metal concentration levels that are considered normal or background for that location. Therefore, any observations that are above background are of scientific interest.

Background Metal Concentrations in Sediment**.** Previous studies (Smith and Schumacher, 1991; Gale et al. 2004; Pavlowsky et al. 2010) have reported average background Pb and Zn concentrations collected above mining influenced segments (Table 6). Smith and Schumacher (1991) and Gale et al. (2004) analyzed the <180 um sediment size fraction, used acid digestion methods to extract the metal, and performed the analysis using an Inductivly Coupled Plasma-Mass Spectrometer. Pavlowsky et al. (2010) collected channel bed sediment and analyzed the <2 mm fraction using the same XRF device as this study.

More background studies are needed but background is clearly below the PEC. Fourteen sediment samples from active bars and glides upstream of known mining influence were collected for this study to determine background Pb, Zn, and Ca concentrations (Table 7). One sample from the Banister Branch segment had 265 ppm Pb, 191 ppm Zn, and 21,542 ppm Ca. The remaining 4 samples in Banister Branch averaged to 41 ppm Pb, 30 ppm Zn, and 8,808 ppm Ca. The Banister Branch coefficient of variation is therefore very high for Pb and Zn. Overall, approximately < 50 ppm Pb, < 40 ppm Zn, and <17,000 ppm Ca can be considered average background concentrations above mining influence in FRC.

Table 6. Summary of average background Pb and Zn concentrations in previous studies.

Study	Size Fract.	Pb (ppm)	Zn (ppm)	Extraction Method
Smith and Schumacher 1991	<180 um	180	100	Hydroflouric, Nitric, Perchloric Acid Digestion
Gale et al. 2004	<180 um	64	147	Nitric and Hydrochloric Acid Digestion
Pavlowsky et al. 2010	<2 mm	50	29	XRF

Table 7. Summary of upstream sediment sampling above mining influence.

			Pb			Zn			Ca		
R-km	Location	n	Avg	Std	Cv%	Avg	Std	Cv%	Avg	Std	Cv%
9.21	Above Harris Branch	4	74	23	31	51	9	18	26,236	17,668	67
10.42	Banister Branch confluence	5	86	101	117	62	72	116	11,355	6,394	56
12.82	Below Rt. 32 Bridge	5	42	8	18	34	11	31	16,658	9,962	60
	Average concentration:		67			49			18,083		

Sediment Metal Concentrations**.** A total of 103 sediment samples were collected from the lower 9.5 km of the study area (Appendix D). Of the 103, all samples are contaminated above the PEC of 128 ppm for Pb (MacDonald et al., 2000) except for 6. These six individual non-contaminated samples are found between R-km 9.5 and 8.0, above Elvins. These sample concentrations are affected by dilution form upstream background sediments. There are 29 samples that are below the PEC threshold of 459 ppm for Zn, and can be found in all segments of the study area. These PEC thresholds are for aquatic organisms.

All sediment deposits averaged together by type are contaminated. Active bar deposits across all segments have the greatest arithmetic average Pb concentration of 2,247 ppm. Stable bars, shadow bars, and channel bed deposits have average Pb concentrations of 1,540, 1,460, and 1,331 ppm, respectively. Channel bed deposits across all segments have the greatest arithmetic average Zn of 3,037 ppm, with stable bars next at 1,369 ppm, and then active and stable bars with 755 and 675 ppm, respectively.

The geometric mean of metal concentrations by deposit type in segments were calculated and plotted similarly to the percent <2 mm sediment size (Figure 28 and 29). The error bars project the ninety-five percent confidence interval, where sufficient sample size allow (i.e. $n \geq 2$). Segments where data was insufficient (i.e. n equals 1) error bars were not included. Metal concentrations for segments with no samples were estimated using the average values upstream and downstream were used for the metal storage calculation, but are not plotted.

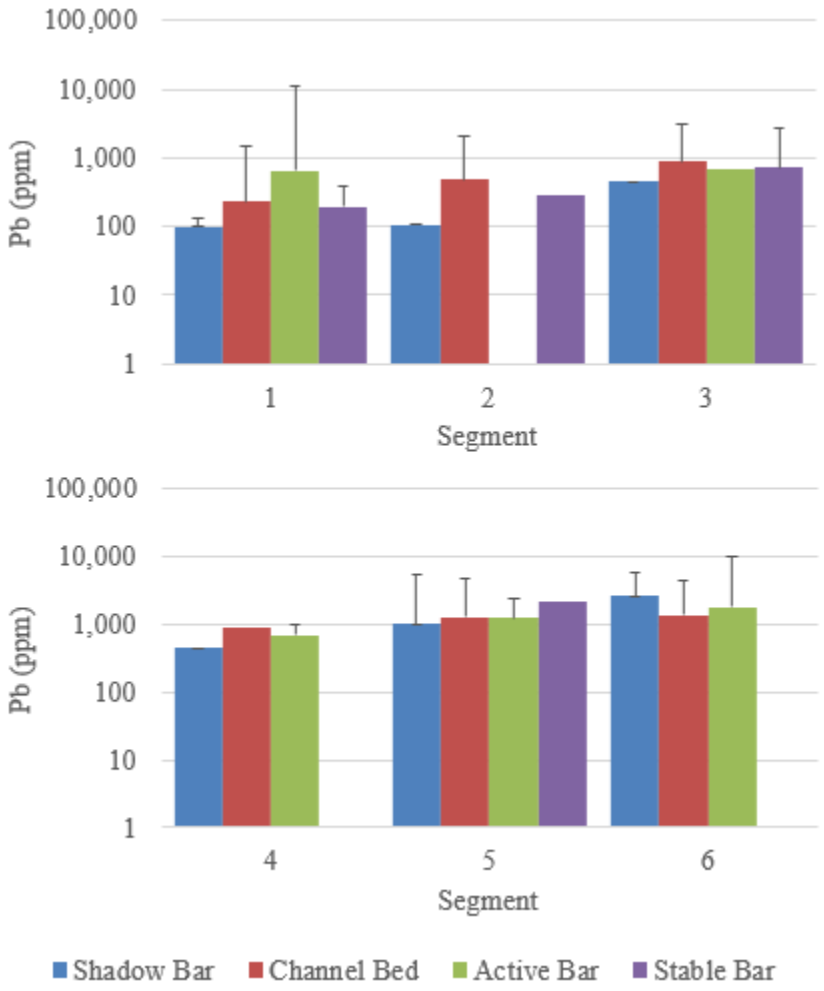

Figure 28. Variations in Pb concentration by deposit type in segments 1-6. Error bars represent 95th confidence interval. Lack of error bars denote n = 1.

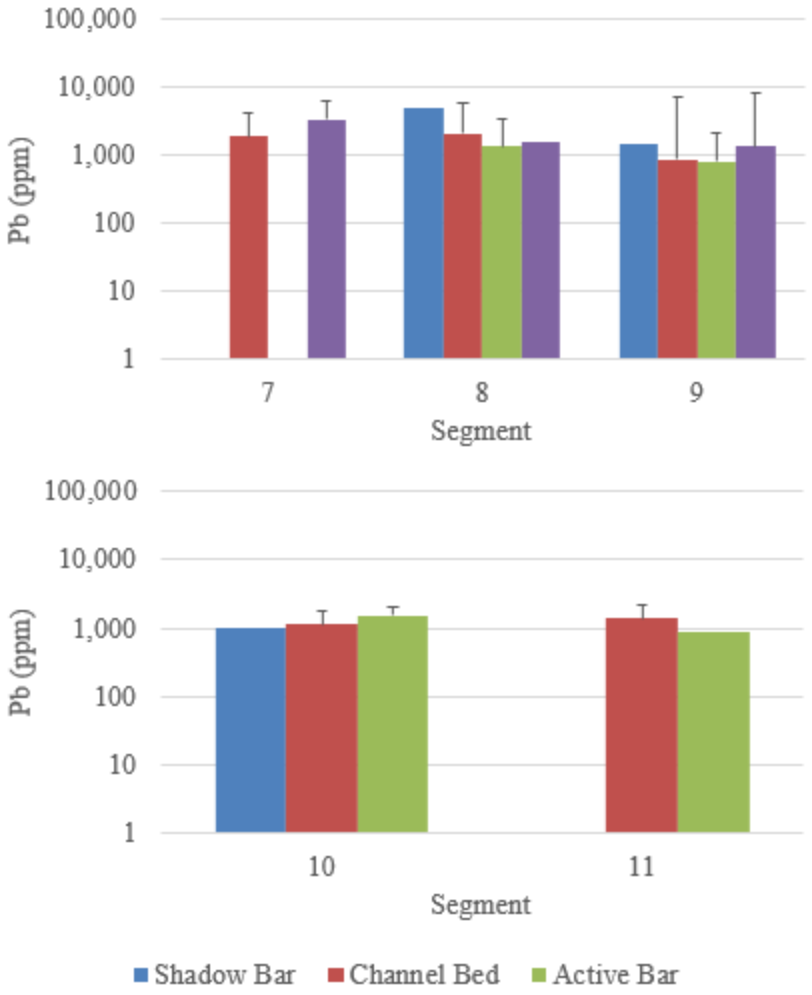

Figure 29. Variations in Pb concentration by deposit type in segments 7-11. Error bars represent 95th confidence interval. Lack of error bars denote n = 1.

Lead and zinc concentrations show little variation between different deposits by segments in FRC since the average concentration of one deposit is usually within the ninety-five percent confidence interval of other deposits. Channel bed deposits have the highest average Pb concentration in segments 2, 3, 4, and 11 (Figure 28 and 29). Channel bed sediments are relatively easily to mobilize during higher discharges and represent a sediment source readily available for transport (Lewin and Macklin, 1987).

Zinc concentration trends mimic Pb trends in all segments except for segments 4 and 10 (Figure 30 and 31). Zinc is marginally higher than Pb in channel bed deposits in segment 4. Additionally, shadow bars in segment 10 have a greater concentration of Zn than active bars and channel bed compared to Pb. Shadow bars in segment 10 have the lowest Pb values (Figure 29). Both Pb and Zn concentrations are greatest in channel bed deposits in segment 2 with 618 for Pb and 3,658 for Zn, with the exception that Zn is an order of magnitude higher than Pb. Segment 2 ends at the confluence of the Elvins tributary, however fluvial processes in confluence zones could have deposited some sediment upstream. Sediment is deposited upstream of confluences in stagnation zone where flow velocity from the tributary encounters the wider channel and shallower slope of the main stem (Wohl, 2014).

The host rock found in FRC is the Bonne Terre Dolomite with a chemical formula of $CaMg(CO_3)_2$ (Smith and Schumacher, 1991; 1993). The Ca abundance in dolomite (i.e. pure tailings) is 21.7 percent by molecular weight. Sediment containing Ca concentrations near 217,000 ppm are therefore assumed to be composed of 100 percent tailings material. Ca concentrations vary between 14,704 ppm and 111,742 ppm in deposits found in segments 1, 2, and 3 with active bar segments having higher concentrations (Figure 32 and 33). The average concentration of each deposit are within the confidence interval of the others. Concentrations in all sediment deposits are around 100,000 ppm Ca in segments 6 to 11. The one exception is segment 9 where concentrations across all deposits slightly decrease, due to dilution from uncontaminated sediment from Walker Branch. Concentrations rise again to 100,000 ppm in segments 10 and 11 (Figure 33).

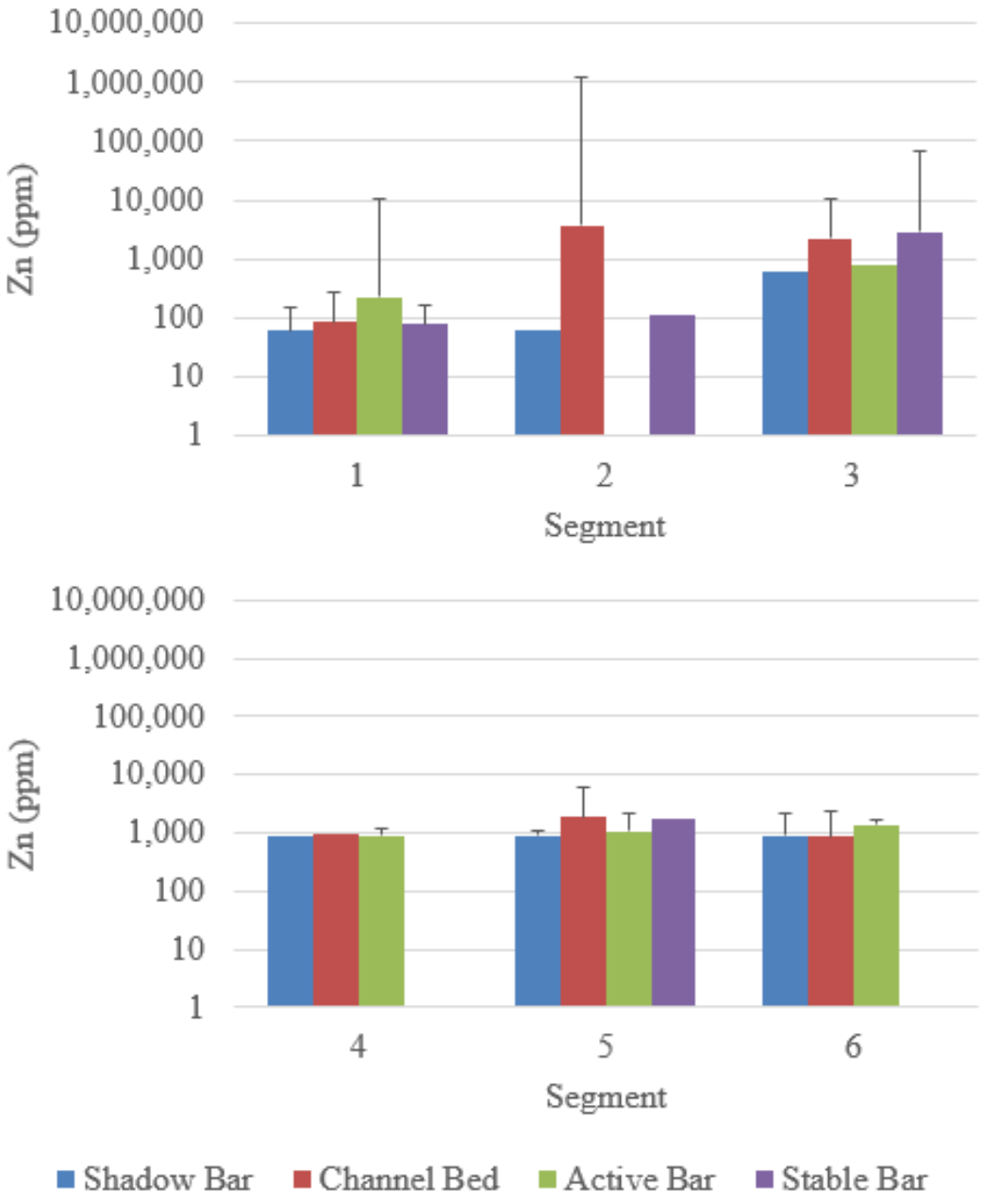

Figure 30. Variations in Zn concentration by deposit in segments 1-6. Error bars represent 95th confidence interval. Lack of error bars denote n = 1.

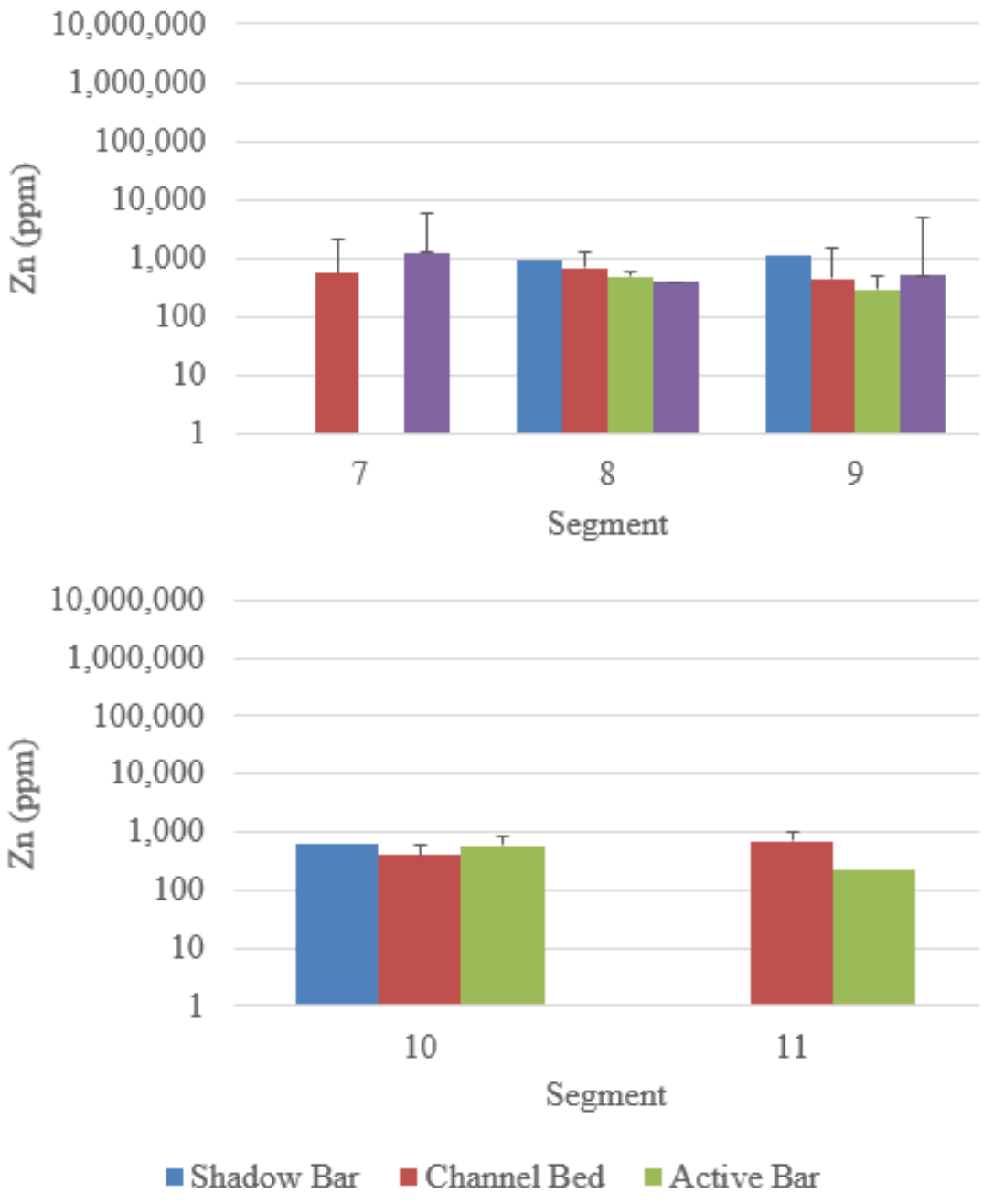

Figure 31. Variations in Zn concentration by deposit in segment 7-11. Error bars represent 95th confidence interval. Lack of error bars denote n = 1.

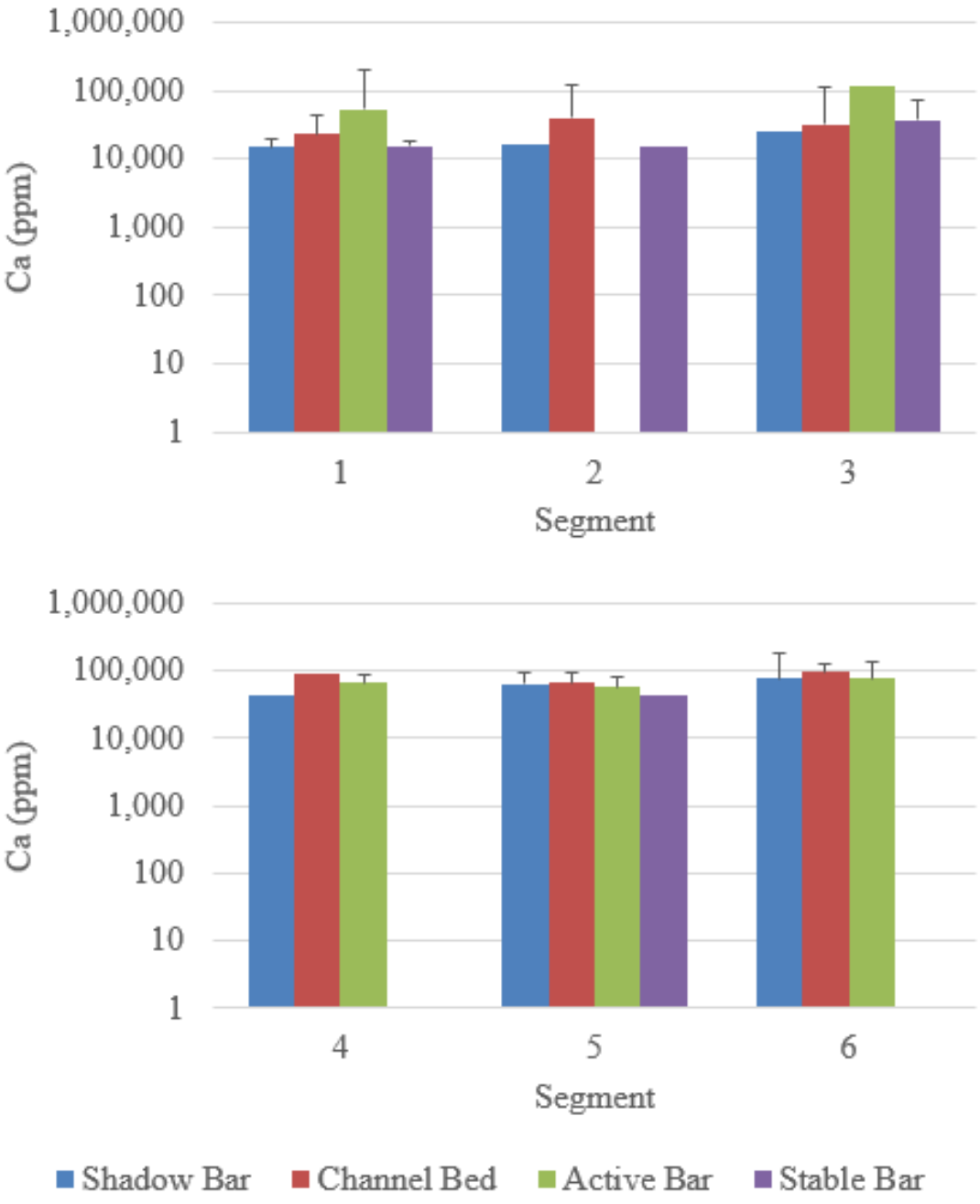

Figure 32. Variations in Ca concentrations by deposit type in segments 1-6. Error bars represent 95th confidence interval. Lack of error bars denote n = 1.

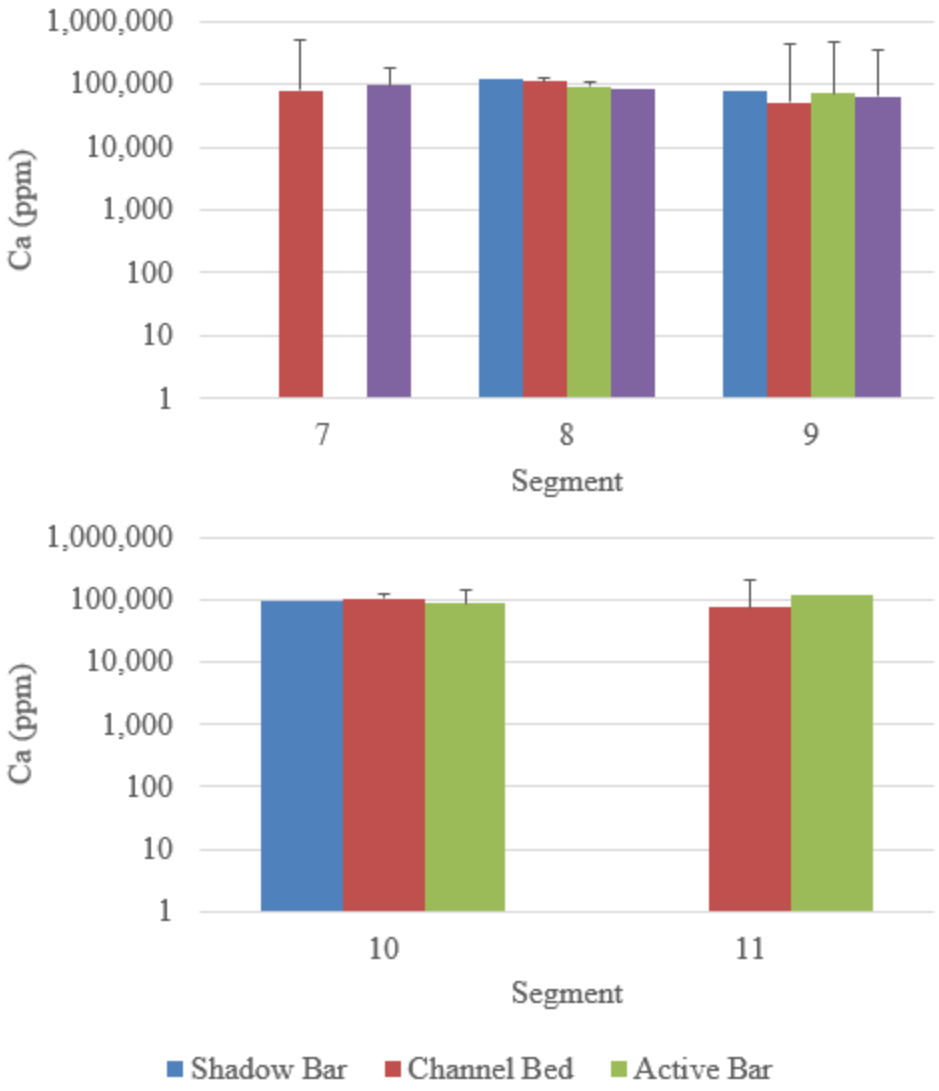

Figure 33. Variations in Ca concentrations by deposit type in segments 7-11. The white dot denote n = 1.

Metal Concentration Trends by Segment**.** Sediment sample concentrations for each metal were averaged together by segment and geomean plotted against river kilometer to reveal the downstream trends in metal concentration (Figure 34). These averaged values were not used for the metal storage calculations and are only used to describe overall longitudinal metal concentration trends. All metal concentrations rise

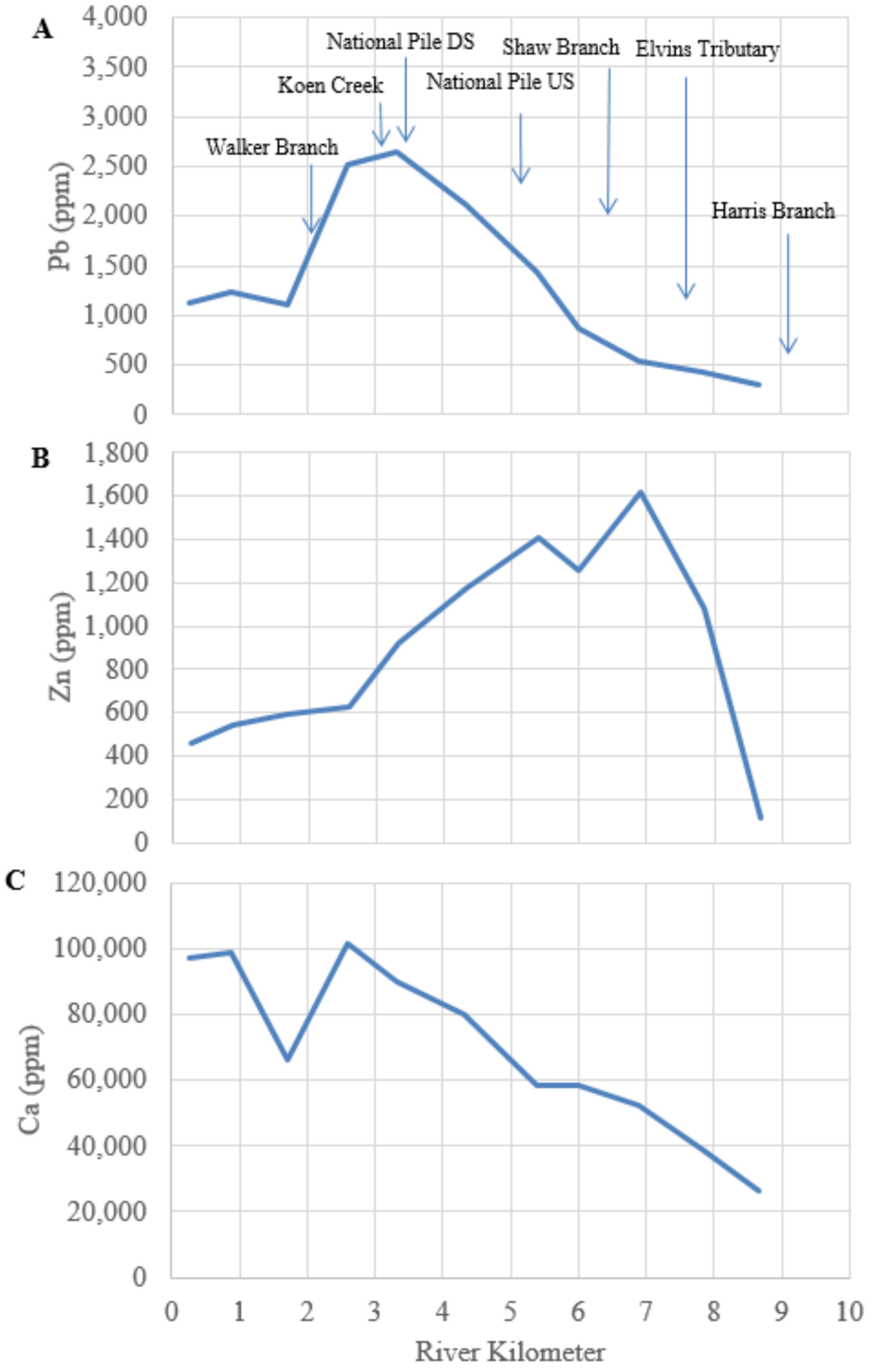

Figure 34. Metal concentration trends for: A- Pb, B- Zn, and C- Ca, by River Kilometer.

sharply past Harris Branch and the Elvins tributary indicating the most upstream source of contaminated tailings and other mine discharge to FRC.

Lead concentrations (Figure 34-A) continue to increase downstream through the mining affected area to peak at 2,600 ppm Pb and then sharply fall past Koen Creek and Walker Branch due to dilution by cleaner sediment. Pb concentrations are highest between R-km 5 and 3 which are just downstream of the National Pile and in segments 8 and 9. Smith and Schumacher (1993) noted the stream bed downstream of the National Pile was composed entirely of sandy mill tailings which can be indicators of Pb contamination.

Zinc concentrations (Figure 34-B) rises sharply with input from the Elvins tributary to 1,600 ppm Zn and then a secondary spike past Shaw Branch at 1,400 ppm Zn. The secondary Zn peak below Shaw Branch could be a combination of additional Zn from the Federal Pile and the movement of sediment from the Elvins Pile tributary confluence at R-km 7.6. Zn concentrations gradually decrease downstream from the source to 450 ppm Zn at the Big River confluence.

Calcium concentration (Figure 34-C) steadily increases downstream with a sharp decrease after the Walker Branch confluence, again due to dilution. Similarly consistent with Smith and Schumacher (1993) channel bed sediments were composed of tailings, just downstream of the National Pile. High Ca concentrations between R-km 4 and 2 could indicate the presences of these observed tailings sediments.

Bar Core Sediment Sampling. An assumption of this study is that metal concentrations in the bar and bed samples collected from 0 to 30 cm depths are representative of average concentrations for the entire depth of the deposit. Bar core

sampling provides metal concentration information with depth to verify this assumption. If metal concentrations vary with depth, then storage calculations would be biased by the near surface samples used in this study. However, if concentrations do not vary with depth, then the samples collected are assumed to be representative of the entire deposit. Bar core samples were collected from active and stable bars within the study area that were at least one meter in height. Bar pits ranged from 0.4 to 0.7 m in depth and samples were collected in 10 cm intervals before hitting the water table. Bar cores were collected at six locations at R-km 7.2, 6.0, 5.8, 4.25, 1.68 and 1.3.

Evaluating the coefficient of variation or the comparing the ratio of the top and bottom samples of the core are two different methods for evaluating contamination trends with depth. The coefficient of variation method assumes variation less than 30 percent of metal concentrations for a core would be representative and within the limits of variability around a mean concentration. The ratio method involves calculating the arithmetic average of metal concentrations in the top two samples divided by the average of the bottom two samples of the core. Values greater than one indicate the top is more contaminated than the bottom, while values less than one are the opposite. Values close to one would represent that contamination does not vary systematically with depth.

All core samples collected were above the PEC threshold of 128 ppm for Pb and above the PEC of 459 ppm for Zn (Table 8). The lowest observed Pb concentration was 496 ppm and highest at 4,443 ppm. All bar cores generally show less than 30 percent variation except for the core at R-km 6.0 which was from a shallow active bar. The bar core at R-km 6 has a Zn ratio well above 1, indicating higher Zn concentrations at the surface, but it also has large coefficient of variation. This sample is from a stable bar just

Table 8. Summary of bar core samples.

Core	Depth	Sample	Pb			Zn			Ca		
R-km	(cm)	(n)	Mean	Cv%	Ratio	Mean	Cv%	Ratio	Mean	Cv%	Ratio
7.2	50	5	698	28	0.99	1,061	15	1.00	43,591	23	0.97
6	40	4	2,347	47	0.93	858	60	1.19	108,429	55	0.91
5.8	40	4	962	21	1.02	1,217	37	0.98	57,328	25	1.04
4.25	70	7	1,164	31	0.95	553	20	0.99	93,880	8	0.99
1.68	60	6	1,321	21	0.96	517	37	0.97	95,519	16	0.99
1.3	40	4	3,262	35	0.93	591	17	0.96	101,668	24	0.97

downstream of Shaw Branch, and the upper 20 cm average 1,300 ppm Zn while the bottom 20 cm averages 420 ppm Zn. All ratios for all metals are very close to 1, indicating little change with depth. These trends indicate that near-surface sediment samples are representative of contamination trends at depth.

Metal Storage Trends. This section will analyze the downstream trends in metal storage and its downstream trends along FRC (Appendix E). There is approximately 130 Mg of Pb, 93 Mg Zn, and 9,700 Mg Ca stored in-channel deposits in FRC (Table 9). The majority of the Pb and Zn mass is stored in active and stable bar deposits. The majority of the Ca mass is found in the active bars. Channel bed sediments contain the least amount of metals due to being composed of relatively thin and coarse deposits. Background concentrations as determined by the upstream sediment sampling were not subtracted from the observed concentrations before storage calculations, therefore the following numbers may be overestimating the mining contribution to metal storage by <5 percent.

Pb Trends**.** There are 133 Mg of Pb stored in channel deposits in FRC.

Table 9. Summary of percent of total by metal and deposit type.

	Pb	Zn	Ca	Sediment
Channel Bed	16	23	14	23
Active Bar	41	32	46	41
Stable Bar Total	43	45	39	35
Sum:	100	100	100	100
Stable Bar Fines	18	24	10	10
Metal Mass (kg)	133,031	93,248	9,672,347	169,909

Stable bar deposits represent the greatest amount of Pb storage of 43 percent of total, then active bars with 41 percent of total, and then channel beds with 16 percent of total (Table 10). The majority of the active and stable bar Pb is found in segments 8 and 9, approximately 32 percent of the total, and are located below the confluence of Koen Creek and Walker Branch. Additionally, the Pb found in these segments have been transported several kilometers downstream from mining sources.

Channel bed deposits contain the lowest percentage of Pb storage of 16 percent. Pb storage in channel bed deposits gradually increases downstream after segment 4, peaks in segment 8, and then decreases in segments 9, 10, and 11. Segment 8 contains the greatest amount of Pb unit storage at 3,245 kg / 100 m (Figure 35-A). This trend can be explained by dilution from the uncontaminated sediment supplied by Walker Branch, and is represented in the relative decrease of Pb unit storage from segment 8 to segment 9 (Figure 35-A). Channel bed storage in segments 6, 7, and 8 compose approximately 12

Table 10. Distribution of Pb across segments in FRC. Red numbers indicate segments with greater than average storage.

	Pb Storage (%)					Metal Storage	
Segment	Channel Bed	Active Bar	Stable Bar Total	Segment Total (%)	Stable Bar Fines Only (%)	Total (kg)	Unit (kg / 100 m)
1	0.2	**5.1**	**4.8**	**10.1**	0.4	13,423	1,278
2	0.6	1.2	0.7	2.6	0.1	3,408	568
3	0.8	3.2	**4.7**	8.7	**2.1**	11,633	895
4	0.3	0.5	**4.0**	4.7	1.4	6,318	1,264
5	1.4	**6.0**	3.8	**11.2**	1.5	14,940	2,134
6	**3.3**	2.3	3.6	**9.1**	**2.8**	12,164	839
7	**2.0**	1.9	3.4	7.2	**2.1**	9,644	1,753
8	**3.7**	**5.6**	**12.6**	**22.0**	**6.4**	29,209	3,245
9	1.3	**8.8**	**5.2**	**15.3**	1.6	20,398	2,266
10	**1.7**	3.1	0.1	5.0	0.0	6,621	883
11	1.0	3.0	0.0	4.0	0.0	5,273	1,055
Average:	1.5	3.7	3.9	9.1	1.7		
Sum:	16.4	40.6	43.0	100.0	18.5	133,031	

percent of total Pb storage and these segments encompass FRC from the upstream National Pile confluence down to the Walker Branch confluence. This general location has a relatively large amount of Pb storage is consistent with findings from Smith and Schumacher (1993) where they noted a large amounts of contaminated sediment storage below the National Pile (Figure 35-B).

Zn Trends**.** There are 93 Mg of Zn stored in channel deposits in FRC. The greatest amount of Zn storage is found in the stable bars at 45 percent of total, then active bars at 32 percent, and the rest in channel bed at 23 percent. Zinc storage trends are highly localized below the Elvins/Rivermines Pile. The downstream

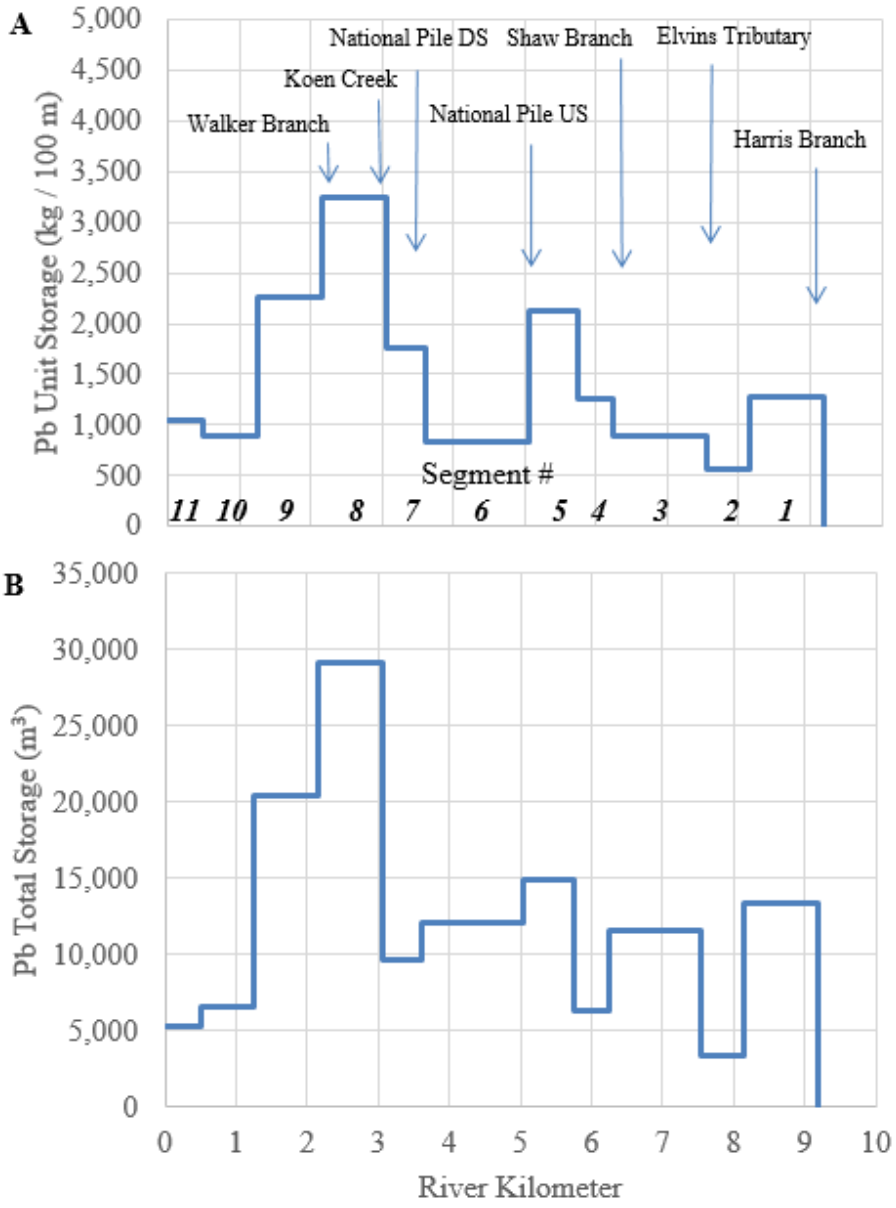

Figure 35. Pb mass: A-Unit storage and B-Total storage per segment.

distribution is very different from Pb and is greatest amount is stored in the mining reaches.

The greatest amount and percent of total Zn storage, 25 Mg and 27 percent respectively, are found in segment 3 which begins with the Elvins/Rivermines Pile confluence and ends above the Shaw Branch confluence (Figure 35). The

Elvins/Rivermines Pile received tailings from mines where Zn mineralization was locally abundant (Smith and Schumacher, 1993, Snyder and Gerdemann, 1968). The Zn mass in channel bed deposits decreases rapidly from the source downstream and is consistent with similar downstream trends from Miller (1997) and Walling et al. (2003) which reported that metal concentrations generally decrease exponentially with distance from the source.

Zinc mass storage in segments 4 to 9 is unevenly distributed between sediment deposits (Table 11). Segment 4 has 8 percent of total Zn in stable bars and less than 1.5 percent in active bar and channel bed deposits. All deposits in segment 5 contain above average percentages of total Zn storage, with 7.4 percent of the total in active bar deposits, 4.6 percent of total in stable bars, and 3 percent of total in channel bed deposits. Segment 5 contains the second highest amount of Zn storage at 14 Mg (Figure 36).

Table 11. Distribution of Zn in FRC. Red numbers indicate segments with greater than average storage.

	Zn Storage (%)					Metal Storage	
Segment	Channel Bed	Active Bar	Stable Bar Total	Segment Total (%)	Stable Bar Fines Only (%)	Total (kg)	Unit (kg / 100 m)
1	0.1	2.5	2.4	5.0	0.2	4,696	447
2	**5.5**	1.3	0.7	7.5	0.1	6,973	1,162
3	**5.4**	**5.4**	**16.1**	**26.9**	**11.7**	25,061	1,928
4	0.4	1.0	**8.0**	**9.3**	**3.3**	8,696	1,739
5	**3.0**	**7.4**	**4.6**	**15.1**	1.8	14,059	2,008
6	**2.9**	2.5	3.1	8.6	**2.2**	7,996	551
7	0.8	1.6	2.2	4.7	1.1	4,383	797
8	1.8	**2.9**	**5.5**	**10.2**	**2.3**	9,526	1,058
9	1.0	**4.5**	2.8	8.3	0.9	7,719	858
10	0.9	1.7	0.1	2.7	0.0	2,488	332
11	0.7	1.0	0.0	1.8	0.0	1,653	331
Average:	2.1	2.9	4.1	9.1	2.1		
Sum:	22.6	31.9	45.5	100.0	23.5	93,248	

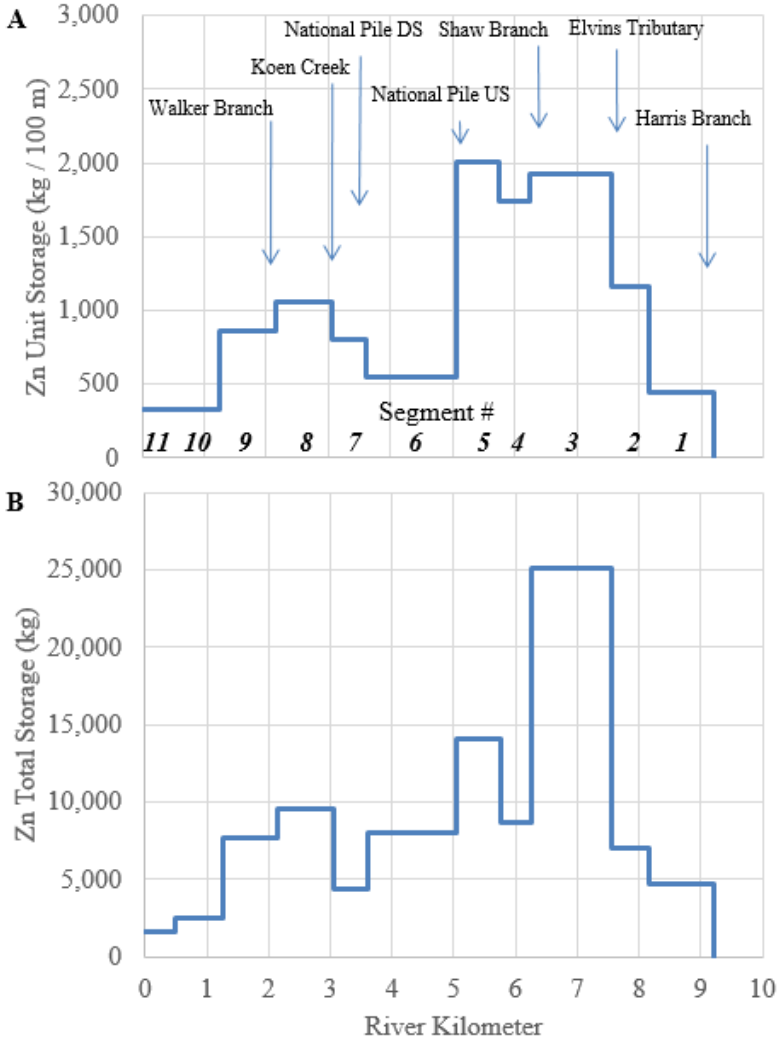

Figure 36. Zn mass: A-unit storage and B-total storage per segment.

This uneven sediment distribution between deposits and between segments is consistent with observations by Graf (1997) where he states sediment transport is unevenly distributed and the sediment deposition rates and associated contaminants increases in places where stream power decreases, or the channel widens.

Ca Trends**.** There are 9,700 Mg of Ca stored in channel deposits in FRC. The greatest amount of Ca mass is stored in active bar deposits at 46 percent, then stable bars

at 39 percent, and 14 percent found in channel bed deposits (Table 12). Calcium follows similar trends to the Pb mass in its segment distribution with the greatest concentrations in segment 8 and 9. There is a generally increasing trend of Ca storage moving downstream, however with a noticeable lack of Ca mass found in segments 4, 5, and 6 (Figure 37-A). This could be caused by sediment removal during remediation and stabilization of the National Pile, however this trend as apparent for Pb or Zn.

Ca mass is concentrated in four segments. Mining affected segments 1 and 3 store approximately 26 percent of total Ca in active bar and stable bar deposits. Downstream segments 8 and 9 store approximately 32 percent of the total in active and stable bars. These segments also have the largest total mass per segment as well as unit storage. This storage trend suggests that segments 4 to 7 are zones of transport.

Table 12. Percent of total distribution of Ca across FRC. Red numbers indicate segments with greater than average storage.

	Ca Storage (%)					Metal Storage	
Segment	Channel Bed	Active Bar	Stable Bar Total	Segment Total (%)	Stable Bar Fines Only (%)	Total (kg)	Unit (kg / 100 m)
1	0.3	**5.7**	**5.4**	**11.4**	0.5	1,099,733	104,736
2	0.6	2.0	1.2	3.7	0.1	361,715	60,286
3	0.8	**7.5**	**7.6**	**15.9**	**1.5**	1,536,383	118,183
4	0.4	0.7	**3.9**	5.0	0.6	479,638	95,928
5	1.0	3.8	1.9	6.7	0.4	650,962	92,995
6	**3.2**	1.4	1.4	6.0	**1.0**	577,166	39,805
7	1.2	1.4	1.8	4.4	0.8	423,234	76,952
8	**2.7**	**5.4**	**10.6**	**18.7**	**4.6**	1,811,366	201,263
9	1.1	**10.7**	**5.5**	**17.2**	**1.1**	1,666,003	185,111
10	**2.3**	2.5	0.1	4.9	0.0	472,187	62,958
11	0.8	**5.4**	0.0	6.1	0.0	593,959	118,792
Average:	1.3	4.2	3.6	9.1	1.0		
Sum:	14.2	46.4	39.3	100.0	10.5	9,672,347	

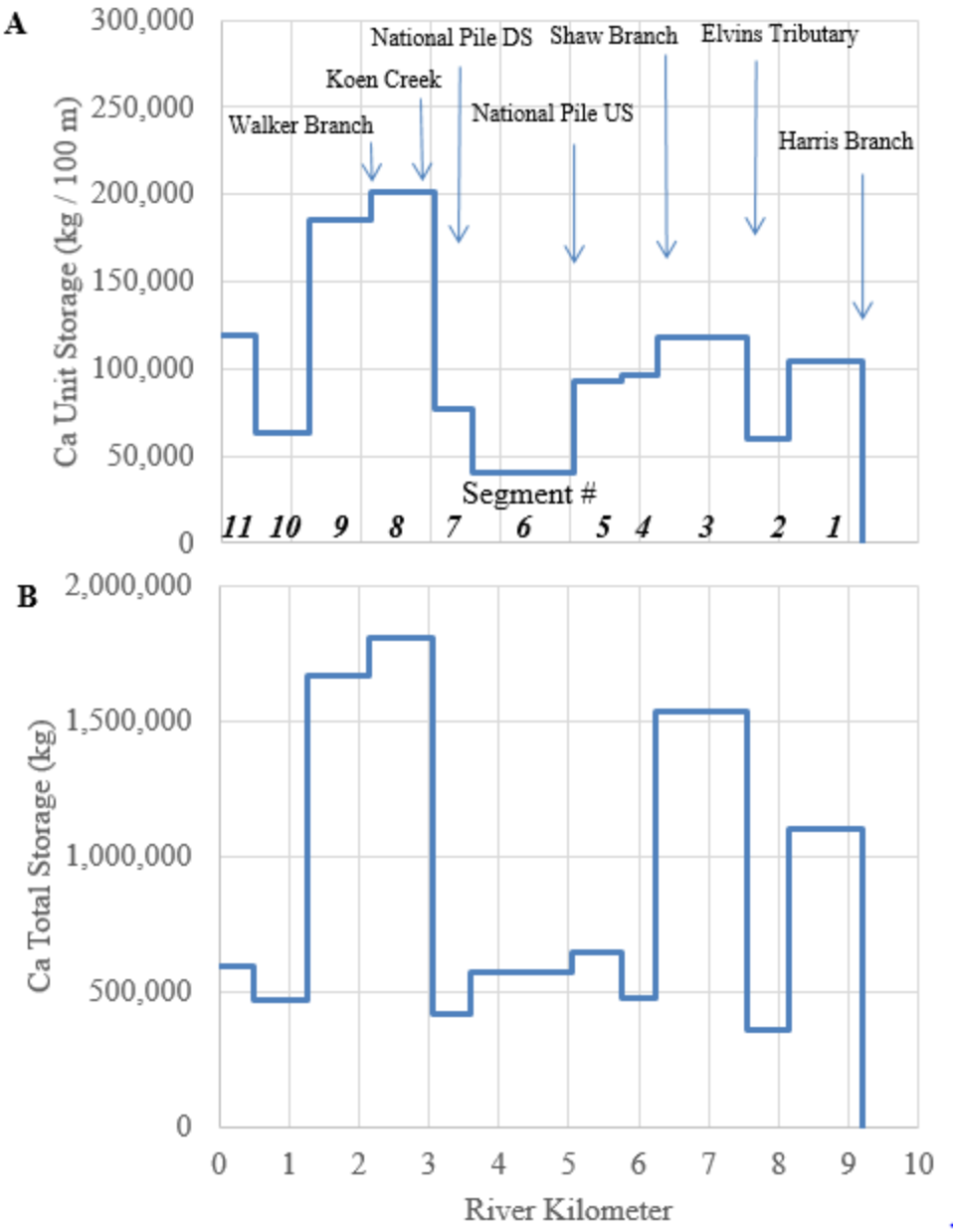

Figure 37. Ca mass: A-unit storage and B-total storage per segment.

Sediment stored long-term in this segment could have been excavated and removed during the stabilization of the National Pile, however a similar trend does not appear in the stable bar fractions for Pb and Zn. There is an overall slightly decreasing trend in Ca mass storage moving downstream in stable bar deposits. This potentially implies large quantities of tailings remain in storage and are available to be reintroduced.

Implications of Storage Trends

The greatest amount of sediment storage is expected to be in wider channel sections where bed slope and low flow velocity decreases and sediment deposition is enhanced (Panfil and Jacobson, 2001). However, there is no relationship of unit sediment and metal storage by segment scale with slope (Figure 38-B and C). Possible variations of channel slope at the segment scale are not sensitive enough to allow adequate analysis. Ikeda (1975) determined an approximate slope of 0.10 is the threshold where slope has a noticeable effect on sediment storage. Slope for segments tend to vary below 0.003 to 0.004 with two segments in 0.007 and 0.009 range (Figure 38-B and C) Unit sediment storage varies between 900 and 3,100 m^3 / 100 m and Pb unit storage varies between 840 and 3,250 kg / 100 m, but have a small range of slopes between 0.0027 and 0.0044. Sediment supply factors can influence sediment depositional patterns in rivers (Lewin and Macklin, 1987; Montgomery and Buffington, 1997). Sediment storage is concentrated in segments 1 and 3 in the mining affected reaches and downstream in segments 8 and 9. Segment 1 receives sediment from Harris Branch, but also from upstream above the study area. An influx of sediment into the main stem from upstream sources could cause the high unit storage rates in segments 1 and 3. Similarly, sediment influx from Koen Creek and Walker Branch could be causing the high unit storage rates in segments 8 and 9.

Geomorphic factors such as valley width, channel bends, and bedrock control have effects on sediment storage (Panfil and Jacobson, 2001; Owen et al., 2011). Owen et al. (2011) observed main stem channels in other Ozark streams confined by valley walls having relatively straight channels with little channel bed sediment deposition.

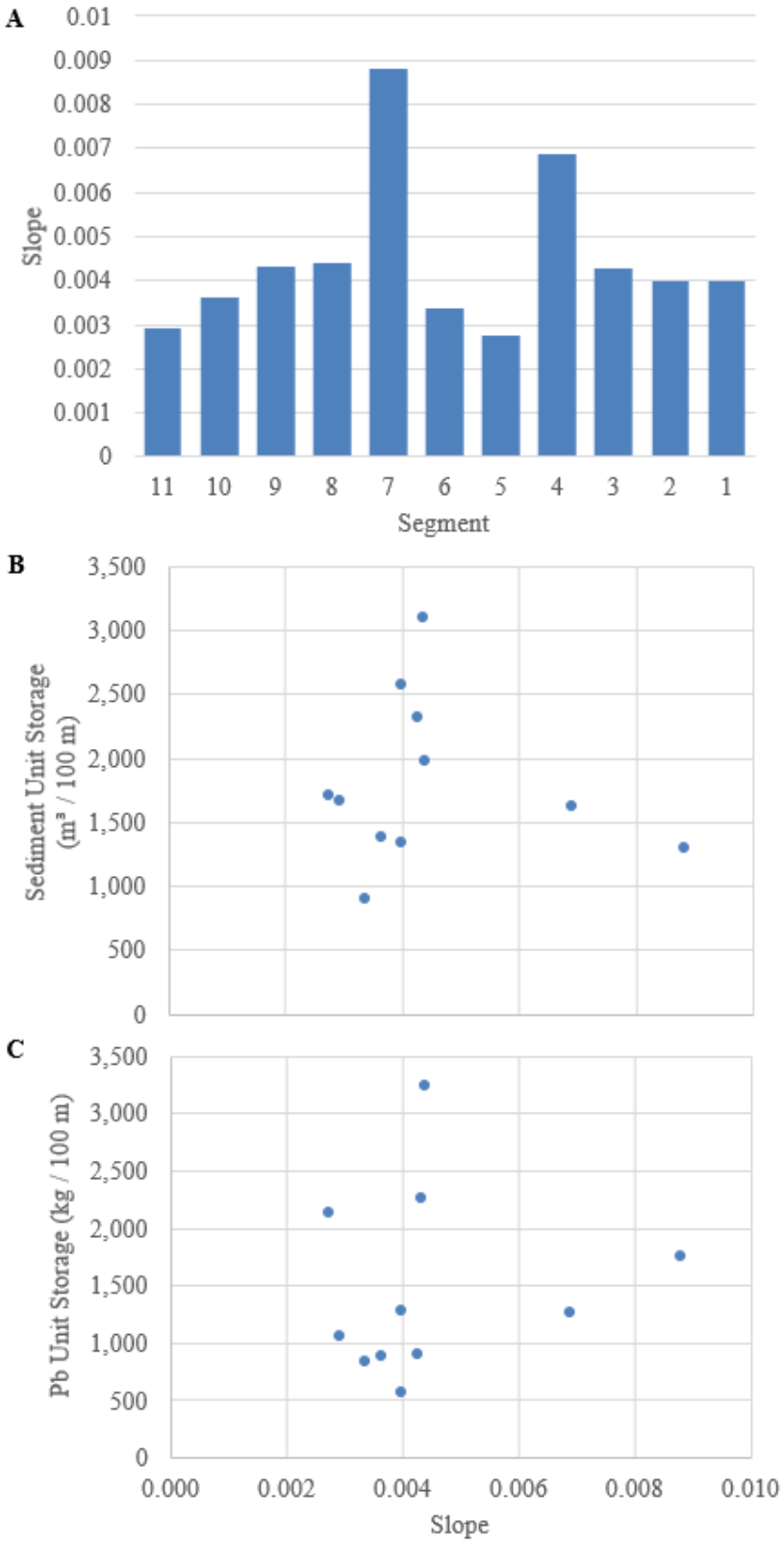

Figure 38. Effect of channel slope (A) on segment unit storage (B) and segment Pb unit storage (C).

Sediment storage is also abundant on the inside bend of channels on the point bar (Panfil and Jacobson, 2001). Many segments in FRC exhibit similar storage patterns based on these geomorphic factors. In segment 3, R-km 7.05 is at a natural bend and sediment storage is amplified by old bridge ties in the channel bed, creating a wide forced channel with abundant channel bed deposition and active bar deposition in the inside bend. In segment 6, R-km 5.05 to 4.3 is a bedrock dominated reach with little storage, however channel bed unit storage below R-km 4.3 is very high with little exposed bedrock and natural channel bends, enhancing storage.

Anthropogenic activities may also have an effect on storage trends in FRC. The Old Lead Belt has been active for over a century and the mining activities and storage of waste have had far reaching environmental impacts (Bussiere, 2007, Gale et al. 2004). In the past decade, humans have altered the landscape through the mining and remediation process in FRC and are evident in photographs collected from field activities (Appendix F). During the remediation process and pile stabilizations, vast quantities of tailings and contaminated sediment were excavated and moved around. The effects of this sediment removal might be a reason segment 6 has the lowest sediment, Pb, Zn, and Ca mass unit storage (Figures 24-A, 35-A, 36-A, and 37-A). Channel modifications such as channel over-widening create areas of wide active channels with greater amounts of storage. Channel straightening also affects sediment storage, creating zones of transport with little opportunities for sediment storage, and forcing greater deposition further downstream. This is evident in segment 6 where it is straight for nearly 1.5 km with one slight bend.

The results of this study are consistent with previous findings. There is an estimated 3,700,000 m^3 of contaminated sediment and 3,000 Mg of Pb stored in channel bed and bar deposits in the main stem of the Big River (Pavlowsky et al. 2010). In comparison, FRC contains an estimated 170,000 m^3 of sediment which represents approximately four percent of contaminated sediment stored in the Big River. The estimated unit storage for in-channel sediment in the Big River is 2,570 m^3 / 100 m in St. Francois County where the Big River is located within the Old Lead Belt (Pavlowsky et al. 2010). However, FRC has an average sediment unit storage of 1,800 m^3 / 100 m. In terms of Pb mass, there is approximately 50 to 60 Mg / km in the Big River segment upstream and downstream to FRC. FRC has an overall Pb unit storage is 9 Mg / km indicating only 15 to 20 percent of Pb unit storage in the Big River.

The results of this study found concentrations in sediment samples and channel morphology measurements were similar to Pavlowsky et al. (2010). Channel bed, bar, and channel sediment data collected around the St. Joe Road bridge at R-km 3.55 had an average concentration of 2,289 ppm Pb, 1,161 ppm Zn, and 151,707 ppm Ca. This study reported average concentrations of 2,000 ppm Pb, 1,200 ppm Zn, and 95,900 ppm Ca for the same segment. Lastly, Pavlowsky et al. (2010) reported an average active channel width of 17.9 m, where this study calculates an average width of 15.1 m at the same location at the St. Joe Road bridge.

The results of this study are also consistent with findings from Smith and Schumacher (1991, 1993). This study similarly found the Pb and Zn concentrations in bed sediment increase downstream from the confluence of Harris Branch. Smith and Schumacher (1993) determined that Pb concentrations in bed sediment increase in the

downstream direction in FRC, which this study also found. Smith and Schumacher (1991) reported Pb concentrations in bed sediments in segment 3, between the Elvins/Rivermines Pile tributary (R-km 7.6) to Shaw Branch (R-km 6.3), ranged from 2,050 ppm to 3,140 ppm. In comparison, this study found the average channel bed Pb concentration in the same segment to be significantly lower at 889 ppm, but one sediment sample had a concentration 3,104 ppm Pb. This difference may suggest that clean-up efforts and dilution from upstream sources may have reduced metal concentrations in these segments over the past 25 years. Conversely, Pb concentrations below the National Pile have remained the same. This study found bed sediments downstream of the National Pile containing Pb concentrations ranging from 1,550 ppm to 5,106 ppm compared to Smith and Schumacher (1993) 1,000 ppm to 7,200 ppm range. If it has taken 25 years for channel sediment Pb concentrations in segment 3 to drop from an average of 2,500 ppm Pb to 900 ppm Pb with little decrease downstream, it is highly probable that Pb contamination problems in FRC will last more than a century into the future. However, remediation and other management efforts may shorten the geochemical recovery time for FRC.

CONCLUSION

Mining-contaminated sediment stored in stream channels can provide a long-term source of metal pollution as deposits become remobilized by fluvial processes. Even though the TMDL for Big River, FRC, and Shaw Branch has been completed, a significant amount of contaminated sediment remains stored in channel bed and bar deposits in FRC. However, FRC storage represents only four percent of contaminated sediment storage in-channel deposits of the Big River with unit storage of about seventy percent of the Big River. There are 9 major findings of this study:

1. **Mining-related metal concentrations in channel sediments tend to exceed PEC and vary downstream due to the effect of tailing pile sources and dilution effect by relatively undisturbed tributaries.** Approximately ninety four percent of all channel sediment samples in the study area are above the PEC for Pb and seventy percent are above PEC for Zn. The highest average concentration used for metal mass calculations is 3,323 ppm for Pb in segment 7 and 3,658 ppm for Zn in segment 2. Pb concentrations peak in segment 8, approximately a kilometer downstream of the lower National Pile confluence, and are affected by dilution of cleaner sediment from Koen Creek and Walker Branch. Zn concentrations peak closest to source at the Elvins tributary confluence in segment 2 with a secondary downstream of Shaw Branch in segment 4.

2. **There is an increasing trend of metal concentrations in sediment as FRC flows past the major mining tributary confluences at R-km 9.1, 7.6, 6.3, 5.05, and 3.65.** Pb concentrations begin to rise past major mine tributaries and concentrations decrease past larger unmined tributaries including Koen Creek at R-km 3.05 and Walker Branch at R-km 2.1. These concentrations become diluted downstream from the input of fresh uncontaminated sediment upstream of the mining reaches and from Koen Creek and Walker Branch downstream. However, Pb and Zn concentrations remain high around 1,127 and 455, respectively at the Big River confluence.

3. **The channel morphology of FRC exhibits bedrock control affecting the width and depth of depositional features.** Segments 3, 4, 6, and 8 have high percentages of exposed bedrock preventing downcutting and creating wider active channels. However, segment 6 for example, has a large percent of exposed bedrock, which would indicate low channel bed storage. Field assessments indicate the upper half of this segment is primarily exposed bedrock, while the

bottom half have relatively thick channel bed deposits. This implies that effects of bedrock control in FRC may have a greater effect on the reach-scale rather than the segment-scale in terms of sediment deposition. Channel widths vary in four different zones with wider widths in segments 1 to 5, significantly narrower widths in segments 6 and 7, and then wider widths in segments 8 and 9, and moderate widths in segments 10 and 11.

4. **In general, unit storage of contaminated sediment decreases slightly downstream in channel bed and bar deposits**. There are 170,000 m^3 of sediment stored in channel bed and bar deposits in FRC. There is 20 percent of total stored in segments 1 and 2, nearly 37 percent of total stored in segments 3 to 6, and 43 percent of total stored in segments 7 to 11. Approximately 23 percent are channel bed deposits, 41 percent are active bar deposits, and 35 percent are stable bar deposits. There is a greater amount of average unit sediment storage in the upstream mining segments 1 to 3 at approximately 2,000 m^3 / 100 m with a total storage of 65,200 m^3. Average unit storage in segments 4 to 7 is approximately 1,400 m^3 / 100 m with a total storage of 40,200 m^3. Average unit storage for the downstream segments 8 to 11 are approximately 1,900 m^3 / 100 m with a total storage of 64,500 m^3.

5. **There is 133 Mg of Pb stored in FRC.** Stable bar deposits contain the greatest amount of Pb storage at 43 percent of total, with active bars at 41 percent of total, and channel beds at 16 percent of total storage. The majority of active and stable bar Pb metal is stored in segments 8 and 9, approximately 32 percent of the total in segments below the confluence of Koen Creek and Walker Branch.

6. **There is 93 Mg of Zn stored in-channel deposits in FRC.** The greatest amount of Zn storage is found in stable bars at 45 percent of total, active bars at 32 percent, and channel bed at 23 percent of total. Zn storage trends reflect source influence of the Elvins/Rivermines Pile. The downstream distribution is different than Pb, with the greatest amount stored below the Elvins/Rivermines Pile and Shaw Branch while the majority of Pb stored in the downstream of the National Pile.

7. **There is 9,700 Mg of Ca stored in-channel deposits in FRC.** The host rock is the Bonne Terre Dolomite with a high Ca abundance (i.e. pure tailings) of 21.7 percent by molecular weight. Therefore, sediment containing Ca concentrations near 217,000 ppm are assumed to be composed of 100 percent tailings materials. Calcium mass is stored in active bar deposits at 46 percent of total, stable bars at 39 percent of total, channel bed at 14 percent of total. Calcium follows similar trends to the Pb mass in its segment distribution with the greatest concentrations are in segment 8 and 9. Generally, Ca storage increases downstream, however there is a noticeable lack of Ca mass found in segments 4, 5, and 6, potentially indicating removal of contaminated sediment or dilution by non-mining sediment.

8. **This study found similar results to previous studies that have included sediment studies in FRC.** Compared to segments in the Big River, Pavlowsky et al. (2010) estimates approximately 50 to 60 Mg / km Pb in the Big River in reaches close to FRC. In comparison, FRC has an average Pb unit storage is 9 Mg / km. Sediment storage and metal concentration values collected by Pavlowsky et al. (2010) at the St. Joe Road bridge are similar to those collected in this study at the same location. The results of this study are also consistent with findings from Smith and Schumacher (1991, 1993), since the present study similarly found that Pb and Zn concentrations in bed sediment increase downstream from Harris Branch in FRC.

9. **FRC is not a significant source of metal contamination to the Big River.** The total sediment volume stored in FRC equates to roughly four percent of sediment in the Big River watershed. The average Pb unit storage in FRC is 9 Mg / km which is significantly lower than 50 to 60 Mg / km in the Big River found upstream and downstream of the confluence. Of total sediment stored, 76 percent is in active and stable bar deposits. These deposits represent sediment in temporary storage that are remobilized by high flow events. An unknown volume of sediment and metals are stored in the floodplain. All together FRC does represent a long-term source of contamination to Big River, but the full impact of sediment Pb and Zn loads to the Big River is not fully understood.

This study represents an initial step in understanding the storage and transport of Pb and Zn in FRC sediments. Future studies should specifically investigate the floodplain deposits in FRC. Sediment stored in floodplains is temporarily removed from the system and may eventually recontaminate the system. Bank erosion, geochemical weathering, and human disturbance can all release Pb and Zn to FRC from floodplain soils. Assessing the volume of floodplain sediment and Pb contaminated sediment will further enhance the understanding of the contamination problem in FRC and the Old Lead Belt. This study focused on the volume and mass of sediment and metal contamination in the tailings sediment size fraction <2 mm in diameter. Sediment contamination may affect other sediment sizes and attention should be given to understanding metal storage in the 2 to 16 mm sized sediment fraction and its distribution since ore mills produce tailings in this size range. While this study has focused on

sediment storage, sediment transport rates leaving FRC and entering the Big River have not been quantified. This information would be valuable to help evaluate the effectiveness of the Big River Lead Remediation Structure recently installed on the Big River downstream of the FRC confluence.

Relatively large volumes of metal contaminated sediment remain stored in channel deposits in FRC and are still located close to their sources of the Federal, Elvins/Rivermines, and National Tailings piles even with mine closure in 1972, however the largest unit storage rates of Pb are below R-km 3 indicating that channel morphology and deposition processes may control the distribution of tailings stored in FRC. Channel bed storage represents a potentially mobile fraction of contamination stored in FRC. The greatest amount of contamination is found in the active bars suggests a slow process of downstream transport over periods of decades to centuries. The long-term problem of contamination is even more evident given that most Pb and Zn is currently stored in channel bar deposits and probably floodplain soil deposits, which slowly release stored contaminated sediment to FRC by fluvial action.

LITERATURE CITED

Ahrens, L.H., 1954, The Log-normal Distribution of the Elements (a Fundamental Law of Geochemistry and its Subsidiary): Geochemica et Cosmochimica Acta, v. 5, p. 49-73.

Besser, J.M., Brumbaugh, W.G., Allert, A.L., Poulton, B.C., Schmitt, C.J., Ingersoll, C.G., 2008, Ecological Impacts of Lead Mining on Ozark Streams: Toxicity of Sediment and Pore Water: Ecotoxicology and Environmental Safety, v. 72, p. 516-526.

Bradley, S.B., 1989, Incorporation of Metalliferous Sediments from Historic Mining into River Floodplains: Supply, Storage, and the Potential for Secondary Pollution in the Fluvial Environment: GeoJournal, v. 19, p. 5-14.

Brown, B.L., 1981, Soil Survey of St. Francois County, Missouri: United States Department of Agriculture, Soil Conservation Service and Forest Service in Cooperation with the Missouri Experiment Station, 142 p.

Buckley, E.R., 1908, Geology of the Disseminated Lead Deposits of St. Francois and Washington Counties: Jefferson City, MO, Hugh Stephens Printing, 259 p.

Buffington, J.M., Montgomery, D.R., 2013, Geomorphic Classification of Rivers: Treatise on Geomorphology, v. 9, 38 p.

Bussiere, B., 2007, Colloquium 2004: Hydrogeotechnical Properties of Hard Rock Tailings from Metal Mines and Emerging Geoenvironmental Disposal Approaches: Canadian Geotechnical Journal, v. 44, p. 1019-1052.

Dennis, I.A., Coulthard, T.J., Brewer, P., Macklin, M.G., 2009, The Role of Floodplains in Attenuating Contaminated Sediment Fluxes in Formerly Mined Drainage Basins: Earth Surface Processes and Landforms, v. 34, p 453-466.

Engelund, F., Hansen, E., 1967, A Monograph on Sediment Transport in Alluvial Streams, 65 p.

EPA, 2007, Field Portable X-Ray Flourescence Spectormetry for the Determination of Elemental Concentrations in Soil and Sediment: Environmental Protection Agency Method 6200, 32p.

EPA, 2011, Record of Decision, Big River Mine Tailings Superfund Site: Environmental Protection Agency Report, CERCLIS ID#: MOD981126899, 133p.

EPA, 2012, Big River Mine Tailings/St. Joe Minerals Corporation Site: Environmental Protection Agency Report, EPA ID# MOD981126899, 7 p.

Evans, D., Davies, B.E., 1993, The Influence of Channel Morphology on the Chemical Partitioning of Pb and Zn in Contaminated River Sediments: Applied Geochemistry, v. 9, p. 45-52.

Fisher, B.G., Bookhagen, B., Amos, C.B., 2013, Channel Planform Geometry and Slopes from Freely Available High-Spatial Resolution Imagery and DEM Fusion: Implications for Channel Width Scalings, Erosion Proxies, and Fluvial Signatures in Tectonically Active Landscapes: Geomorphology v. 194, p. 46-56.

Gale, N.L., Adams, C.D., Wixson, B.G., Loftin, K.A., Huang, Y.W., 2004, Lead, Zinc, Copper and Cadmium in Fish and Sediments from the Big River and Flat River Creek of Missouri's Old Lead Belt: Environmental Geochemistry and Health, v. 26, p. 37-49.

Graf, W.L., 1997, Transport and Deposition of Plutonic-contaminated Sediments by Fluvial Processes, Los Alamos Canyon, New Mexico: Geological Society of America Bulletin, v. 108, p. 1342-1355.

Gran, K.B., Belmont, P., Day, S.S., Jennings, C., Johnson, A., Perg, L., Wilcock, P.R., 2009, Geomorphic Evolution of the Le Sueur River, Minnesota, USA, and Implications for Current Sediment Loading: Geological Society of America Special Paper 451, p. 12.

Gulson, B.L., Davies, J.J., Mizon, K.J., Korsch, M.J., Law, A.J., Howrath, D., 1994, Lead Bioavailability in the Environment of Children: Blood Lead Levels in Children Can Be Elevated in a Mining Community: Archives of Environmental Health, v. 49, p. 326-331.

Ikeda, H., 1975, On the Bed Configuration in Alluvial Channels; Their Types and Conditions of Formation with Reference to Bars: Geographical Review of Japan, v. 48, p. 712-730.

Jacobson, R.B., Primm, A.T., 1997, Historical Land-Use Changes and Potential Effects on Stream Disturbance in the Ozark Plateaus, Missouri: U.S. Geological Survey Water-Supply Paper 2484, 92. p.

Jacobson, R.B., Pugh, A.L., 1992, Effects of Land Use and Climate Shifts on Channel Instability, Ozark Plateaus, Missouri: Proceedings of the Workshop on the Effects of Global Climate Change on Hydrology and Water Resources at the Catchment Scale, Japan-U.S. Committee on Hydrology, Water Resources and Global Climate Change, p 423-444.

James A. L., 1989, Sustained Storage and Transport of Hydraulic Gold Mining Sediment in the Bear River, California: Annals of the Association of American Geographers, v. 79, p. 570-592.

Knighton, D., 1998, Fluvial Forms and Processes: A new perspective. Oxford University Press, 383 p.

Lead Belt News, 1917, To Incorporate Flat River: http://www.rootsweb.ancestry.com/~mostfran/towns/to_incorporate_flatriver.htm (accessed 6/15/16)

Lecce, S.A., Pavlowsky, R.T., 1997, Storage of Mining-Related Zinc in Floodplain Sediments, Blue River, Wisconsin: Physical Geography, v. 18, p. 424-439.

Lecce, S.A., Pavlowsky, R.T., 2001, Use of Mining-Contaminated Sediment Tracers to Investigate the Timing and Rates of Historical Floodplain Sedimentation: Geomorphology, v. 38, p. 85-108.

Lecce, S.A., Pavlowsky, R.T., Bassett, G.S., Martin, D.J., 2011, Metal Contamination from Gold Mining in the CID District, North Carolina: Physical Geography, v. 32, pp. 469-495.

Lecce, S.A., Pavlowsky, R.T., 2014, Floodplain Storage of Sediment Contaminated by Mercury and Copper from Historic Gold Mining at Gold Hill, North Carolina, USA: Geomorphology, v. 206, p. 122-132.

Lewin, J., Macklin, M.G., 1987, Metal Mining and Floodplain Sedimentation in Britain, in Gardiner, V, ed. International Geomorphology, p. 1009–1027.

MacDonald, D.D., Ingersoll, C.G., Berger, T.A., 2000, Development and Evaluation of Consensus-Based Sediment Quality Guidelines for Freshwater Ecosystems: Environmental Contamination and Toxicology, v. 39, p. 20-31.

Macklin, M.G., Brewer, P.A., Hudson-Edwards, K.A., Bird, G., Coulthard, T.J., Dennis, I.A., Lechler, P.J., Miller J.R., Turner, J.N., 2006, A Geomorphological Approach to the Management of Rivers Contaminated by Metal Mining: Geomorphology, v. 79, p. 423- 447.

Magilligan, F.J., 1985, Historical Floodplain Sedimentation in the Galena River Basin, Wisconsin and Illinois: Annals of the Association of American Geographers, v. 75, p. 583-594.

McGraw, 1936, A Brief History of Flat River: http://www.rootsweb.ancestry.com/~mostfran/brief_history_flat_river.htm (accessed 6/15/16).

MDNR, 2007. Total Maximum Daily Load Information Sheet: Big River and Flat River Creek. http://www.dnr.mo.gov/env/wpp/tmdl/info/2074-2080-2168-big-r-info.pdf

MDNR, 2008, EPA Approved 303(d) List: Missouri Department of Natural Resources.

MDNR, 2009, Final Phase I Damage Assessment Plan for Southeast Missouri Lead Mining District: Big River Mine Tailings Superfund Site, St. Francois County and Viburnum Trend Sites, Reynolds, Crawford, Washington, and Iron Counties: Missouri Department of Natural Resources, 84 p.

Miller, J.R., 1997, The Role of Fluvial Geomorphic Processes in the Dispersal of Heavy Metals from Mine Sites: Journal of Geochemical Exploration, v. 58, p. 101-118.

Montgomery, D.R., Buffington, J.M., 1997, Channel-Reach Morphology in Mountain Drainage Basins, Geological Society of America Bulletin, v. 109, p.596-611.

Newfields, 2007, Volume of sediment in Big River, Flat River Creek, and Owl Creek-St. Francois County mined Areas, Missouri: Focused Remediaial Investigation of Mined Areas in St. Francois County, Missouri.

Notebaert, B., Verstraeten, G., Govers, G., Poesen, J., 2009, Qualitative and Quantitative Applications of LiDAR Imagery in Fluvial Geomorphology: Earth Surface Processes and Landforms v. 34, p. 217-231.

Owen, M.R., Pavlowsky, R.T., Womble, P.J., 2011, Historical Disturbance and Contemporary Floodplain Development along an Ozark River, Southwest Missouri: Physical Geography: v 32. 22 p.

OEWRI, 2011. Standard Operating Procedure for: X-MET3000TXS+ Handheld XRF Analyzer, Ozark Environmental and Water Resources Institute, Missouri State University.

Panfil, M.S., Jacobson, R.B., 2001, Relations Among Geology, Physiography, Land Use, and Stream Habitat Conditions in the Buffalo and Current River Systems, Missouri and Arkansas: USGS/BRD/BSR- 2001-0005, 111 p.

Pavlowsky, R.T., Owen, M.R., Martin, D.J., 2010, Distribution, Geochemistry, and Storage of Mining Sediment in Channel and Floodplain Deposits of the Big River System in St. Francois, Washington, and Jefferson Counties, Missouri: Missouri State University Ozark Environmental and Water Resource Institute, 141 p.

Podhoranyi, M., Fedorcak, D., 2015, Inaccuracy introduced by LiDAR-generated cross sections and its impact on 1D hydrodynamic simulations: Environmental Earth Science, v 73, 11 p.

Reid, L.M., Dunne, T., 1996, Rapid Evaluation of Sediment Budgets, GeoEcology.

Reimann, C., Filzmoser, P., 2000, Normal and Lognormal Data Distribution in Geochemistry: Death of a Myth. Consequences for the Statistical Treatment of Geochemical and Environmental Data: Environmental Geology, v. 39, n. 9, 14 p.

Roberts, A.D., Mosby, D., Weber, J., Besser, J., Hundley, J., McMurray, S., Faiman, S., 2009, An Assessment of Freshwater Mussel (Bivalvia: Margaritiferidae and Unionidae) Populations and Heavy Metal Sediment Contamination in the Big River, Missouri: U.S. Fish and Wildlife Service, 114 p.

Schumm, S.A., 1977, The Fluvial System, John Wiley and Sons, New York, NY, 338 p.

Seeger, C.M., 2008, History of Mining in the Southeast Missouri Lead District and Description of Mine Processes, Regulatory Controls, Environmental Effects, and Mine Facilities in the Viburnum Trend Subdistrict: U.S. Geological Survey Scientific Investigations Report 2008-5140.

Shefsky, S., 1997, Comparing Field Portable X-Ray Fluorescence (XRF) to laboratory analysis of heavy metals in soil: International Symposium of Field Screening Methods for Hazardous Wastes and Toxic Chemicals, 10 p.

Singer, D.A., 2013, The Lognormal Distribution of Metal Resources in Mineral Deposits: Ore Geology Reviews, v. 55, p. 80-86.

Smith, B.J., Schumacher, J.G., 1991, Hydrochemical and Sediment Data for the Old Lead Belt, Southeastern Missouri – 1988-89: United States Geological Survey Open-File Report 91-211, 104 p.

Smith, B.J., Schumacher J.G., 1993, Surface-water and sediment quality in the Old Lead Belt, Southe Eastern Missouri 1988-89: USGS Water-Resources Investigations Report 93-4012, 141 p.

St. Francois Herald, 1902, Federal Lead Company to Erect 1000 Houses in Flat River District: http://www.rootsweb.ancestry.com/~mostfran/chatdumps_mining/images2/1000_houses_1902.jpg, (accessed 6/15/15).

Ste. Gen. Herald, 1893, Rich Lead Strike: http://www.rootsweb.ancestry.com/~mostfran/chatdumps_mining/images/rich_lead_strike_1893.jpg (accessed 6/15/16).

Stoeser, D.B., Green, G.N., Morath, L.C., Heran, W.D., Wilson, A.B., Moore, D.W., Van Gosen, B.S., 2007, Preliminary Integrated Geologic Map Database for the United States: Central States: Montana, Wyoming, Colorado, New Mexico, North Dakota, South Dakota, Nebraska, Kansas, Oklahoma, Texas, Iowa, Missouri, Arkansas, and Louisiana: U.S. Geological Survey Open File Report 2005-1351.

Stout, J.C., Belmont, P., 2014, TerEx Toolbox for Semi-Automated Selection of Fluvial Terrace and Floodplain Features from LiDAR: Earth Surface Processes and Landforms, v. 39, p. 569-580.

Snyder, F.G., Gerdemann, P.E., 1968, Geology of the Southeastern Missouri Lead District in Ridge, J.S., Ore Deposits of the United States, p. 326 – 369.

Thoma, D.P., Gupta, S.C., Bauer, M.E., Kirchoff, C.E., 2005, Airborne Laser Scanning for Riverbank Erosion Assessment: Remote Sensing of Environment, v. 95, p. 493 – 501.

Trimble, S.W., Lund, S.W., 1982, Soil Conservation and the Reduction of Erosion and Sedimentation in the Coon Creek Basin, Wisconsin: United States Geological Survey Professional Paper 1234, 37 p.

Trimble, S.W., 1999, Decreased Rates of Alluvial Sediment Storage in the Coon Creek Basin, Wisconsin, 1975-93: Science, v. 285, p. 1244 – 1246.

U.S. Census Bureau, 2010, American FactFinder: http://factfinder.census.gov/ (accessed 9 July 2010).

Vianello, A., Cavalli, M., Tarolli, P., 2009, LiDAR-derived Slopes for Headwater Channel Network Analysis: Catena, v. 76, p. 97-106.

Walling, D.E., 1983, The Sediment Delivery Problem: Journal of Hydrology, v. 65, p. 209-237.

Walling, D.E., Owens, P.N., Leeks, G.J.L., 1998, The Role of Channel and Floodplain Storage in the Suspended Sediment of the River Ouse, Yorkshire, UK: Geomorphology, v. 22, p. 225-242.

Walling, D.E., Owens. P.N., Carter, J., Leeks, G.J.L., Lewis, S., Meharg, A.A., Wright, J., 2003, Storage of Sediment-Associated Nutrients and Contaminants in River Channel and Floodplain Systems: Applied Geochemistry, v. 18, p. 195-220.

Wharton, H.M., 1975, Guidebook to the Geology and Ore Deposits of Selected Mines in the Viburnum Trend, Missouri: Missouri Geological Survey Report 58, p.60.

Wohl, E., 2014, Rivers in the Landscape: Science and Management, Wiley. 318 p.

APPENDICES

Appendix A-1. LiDAR Channel Planform and Segment Data.

R-km	Total Channel Width (m)	Active Channel Width (m)	Bank Average Width (m)	Bed Average Width (m)	Active Bar Average Width (m)	Stable Bar Average Width (m)
9.45	25.23	18.25	3.49	12.86	5.39	
9.35	23.34	12.88	5.23	12.88		
9.25	21.56	13.34	4.11	13.34		
9.15	28.77	19.64	4.57	15.59	4.05	
9.05	35.43	21.21	7.11	19.04	1.38	0.79
8.95	35.24	22.72	6.26	8.39		14.33
8.85	26.55	16.65	4.95	10.49		6.17
8.75	34.89	20.58	7.15	20.58		
8.65	46.67	33.45	6.61	18.66		14.79
8.55	44.76	29.93	7.41	14.48	4.89	5.67
8.45	40.75	27.04	6.86	13.93	4.37	
8.35	33.54	20.32	6.61	16.49	3.83	
8.25	37.12	23.65	6.73	15.89	7.76	
8.15	40.79	24.38	8.21	10.99	6.70	
8.05	30.75	20.96	4.89	18.99	0.66	
7.95	22.57	18.13	2.22	12.59	2.84	2.70
7.85	16.93	12.78	2.08	12.78		
7.75	21.19	13.01	4.09	13.01		
7.65	23.85	15.62	4.11	13.11	2.51	
7.55	32.83	24.27	4.28	15.93	8.34	
7.45	22.86	13.73	4.57	11.93	1.80	
7.35	24.32	14.61	4.85	9.60		5.02
7.25	24.77	14.37	5.20	9.31	1.34	2.39
7.15	31.30	20.55	5.38	6.32	11.93	2.30
7.05	40.92	30.60	5.16	8.36	9.11	4.02
6.95	30.87	19.48	5.69	18.00	1.49	
6.85	34.05	18.75	7.65	16.86		1.89
6.75	32.10	23.44	4.33	20.56		2.88

Appendix A-1 continued. LiDAR Channel Planform and Segment Data.

R-km	Total Channel Width (m)	Active Channel Width (m)	Bank Average Width (m)	Bed Average Width (m)	Active Bar Average Width (m)	Stable Bar Average Width (m)
6.65	29.48	23.78	2.85	11.45		12.33
6.55	31.50	25.06	3.22	7.66		17.40
6.45	28.76	23.50	2.63	7.80		15.70
6.35	22.20	15.85	3.18	13.20		1.32
6.25	36.60	28.50	4.05	12.31		16.19
6.15	37.09	30.29	3.40	9.29	3.38	17.63
6.05	47.99	37.26	5.36	11.63	1.51	24.12
5.95	38.36	27.39	5.48	15.95		11.44
5.85	33.05	25.21	3.92	17.59	0.89	6.73
5.75	24.82	19.16	2.83	13.50	1.97	1.72
5.65	28.57	18.65	4.96	13.34	2.66	
5.55	34.15	16.65	8.75	15.71		0.94
5.45	45.72	34.12	5.80	18.49	2.43	10.77
5.35	39.91	30.84	4.53	16.38	13.69	0.77
5.25	49.24	29.91	9.67	14.42	15.49	
5.15	38.09	19.04	9.52	17.26	1.78	
5.05	32.85	16.12	8.37	16.12		
4.95	25.71	14.96	5.37	13.49		0.73
4.85	31.28	19.38	5.95	10.66	0.88	7.84
4.75	19.64	10.38	4.63	6.79	0.21	3.38
4.65	19.06	13.52	2.77	10.30	0.10	3.12
4.55	20.71	15.15	2.78	11.93		1.61
4.45	22.79	17.13	2.83	14.48		1.32
4.35	24.58	18.08	3.25	11.67	3.21	
4.25	20.40	12.88	3.76	9.47	1.14	
4.15	20.96	14.83	3.06	10.92	3.91	
4.05	24.23	17.35	3.44	14.75	1.30	
3.95	30.43	18.31	6.06	14.24	4.06	

Appendix A-1 continued. LiDAR Channel Planform and Segment Data.

R-km	Total Channel Width (m)	Active Channel Width (m)	Bank Average Width (m)	Bed Average Width (m)	Active Bar Average Width (m)	Stable Bar Average Width (m)
1.05	29.03	19.21	4.91	15.22	2.00	
0.95	32.41	23.98	4.21	15.53	2.82	
0.85	29.57	20.92	4.33	12.39	2.84	
0.75	35.56	27.08	4.24	15.87	5.61	
0.65	38.40	27.47	5.47	17.88	9.59	
0.55	34.43	25.38	4.52	21.16	2.11	
0.45	33.74	25.66	4.04	19.56	3.05	
0.35	38.44	28.01	5.21	13.91	3.53	
0.25	40.23	28.22	6.00	11.93	8.15	
0.15	38.76	33.02	2.87	18.04	14.98	
0.05	24.69	18.70	2.99	15.90	2.79	

Appendix A-2. Channel widths from LiDAR derived cells.

				LiDAR Channel Width (m)		
Segment	R-km	Deposit	n	Avg	Std	Cv%
1	9.2	Active	7	7.62	4.73	62.10
		Bed	12	14.82	3.67	24.76
		Stable	5	8.35	6.05	72.43
2	8.15	Active	4	3.92	2.97	75.88
		Bed	6	14.40	2.57	17.82
		Stable	1	2.70		
3	7.55	Active	5	7.22	7.52	104.14
		Bed	13	11.79	4.37	37.06
		Stable	11	7.53	6.42	85.30
4	6.25	Active	4	2.43	1.46	60.20
		Bed	5	13.59	3.31	24.38
		Stable	5	12.33	8.83	71.61
5	5.75	Active	5	8.22	6.00	72.96
		Bed	7	15.96	1.71	10.74
		Stable	3	4.16	5.73	137.67
6	5.05	Active	11	2.34	2.13	91.10
		Bed	14	11.67	2.55	21.87
		Stable	7	3.26	2.21	67.83
7	3.6	Active	3	3.36	2.46	73.19
		Bed	6	13.71	3.32	24.19
		Stable	3	4.66	3.72	79.82
8	3.05	Active	6	5.77	5.84	101.26
		Bed	9	16.58	3.51	21.19
		Stable	3	9.98	8.85	88.68
9	2.15	Active	6	9.88	4.30	43.54
		Bed	9	18.39	4.83	26.27
		Stable	6	4.04	2.98	73.92
10	1.25	Active	7	7.34	2.82	38.39
		Bed	7	16.39	2.69	16.42
		Stable	1	0.19		
11	0.5	Active	5	10.85	6.01	55.41
		Bed	5	15.87	3.07	19.35
	0	Stable	0			

Appendix A-3. Channel bed sediment thickness data.

Channel Bed		Thickness		
Segment	n	Avg (m)	Std	Cv%
1	0	0.33		
2	0	0.33		
3	17	0.33	0.43	129.46
4	3	0.06	0.10	173.21
5	7	0.29	0.20	70.81
6	15	0.32	0.39	121.29
7	7	0.35	0.25	70.85
8	6	0.24	0.19	81.04
9	8	0.26	0.18	69.27
10	9	0.38	0.16	42.34
11	9	0.28	0.34	120.63

Appendix A-4. Active bar sediment thickness data.

Active Bar		Thickness		
Segment	n	Avg (m)	Std	Cv%
1	0	1.28		
2	0	1.28		
3	6	1.28	0.28	21.95
4	1	0.85		
5	5	0.95	0.15	15.84
6	11	1.28	0.48	37.26
7	4	1.13	0.27	24.15
8	5	0.94	0.20	21.48
9	3	1.77	0.21	11.78
10	7	1.00	0.18	18.24
11	10	1.13	0.45	40.02

Appendix A-5. Stable Bar sediment thickness data.

Stable Bar		Total Thickness	Fines Thickness	Coarse Thickness	Total Thickness		Fines Thickness	Fines Thickness
Segment	n	Avg (m)	Avg (m)	(m)	Std	Cv%	Std	Cv%
1	0	1.33	0.33	1.00		45.08		
2	0	1.33	0.33	1.00		45.08		
3	10	1.33	0.33	1.00	0.60	45.08	0.21	63.96
4	3	1.08	0.27	0.82	0.26	23.68	0.12	43.30
5	3	1.12	0.40	0.72	0.34	30.01	0.00	0.00
6	2	0.68	0.35	0.33	0.04	5.24	0.07	20.20
7	1	0.95	0.40	0.55				
8	1	1.05	0.45	0.60				
9	5	2.20	0.40	1.80	0.47	21.56	0.18	45.64
10	2	1.70	0.15	1.55	0.71	41.59	0.07	47.14
11	0							

Appendix A-6. Deposit dimensions for channel bed sediment volume calculation.

	Channel Bed (m)		
Segment	Width	Depth	Length
1	14.82	0.33	1050
2	14.40	0.33	600
3	11.79	0.33	1300
4	13.59	0.06	500
5	15.96	0.29	700
6	11.67	0.32	1450
7	13.71	0.35	550
8	16.58	0.24	900
9	18.39	0.26	900
10	16.39	0.38	750
11	15.87	0.28	500

Appendix A-7. Deposit dimensions for active bar sediment volume calculation.

	Active Bar (m)		
Segment	Width	Depth	Length
1	7.62	1.28	1050
2	3.92	1.28	600
3	7.22	1.28	1300
4	2.43	0.85	500
5	8.22	0.95	700
6	2.34	1.28	1450
7	3.36	1.13	550
8	5.77	0.94	900
9	9.88	1.77	900
10	7.34	1.00	750
11	10.85	1.13	500

Appendix A-8. Deposit dimensions for stable bar sediment volume calculation.

	Stable Bar Coarse (m)		
Segment	Width	Depth	Length
1	8.35	1.00	1050
2	2.70	1.00	600
3	7.53	1.00	1300
4	12.33	0.82	500
5	4.16	0.72	700
6	3.26	0.33	1450
7	4.66	0.55	550
8	9.98	0.60	900
9	4.04	1.80	900
10	0.19	1.55	750
11	0	0	500

Appendix A-9. Deposit dimensions for stable bar sediment volume calculation.

	Stable Bar Fine (m)		
Segment	Width	Depth	Length
1	8.35	0.33	1050
2	2.70	0.33	600
3	7.53	0.33	1300
4	12.33	0.27	500
5	4.16	0.40	700
6	3.26	0.35	1450
7	4.66	0.40	550
8	9.98	0.45	900
9	4.04	0.40	900
10	0.19	0.15	750
11	0	0	500

Appendix A-10. Segment maps. Segment 1.

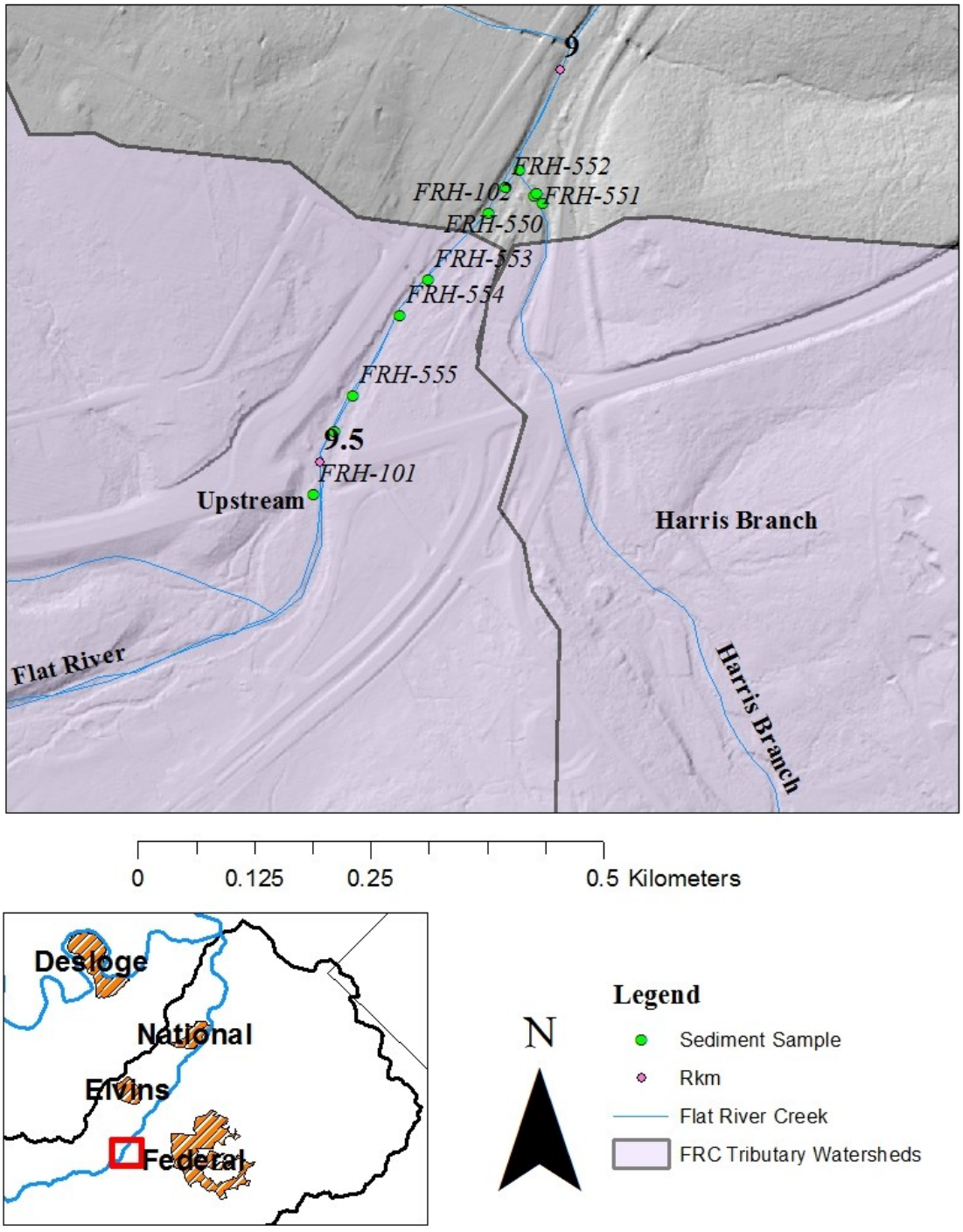

Appendix A-10 continued. Segment 2.

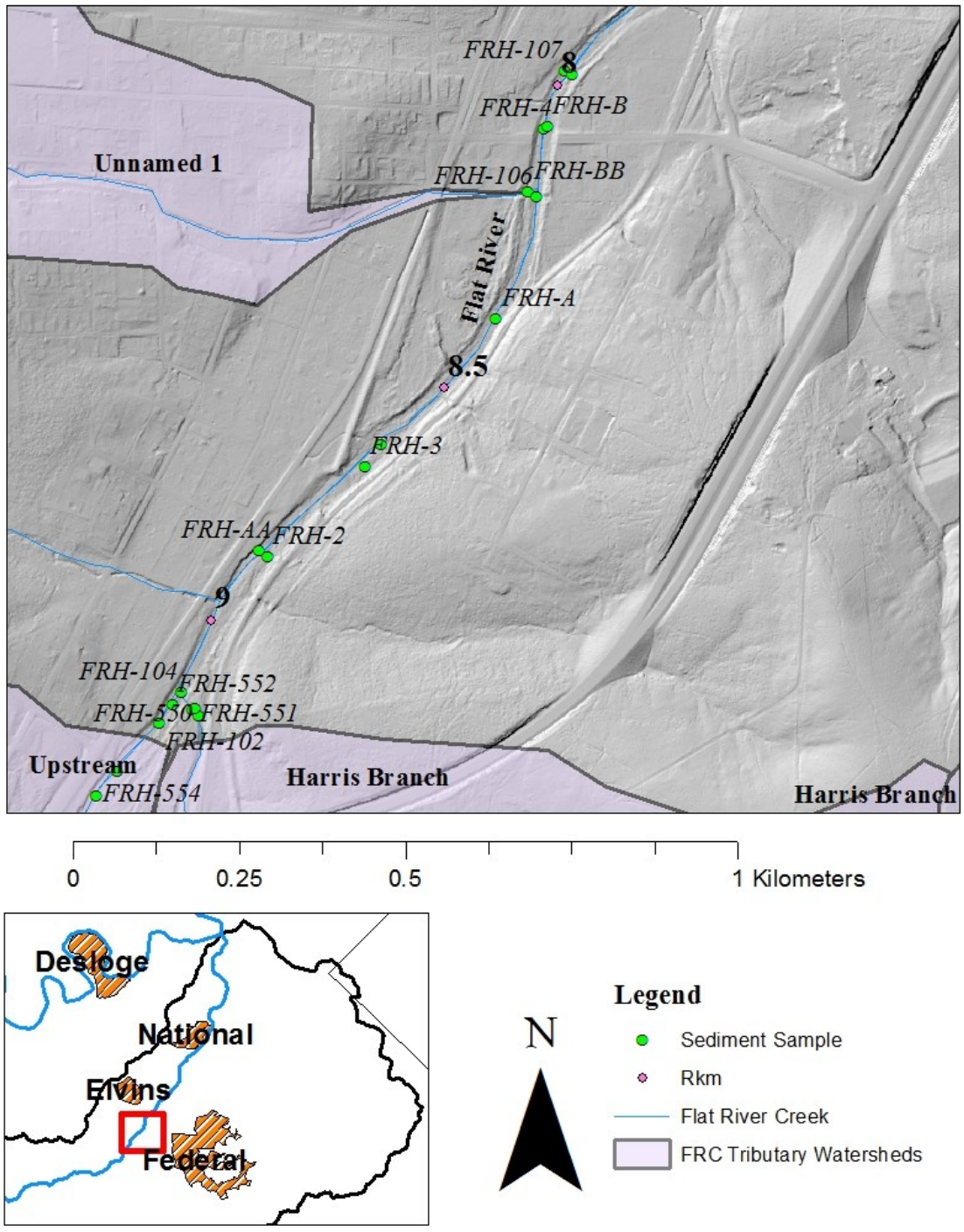

Appendix A-10 continued. Segment 3.

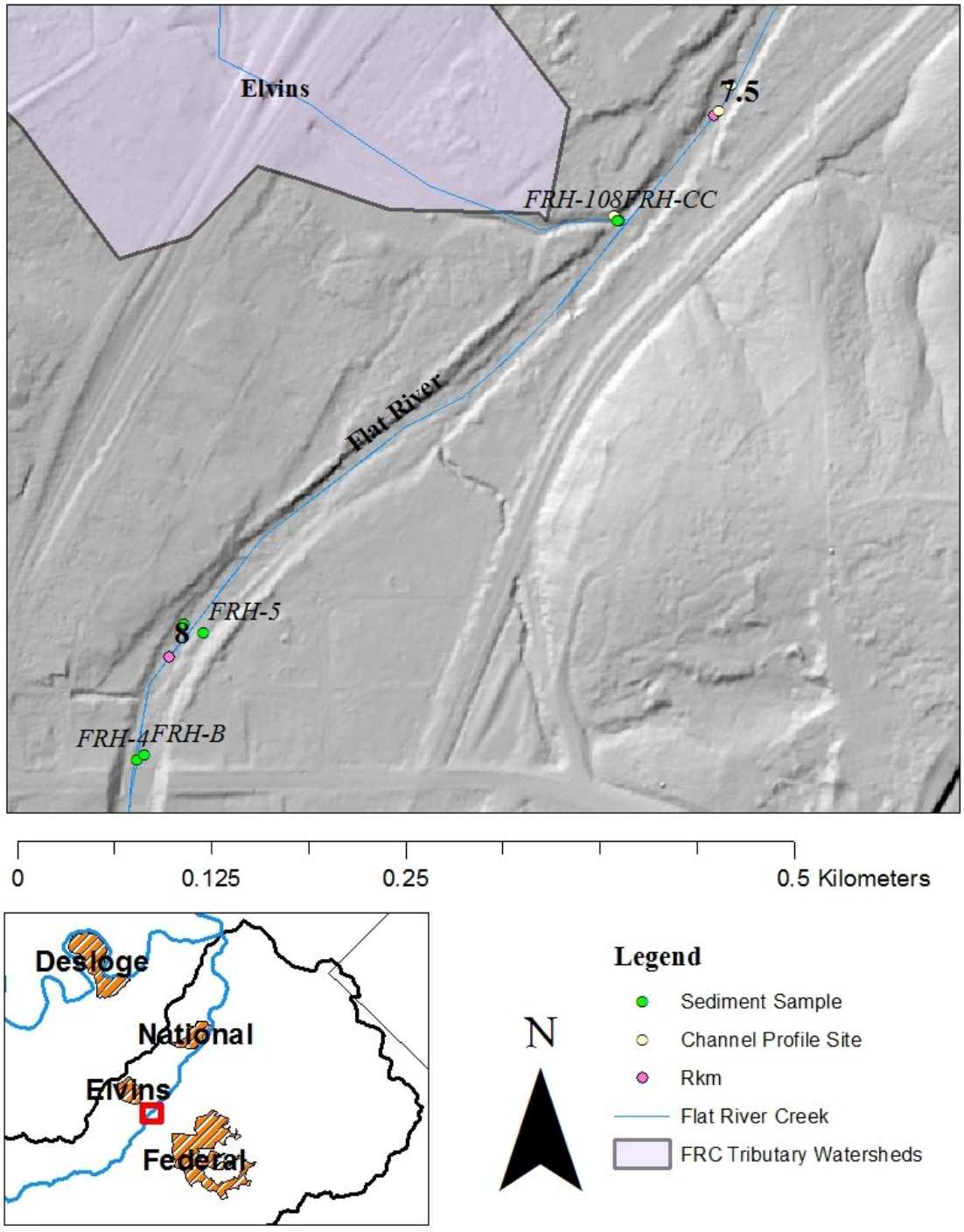

Appendix A-10 continued. Segment 4.

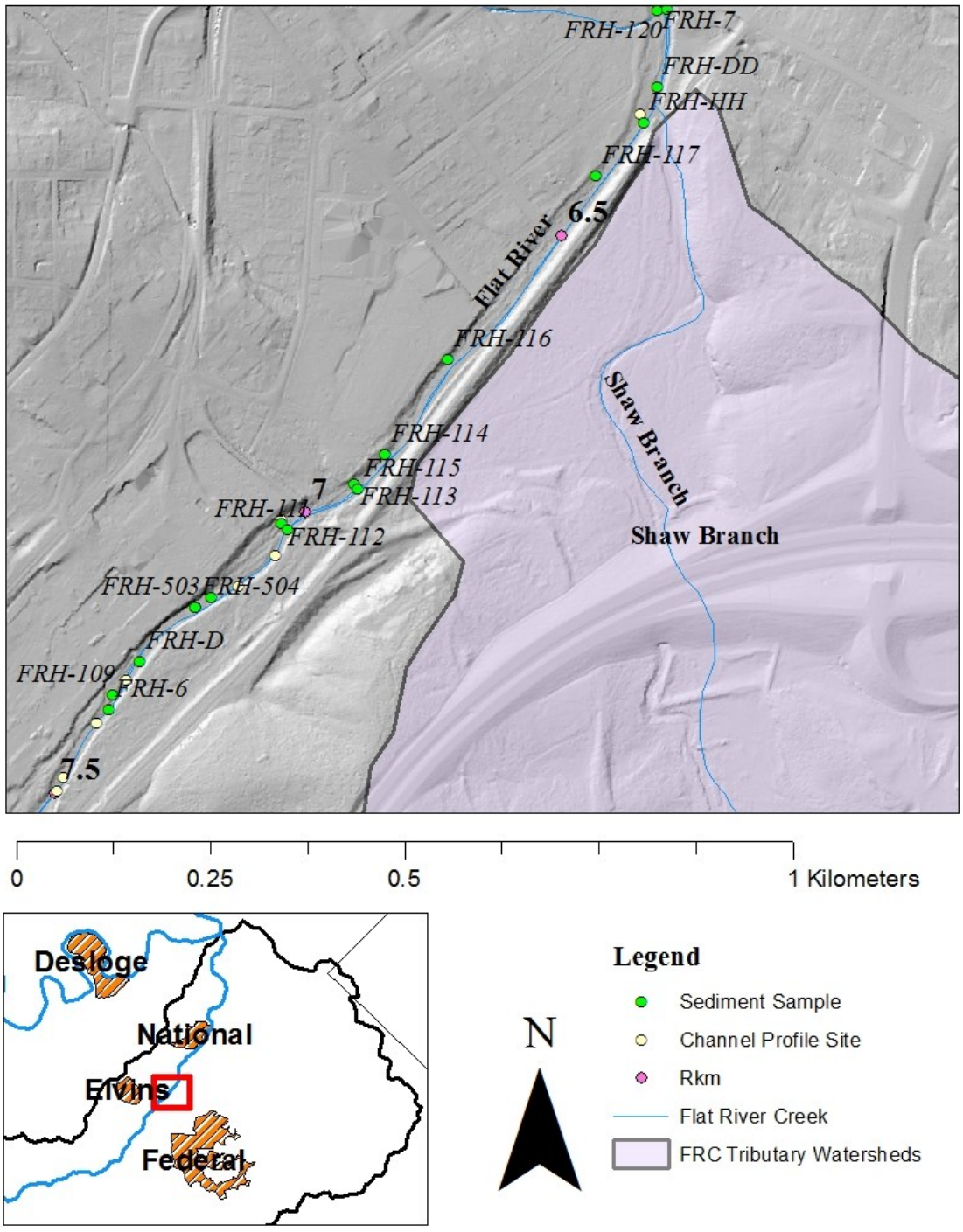

Appendix A-10 continued. Segment 5.

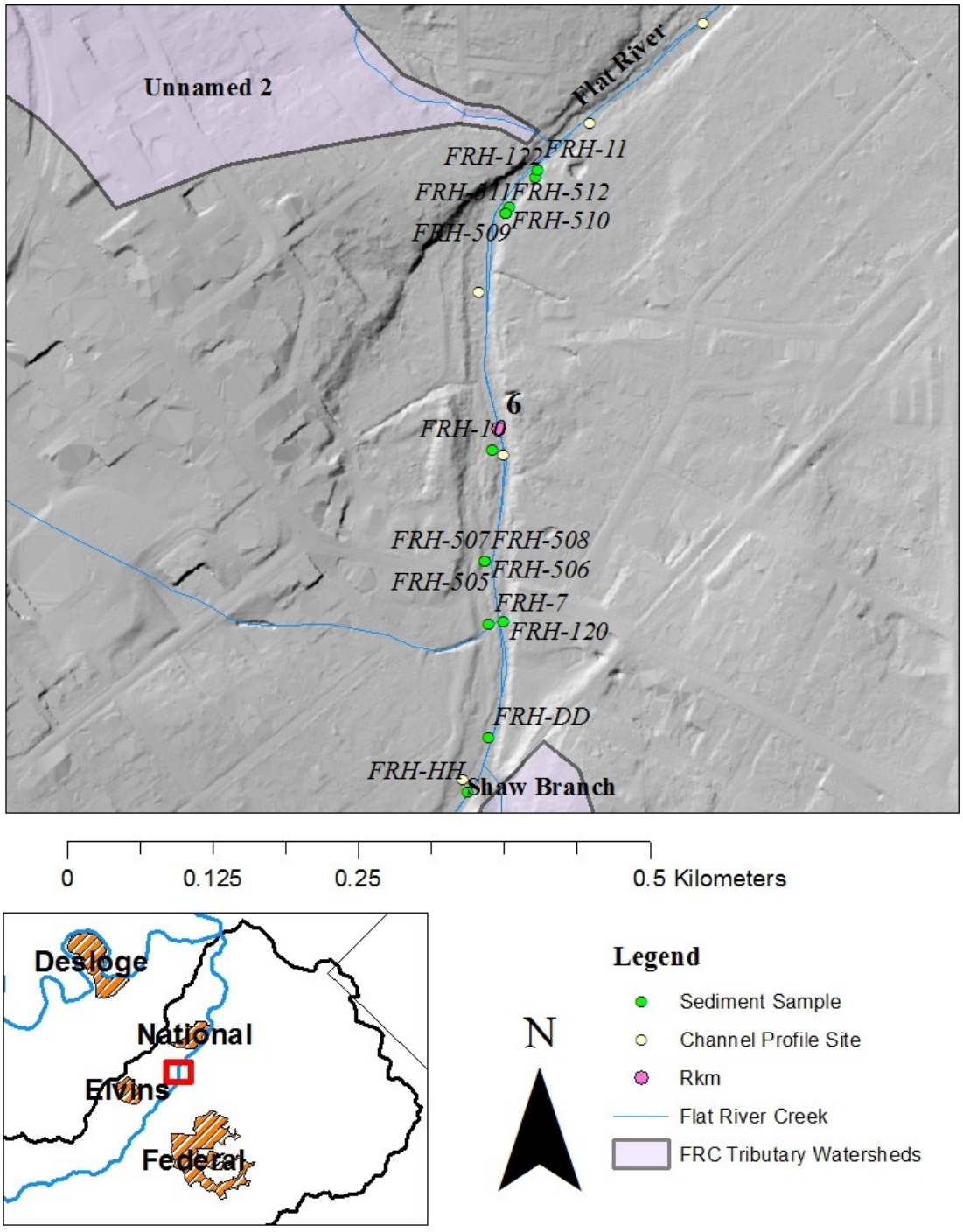

Appendix A-10 continued. Segment 6.

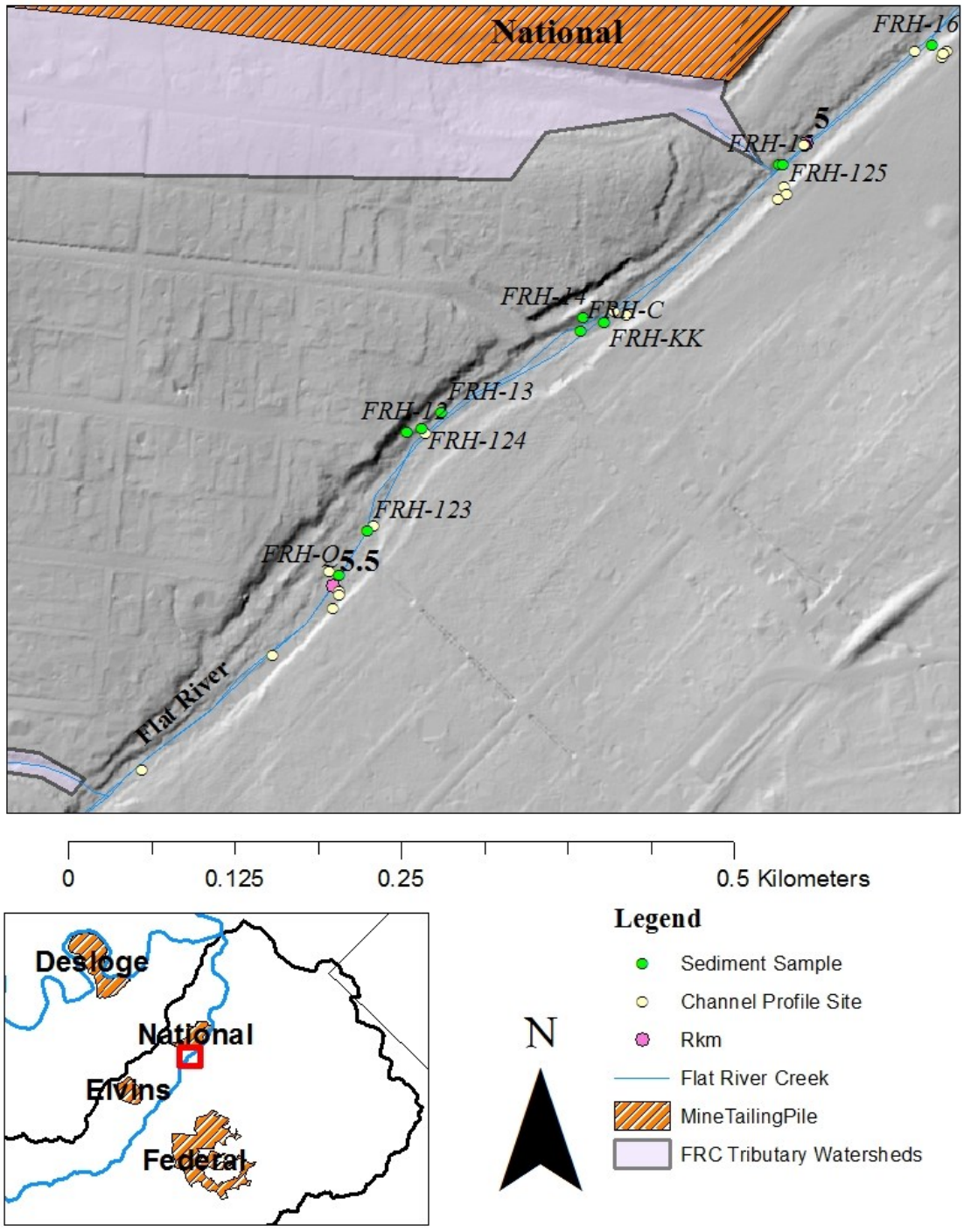

Appendix A-10 continued. Segment 7.

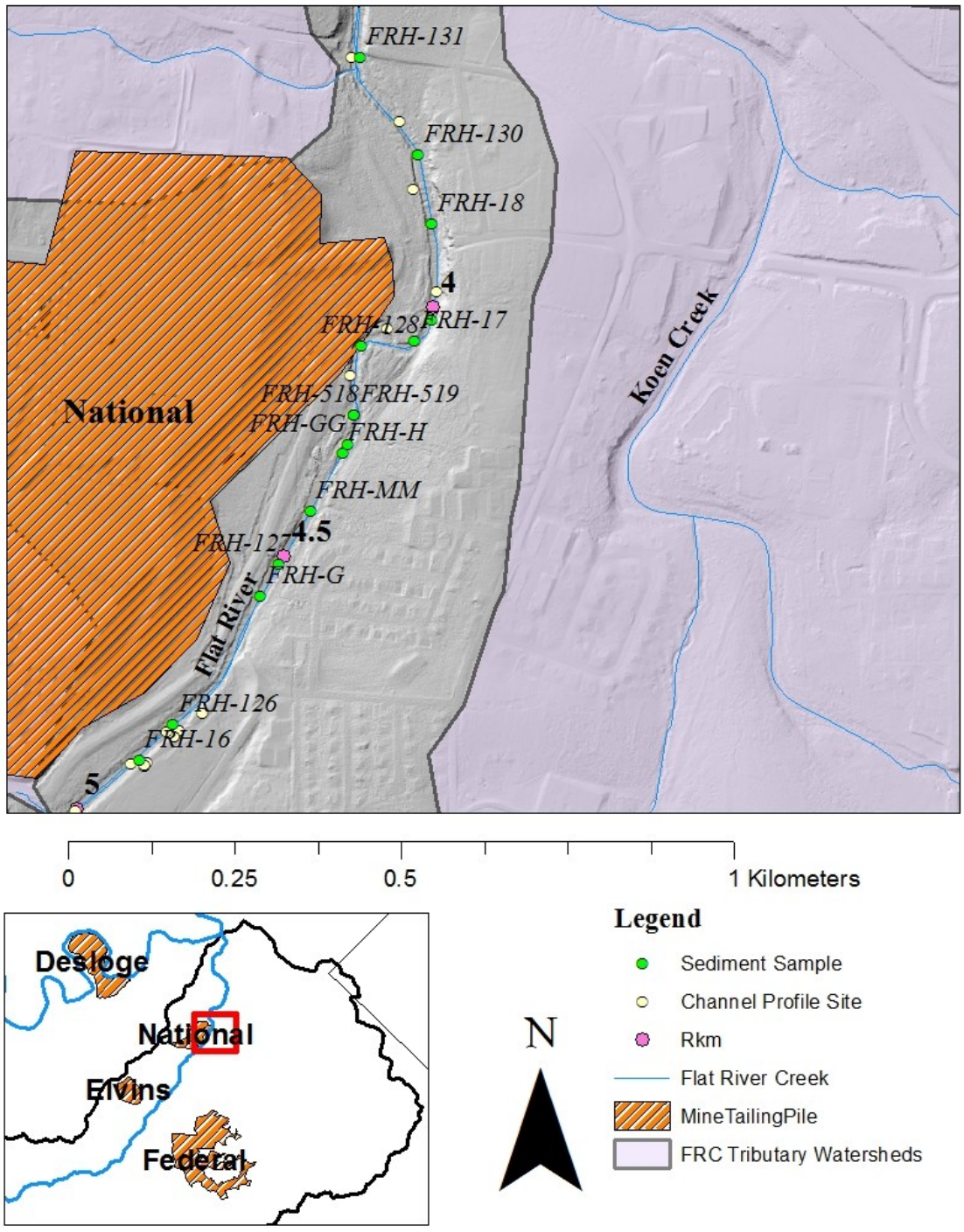

Appendix A-10 continued. Segment 8.

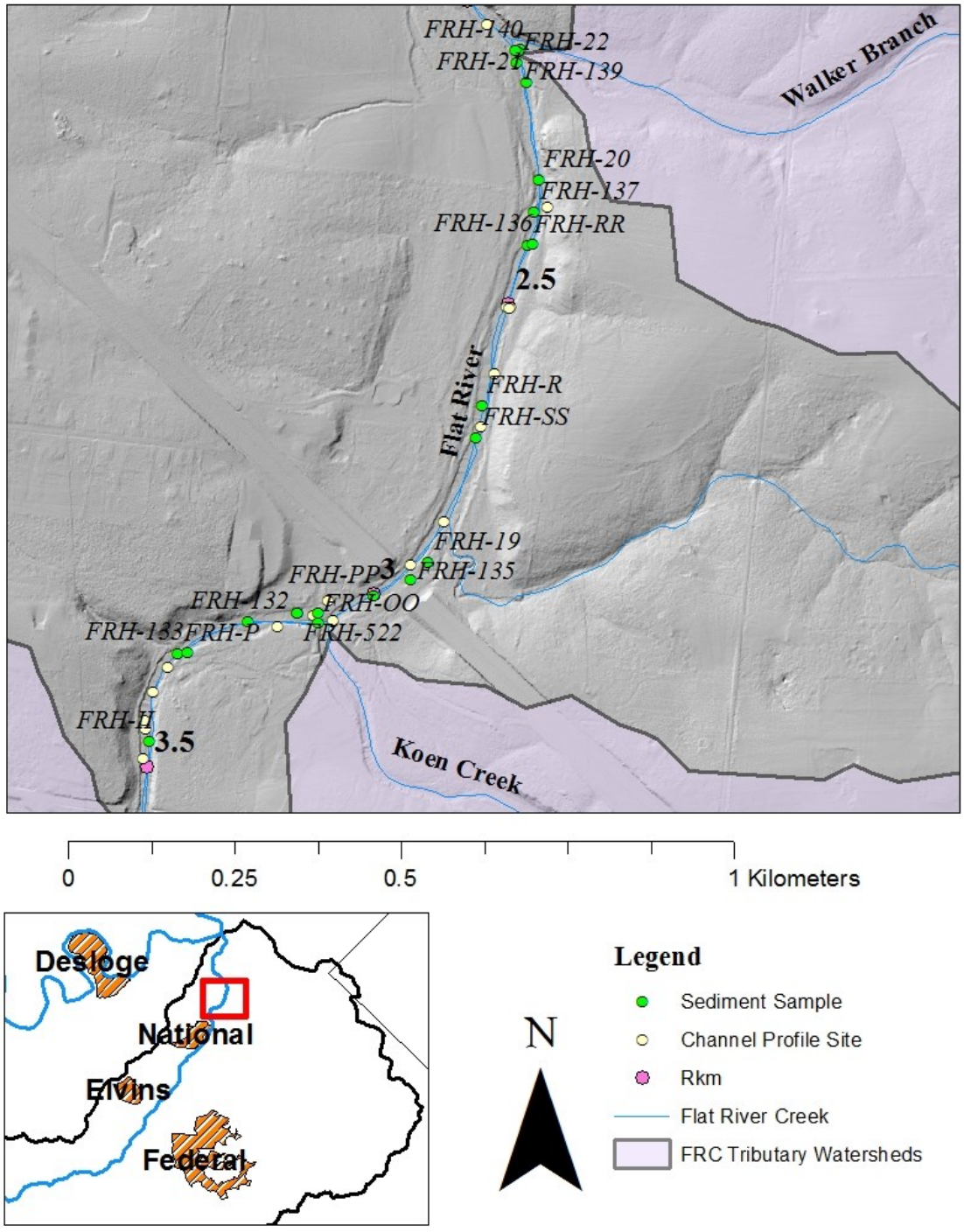

Appendix A-10 continued. Segment 9.

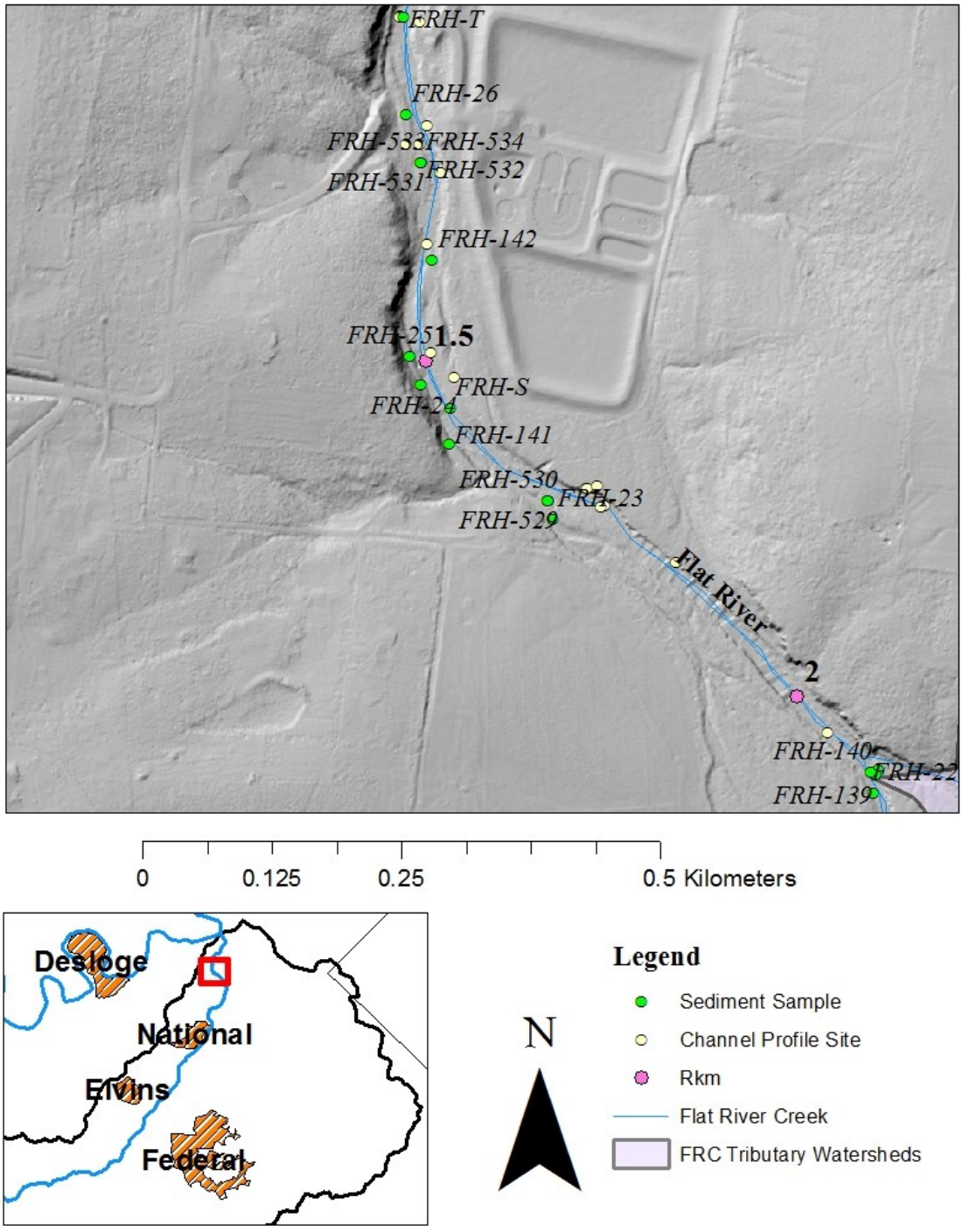

Appendix A-10 continued. Segment 10.

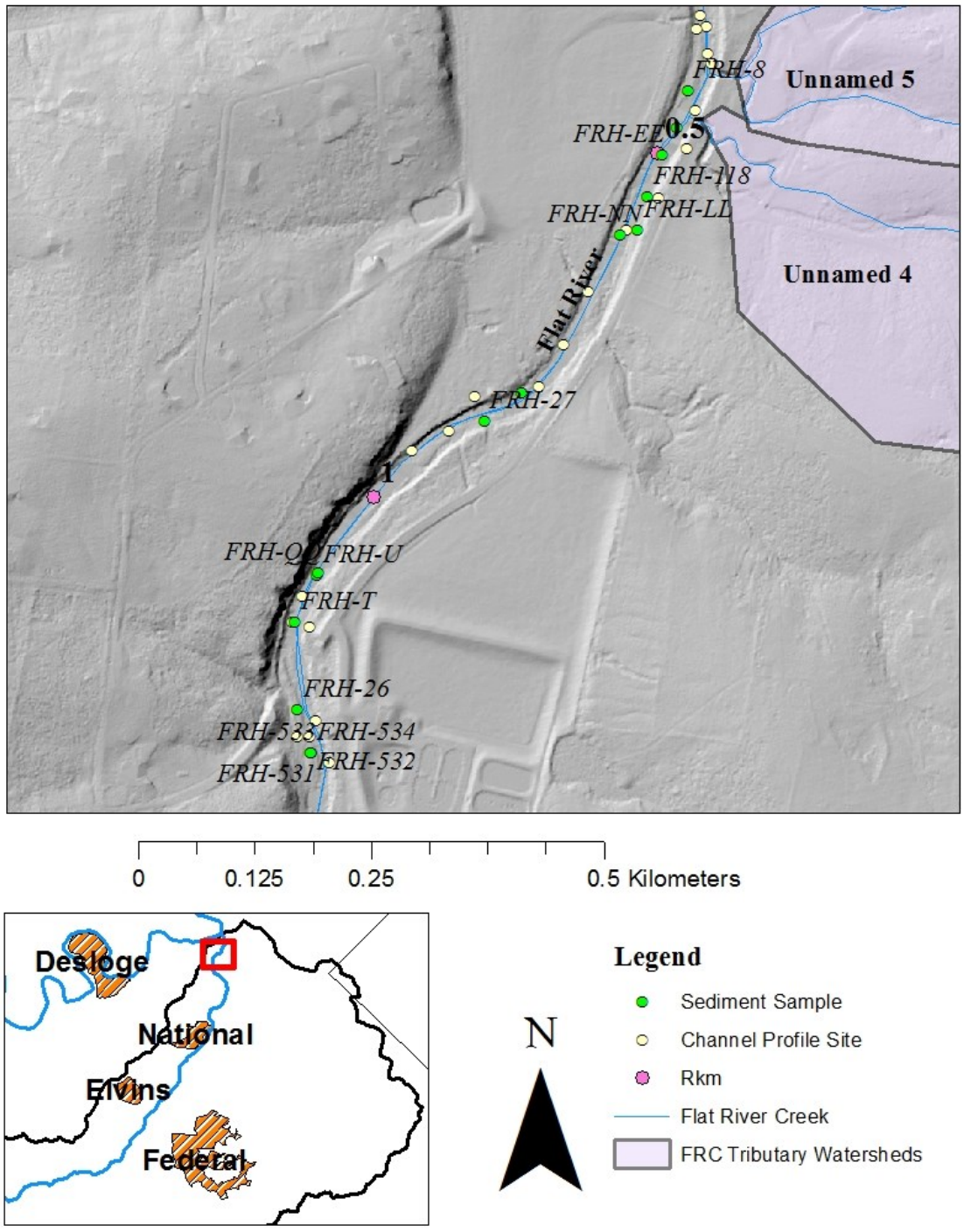

Appendix A-10 continued. Segment 11.

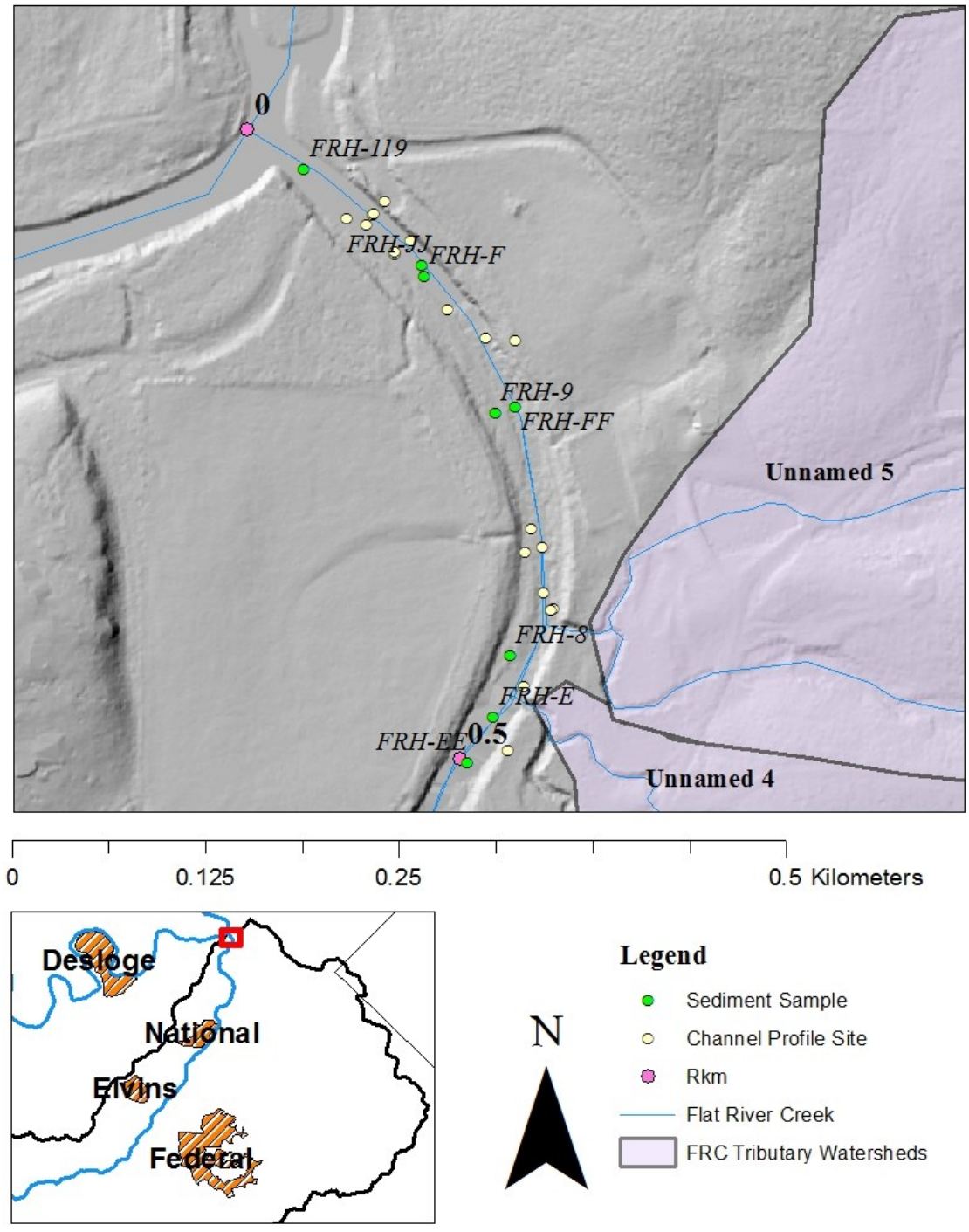

Appendix B-1. Field Data. Width Data.

Rkm	Bank L-Bk (m)	Active Ch. (m)	Bed W (m)	BA W (m)	BS W (m)	Other Unit	Other W (m)	Bank R-Bk (m)	Total Ch. Field (m)
7.444	3	13.6	13.6					0.7	17.3
7.422	2	15.2	15.2					1	18.2
7.4	2.6	11	11					1.7	15.3
7.378	1	19	13		6			8	28
7.356	0.7	18	10		5	Chute	3	0.5	19.2
7.334	2	16	11		5			3	21
7.256	2	23.4	4.9	13	5.5			2.4	27.8
7.204	5	24.4	7	17.4				2.3	31.7
7.152	2	24	7	13	4			0	26
7.1	5	26	8.7	12	5.3			2	33
7.048	1	24	14.3	9.7				0	25
6.996	1.5	26.5	12.5		10	Chute	4	0.5	28.5
6.944	1	16	8.8	7.2				2	19
6.35	1.5	25.3	12.3		13			2	28.8
6.33	1.5	17.8	13.8		4			2	21.3
6.31	5	16.7	16.7					1	22.7
6.3	6	16.3	16.3					1	23.3
6.2	5	27.6	9.1		18.5			3	35.6
6.1	3	37	10	17	10			5	45
5.85	5	19.5	16.8		2.7			2.5	27
5.5	6	30	15	5	10			0.2	36.2
5.45	5	34	17	6.3	11.7			1	40
5.42	5	28	13	8	7			2.5	35.5
5.3	1.5	25.5	15	10.5				2.3	29.3
5.2	3	23.5	16	5		Chute	2.5	5	31.5

Appendix B-1 continued. Width data.

Rkm	Bank L-Bk (m)	Active Ch. (m)	Bed W (m)	BA W (m)	BS W (m)	Other Unit	Other W (m)	Bank R-Bk (m)	Total Ch. Field (m)
5.1	2.4	17.5	17.5					6	25.9
5.06	3	16	16					5	24
5	2	18	10		6.5	Chute	1.5	4	24
4.8	2	20	10		10			2	24
4.77	2	14	9.5	4.5				3	19
4.5	2	16	16					0.5	18.5
4.45	0.7	17.2	17.2					0	17.9
4.4	1	16	16					2	19
4.35	0.5	32	7.7	17.5		2nd Channel	6.8	0.2	32.7
4.28	2	18.5	8.5	10				1.5	22
4.15	0	12.7	7.9	4.8				2.5	15.2
4.02	2	12	6.6	5.4				0	14
3.95	3	14	3	11				2	19
3.9	3	14.5	9.5	5				2	19.5
3.85	1.3	17	17					2	20.3
3.8	3	19.6	10	9.6				0	22.6
3.7	2.3	11.7	9.8	1.9				5	19
3.57	2.4	16	8	5.4	2.6			Bridge	22.4
3.47	1	17.7	17.7					5	23.7
3.4	1	21.7	17.2	4.5				5	27.7
3.3	1.6	14	14					1.5	17.1
3.2	0.5	18	18					1.3	19.8
3.15	1.5	17.5	13	4.5				4	23
3.1	2	26	7	19				1.5	29.5
2.9	0	36	9.7	26.6				0	36

Appendix B-1 continued. Width data.

Rkm	Bank L-Bk (m)	Active Ch. (m)	Bed W (m)	BA W (m)	BS W (m)	Other Unit	Other W (m)	Bank R-Bk (m)	Total Ch. Field (m)
2.75	3	33.4	16.4	17				6	42.4
2.7	1.5	27	27					5	33.5
2.65	1	18.5	18.5					2	21.5
2.6	2	22	22					2	26
2.31	2	37.5	14	10.5	13			0.3	39.8
2.1	2	20	8.5		11.5			1.5	23.5
1.9	1.7	17.5	17.5					2	21.2
1.8	4	19	19					2.5	25.5
1.65	1	46	8		32	Chute	6	0	47
1.6	3	27	17.7		9.3			3	33
1.4	2.7	43	14	19	7.5	Chute	2.5	2	47.7
1.35	4	22	10.1	11.9				3	29
1.3	Bluff	36	11.4		24.6			5	42
1.2	Hill	29	11		18			5	34
1.1	0	19.5	14	5.5				6	25.5
1	0	22.5	22.5					3	25.5
0.95	4	26	7	19				3	33
0.9	2	26	8	18				2	30
0.75	1	22	10.5	11.5				6	29
0.7	3	27	19	8		Bedrock Bench	7.5	3	33
0.65	4	20	15.5	4.5				3	27
0.6	6	28	7.8	11.2		Chute	4	3	37

Appendix B-1 continued. Width data.

Rkm	Bank L-Bk (m)	Active Ch. (m)	Bed W (m)	BA W (m)	BS W (m)	Other Unit	Other W (m)	Bank R-Bk (m)	Total Ch. Field (m)
0.4	5	24	24					6	35
0.35	2	28	11.5	13.5		Bedrock Bench	3	2	32
0.32	5	28	13	11		Chute	4	2	35
0.3	7	27	13.5	13.5				6	40
0.25	10	24	14	10				13	47
0.15	10	25	13	12				5	40
0.1	4	31	16	15				0	35
0.05	2	35	26	9				0	37
0.02	3	30	25	5				3	36

Appendix B-2. Depth and thickness data.

		Bed (m)			BA (m)		BS (m)			Other			
Rkm	L-Bk Ht	Avg	Max	Thick.	Ht	Thick.	Ht	D-fine	Thick.	Unit	Depth (m)	R-Bk Ht	BR%
7.444	1.4	0.468	0.66	0.192								2.2	0
7.422	1	0.6	0.8	0.2								2.2	0
7.4	1.8	0.486	1.15	0.664								1.9	0
7.378	0.06	0.116	1.8	1.684			0.2	0.8	2			1.4	0
7.356	1	0.158	0.36	0.202			0.7		1.06	Chute	0.3	2.4	0
7.334	0.7	0.488	0.8	0.312			0.2	0.4	1			2.5	40
7.256	1.5	0.136	0.68	0.544	0.6	1.28	1	0.2	1.68			1.3	0
7.204	1.7	0.384	0.7	0.316	0.6	1.3						2.2	0
7.152	1.3	0.82	0.9	0.08	0.6	1.5	0.8	0.2	1.7			1.6	100
7.1	1.5	0.604	1	0.396	0.5	1.5	1.5	0.3	2.5			1.8	0
7.048	0.8	0.332	1.2	0.868	0.15	1.35						1.8	0
6.996	0.4	0.15	0.45	0.3		0.45	0.3	0.2	0.75	Chute	0.4	2.1	10
6.944	2	0.6	0.64	0.04	0.1	0.74						1.5	100
6.35	1.4	0.156	0.5	0.344			0.4	0.2	0.9			1.2	100
6.33	1.5	0.236	0.6	0.364			0.1		0.7			0.7	100
6.31	1.7	0.42	0.6	0.18								1.7	100
6.3	1.9	0.248	0.36	0.112								1.9	100
6.2	1.8	0.43	0.6	0.17			0.2	0.2	0.8			1.9	70
6.1	3	0.14	0.65	0.51	0.2	0.85	0.5	0.2	1.15			3	100
5.85	1.5	0.196	0.5	0.304		0.5	0.8	0.4	1.3			1.8	100
5.5	2	0.392	0.6	0.208	0.25	0.85	0.25	0.4	0.85			2.3	100
5.45	2	0.376	0.62	0.244	0.25	0.87	0.4	0.4	1.02			1.9	50
5.42	1.9	0.21	0.8	0.59	0.4	1.2	0.7	0.4	1.5			1.4	0
5.3	1.5	0.186	0.7	0.514	0.3	1						1.4	20
5.2	0.4	0.37	0.65	0.28	0.2	0.85				Chute	0.01	2.6	20

Appendix B-2 continued. Depth and thickness data.

		Bed (m)			BA (m)		BS (m)			Other			
Rkm	L-Bk Ht	Avg	Max	Thick.	Ht	Thick.	Ht	D-fine	Thick.	Unit	Depth (m)	R-Bk Ht	BR%
5.1	1.7	0.188	0.32	0.132								2	10
5.06	1.6	0.184	0.45	0.266								2	10
5	1.5	0.16	0.35	0.19			0.3	0.3	0.65	Chute	0.01	2.5	95
4.8	0.8	0.132	0.3	0.168			0.4	0.4	0.7			1.9	100
4.77	0.5	0.264	0.4	0.136	0.2	0.6						1.9	100
4.5	1.7	0.68	0.8	0.12								1.3	100
4.45	1.4	0.386	0.9	0.514								0.7	100
4.4	1.3	0.442	0.9	0.458								1.4	100
4.35	0.7	0.176	0.7	0.524	1.6	2.3				2nd Channel	0.5	1.7	100
4.28	1.7	0.316	0.8	0.484	0.7	1.5						1.7	50
4.15	2.3	0.184	0.9	0.716	0.3	1.2						2.3	10
4.02	1.2	0.296	0.7	0.404	0.5	1.2						2.5	0
3.95	1.7	0.442	1.7	1.258	0.01	1.71						2	20
3.9	2.2	0.51	0.6	0.09	0.01	0.61						2.2	0
3.85	2.1	0.52	1.05	0.53								2.1	20
3.8	2.6	0.154	0.85	0.696	0.6	1.45						2.6	10
3.7	2.4	0.246	0.9	0.654	0.2	1.1						1.7	20
3.57	1.6	0.288	0.45	0.162	0.3	0.75	0.5	0.4	0.95			1	100
3.47	1.3	0.6	1.1	0.5								6	70
3.4	1.4	0.39	1	0.61	0.2	1.2						6	30
3.3	2	0.646	1.1	0.454								1.3	20
3.2	1.7	0.81	1.2	0.39								1.1	0
3.15	1.5	0.51	1	0.49	0.1	1.1						2	0
3.1	2	0.386	0.48	0.094	1	1.48						1.6	100
2.9	1.1	0.28	0.5	0.22	0.6	1.1						1	50

Appendix B-2 continued. Depth and thickness data

		Bed (m)		BA (m)		BS (m)			Other			
Rkm	L-Bk Ht	Avg	Max	Thick.	Ht	Thick.	Ht	D-fine	Thick.	Unit	Depth (m)	R-Bk Ht	BR%
2.75	1.4	0.22	0.31	0.09	0.6	0.91						1.5	60
2.7	1.6	0.4	1	0.6								1.7	20
2.65	1.1	0.43	0.5	0.07								1.2	60
2.6	1.3	0.55	0.8	0.25								1.2	30
2.31	2.8	0.41	0.6	0.19	0.01	0.61	0.45	0.45	1.05			2.2	60
2.1	1.9	0.36	0.4	0.04		0.4	1.2	0.3	1.6			2.5	100
1.9	1.6	0.57	1	0.43								2.2	100
1.8	2.3	0.53	1	0.47								1.7	20
1.65	1.7	0.326	0.6	0.274			1.3	0.5	1.9	Chute	0.1	5.6	0
1.6	3	0.402	0.6	0.198			1.9	0.6	2.5			2.3	0
1.4	2	0.412	0.8	0.388	1.2	2	2		2.8	Chute	0.01	1.8	20
1.35	3	0.264	0.6	0.336	1	1.6						2.4	20
1.3	Bluff	0.522	0.9	0.378			1.3	0.2	2.2			3	20
1.2	Hill	0.626	0.9	0.274			1.3	0.2	2.2			2.8	20
1.1	Bluff	0.42	1	0.58	0.01	1.01						2.8	0
1	Bluff	0.35	1	0.65								2	0
0.95	3	0.26	0.6	0.34	0.4	1						2.3	0
0.9	3.5	0.15	0.6	0.45	0.5	1.1						2	0
0.75	3	0.37	0.7	0.33	0.3	1						0.8	20
0.7	0.3	0.376	0.6	0.224	0.3	0.9				Bedrock Bench	0.5	1.8	60
0.65	0.2	0.33	0.5	0.17	0.2	0.7						1.7	60
0.6	2.6	0.242	0.6	0.358	0.7	1.3				Chute	0.3	3.5	0

Appendix B-2 continued. Depth and thickness data

		Bed (m)			BA (m)		BS (m)		Other			
Rkm	L-Bk Ht	Avg	Max	Thick.	Ht	Thick.	Ht	D-fine Thick.	Unit	Depth (m)	R-Bk Ht	BR%
0.4	3	0.24	0.5	0.26							3.5	0
0.35	3	0.19	0.3	0.11	0.3	0.6			Bedrock Bench	0.1	3	20
0.32	3	0.148	0.3	0.152	1	1.3			Chute	0.01	3.5	80
0.3	3.5	0.21	0.3	0.09	0.5	0.8					4	100
0.25	3	0.3	0.6	0.3	0.4	1					3	80
0.15	1.5	0.44	0.6	0.16	0.5	1.1					3	0
0.1	2.5	0.36	0.5	0.14	0.8	1.3					3	10
0.05	3.5	0.26	0.5	0.24	0.2	0.7					3	0
0.02	4	0.36	1.5	1.14	0.2	1.7					2.7	0

Appendix C-1. Sediment volumes by segment

	Sediment Storage (m^3)				Sediment Storage	
Segment	Channel Bed	Active Bar	Stable Bar Total	Stable Bar Fines Only	Total (m^3)	Unit (m^3 / 100 m)
1	5,136	10,222	11,663	2,894	27,020	2,573
2	2,851	3,004	2,155	535	8,010	1,335
3	5,121	12,002	13,050	3,228	30,174	2,321
4	385	1,031	6,679	1,644	8,095	1,619
5	3,234	5,492	3,271	1,165	11,998	1,714
6	5,453	4,333	3,186	1,652	12,972	895
7	2,632	2,092	2,433	1,025	7,157	1,301
8	3,530	4,899	9,432	4,042	17,861	1,985
9	4,229	15,703	7,993	1,453	27,925	3,103
10	4,611	5,510	237	21	10,359	1,381
11	2,206	6,133	0	0	8,338	1,668
Average:	3,581	6,402	5,464	1,605		
Sum:	39,388	70,421	60,100	17,659	169,909	

Appendix C-2. Fine sediment volumes by segment

	Sediment Storage < 2 mm (m^3)				Sediment Storage	
Segment	Channel Bed	Active Bar	Stable Bar Total	Stable Bar Fines Only	Total (m^3)	Unit (m^3 / 100 m)
1	924	7,462	8,398	1,997	16,784	1,599
2	998	1,652	1,298	406	3,948	658
3	1,639	4,561	6,444	2,712	12,644	973
4	281	712	4,411	937	5,404	1,081
5	1,067	4,559	2,412	664	8,038	1,148
6	2,290	1,213	1,388	958	4,891	337
7	1,000	1,150	1,379	605	3,530	642
8	1,695	4,017	8,260	3,840	13,971	1,552
9	1,438	10,364	5,435	1,119	17,237	1,915
10	1,476	1,929	92	16	3,496	466
11	706	3,138	0	0	3,843	769
Average:	1,229	3,705	3,592	1,205		
Sum:	13,514	40,756	39,517	13,254	93,787	

Appendix D-1. Sediment Data. FRC main stem sediment sampling.

R-km	Sample ID	Dep. Type	Frac. <2 (%)	Pb (ppm)	Zn (ppm)	Ca (ppm)
9.5	FRH-101	Active Bar	34.47	91	51	13,457
9.45	FRH-1	Shadow Bar	45.41	47	36	2,419
9.15	FRH-102	Shadow Bar	94.63	110	84	13,276
9.1	FRH-103	Glide	23.60	657	165	33,303
9.1	FRH-104	Active Bar	50.59	238	57	33,106
8.85	FRH-2	Stable Bar	53.75	251	89	15,245
8.85	FRH-AA	Glide	9.10	109	61	19,271
8.65	FRH-3	Stable Bar	77.56	135	51	14,948
8.62	FRH-105	Stable Bar	78.54	223	103	17,100
8.35	FRH-A	Glide	23.38	175	62	18,227
8.15	FRH-106	Shadow Bar	52.64	90	44	16,286
8.15	FRH-BB	Active Bar	96.59	1,762	886	84,473
8.06	FRH-4	Glide	49.29	492	469	68,195
8.05	FRH-B	Glide	23.04	379	200	47,247
7.95	FRH-5	Shadow Bar	76.55	108	62	15,764
7.95	FRH-107	Stable Bar	76.92	279	111	14,997
7.6	FRH-108	Pool	50.88	1,602	73,769	45,699
7.6	FRH-CC	Glide	19.28	491	25,945	18,232
7.35	FRH-6	Glide	20.04	222	6,430	21,214
7.35	FRH-109	Stable Bar	73.33	1,163	8,886	47,824
7.27	FRH-D	Glide	14.15	357	1,844	20,403
7.15	FRH-110	Pool/Glide	31.37	418	2,877	24,438
7.02	FRH-111	Glide	28.56	432	4,461	30,003
7.02	FRH-112	Shadow Bar	77.83	276	605	26,215
6.9	FRH-113	Stable Bar	95.39	452	925	29,329
6.9	FRH-115	Pool	69.77	303	1,746	20,679
6.3	FRH-HH	Pool	26.80	435	1,559	49,534
6.25	FRH-DD	Glide	35.05	3,104	610	107,582
6.15	FRH-7	Active Bar	79.66	729	982	70,974

Appendix D-1 continued. FRC main stem sediment sampling.

R-km	Sample ID	Dep. Type	Frac. <2 (%)	Pb (ppm)	Zn (ppm)	Ca (ppm)
6.15	FRH-120	Pool	73.73	889	943	93,406
6	FRH-10	Active Bar	98.33	575	785	56,282
5.8	FRH-121	Active Bar	30.85	792	948	73,533
5.75	FRH-122	Shadow Bar	82.98	449	876	44,767
5.74	FRH-11	Active Bar	78.89	994	843	64,442
5.45	FRH-Q	Glide	24.33	832	4,242	52,018
5.43	FRH-123	Pool	60.62	3,318	1,136	69,491
5.35	FRH-12	Stable Bar	57.82	2,190	1,775	43,898
5.35	FRH-124	Shadow Bar	47.86	569	850	55,572
5.34	FRH-13	Shadow Bar	51.19	1,823	967	74,553
5.2	FRH-14	Active Bar	87.22	1,556	1,404	51,627
5.2	FRH-C	Glide	19.93	790	1,617	77,857
5.2	FRH-KK	Pool/Glide	30.52	1,260	1,594	73,757
5.02	FRH-15	Shadow Bar	94.43	3,465	985	50,719
5.02	FRH-125	Shadow Bar	96.39	2,142	681	129,729
4.85	FRH-16	Active Bar	31.19	970	1,508	64,310
4.8	FRH-126	Shadow Bar	60.42	3,638	1,599	56,582
4.55	FRH-G	Pool	21.75	1,336	818	76,285
4.5	FRH-127	Pool	21.03	942	1,278	82,941
4.4	FRH-MM	Pool	28.68	1,925	1,456	103,822
4.3	FRH-H	Glide	41.89	1,560	999	97,603
4.27	FRH-GG	Pool	59.92	1,787	1,298	105,503
4.13	FRH-128	Pool	55.20	1,395	754	86,571
4.05	FRH-17	Active Bar	26.44	3,271	1,299	93,867
4.025	FRH-129	Pool	66.59	1,388	346	101,873
3.87	FRH-18	Pool	43.54	908	550	112,375
3.77	FRH-130	Shadow Bar	50.49	1,618	638	98,043

Appendix D-1 continued. FRC main stem sediment sampling.

R-km	Sample ID	Dep. Type	Frac. <2 (%)	Pb (ppm)	Zn (ppm)	Ca (ppm)
3.57	FRH-131	Stable Bar	51.59	2,628	2,052	79,931
3.45	FRH-II	Pool	31.71	1,653	1,127	109,779
3.3	FRH-P	Pool	36.24	1,404	339	131,930
3.27	FRH-133	Stable Bar	87.92	4,694	513	138,078
3.17	FRH-132	Glide	54.78	3,359	824	138,442
3.07	FRH-134	Stable Bar	39.23	2,976	1,915	78,877
3.07	FRH-OO	Glide	29.67	1,597	296	20,452
2.98	FRH-PP	Pool	75.26	2,450	733	119,529
2.95	FRH-135	Active Bar	68.77	1,879	455	94,826
2.89	FRH-19	Stable Bar	95.44	1,592	399	82,851
2.7	FRH-SS	Pool	41.95	1,754	1,043	104,543
2.65	FRH-R	Pool	29.96	1,442	493	105,619
2.4	FRH-RR	Pool	37.20	5,420	855	110,803
2.398	FRH-136	Shadow Bar	57.74	5,106	935	119,444
2.35	FRH-137	Active Bar	96.68	949	516	91,678
2.3	FRH-20	Glide	56.64	1,350	680	108,329
2.15	FRH-21	Glide	48.74	1,663	531	121,687
2.13	FRH-22	Stable Bar	70.81	2,428	384	119,635
2.12	FRH-139	Stable Bar	80.51	459	202	24,562
2.12	FRH-140	Pool	43.87	295	233	14,918
1.7	FRH-23	Glide	31.89	2,351	694	106,066
1.6	FRH-141	Stable Bar	82.22	2,090	1,770	92,896
1.55	FRH-S	Glide	26.98	983	580	87,223
1.52	FRH-24	Active Bar	62.36	1,124	351	82,231
1.5	FRH-25	Active Bar	70.83	577	243	61,398
1.4	FRH-142	Shadow Bar	28.08	1,429	1,130	76,611
1.25	FRH-26	Active Bar	41.19	1,347	600	108,776
1.15	FRH-T	Glide	41.16	804	432	109,204

Appendix D-1 continued. FRC main stem sediment sampling.

R-km	Sample ID	Dep. Type	Frac. <2 (%)	Pb (ppm)	Zn (ppm)	Ca (ppm)
1.1	FRH-U	Glide	30.02	1,474	296	110,798
1.1	FRH-QQ	Pool	27.76	1,136	480	112,856
0.85	FRH-27	Active Bar	38.94	1,730	460	101,664
0.8	FRH-143	Active Bar	29.45	1,692	624	63,655
0.6	FRH-NN	Pool	32.80	1,138	427	91,881
0.57	FRH-LL	Active Bar	30.49	1,388	685	92,508
0.55	FRH-118	Shadow Bar	62.67	1,033	648	100,549
0.5	FRH-EE	Glide	35.95	1,840	1,069	99,446
0.47	FRH-E	Pool	20.23	1,534	559	33,179
0.45	FRH-8	Stable Bar	28.06	1,612	649	76,712
0.25	FRH-9	Active Bar	51.16	895	221	118,170
0.25	FRH-FF	Glide	20.66	1,600	682	110,425
0.15	FRH-F	Pool	33.41	1,577	806	115,980
0.15	FRH-JJ	Glide	44.60	924	827	67,175
0.04	FRH-119	Pool	43.44	1,298	616	87,573

Appendix D-2. FRC bar core sediment sampling.

R-km	Sample ID	Dep. Type	Depth (cm)	Fract <2 (%)	Pb (ppm)	Zn (ppm)	Ca (ppm)
7.2	FRH-500	Active Bar	0-10	34	496	881	29,659
7.2	FRH-501	Active Bar	10-20	31	860	1,148	48,294
7.2	FRH-502	Active Bar	20-30	23	638	1,178	37,637
7.2	FRH-503	Active Bar	30-40	33	546	904	46,196
7.2	FRH-504	Active Bar	40-50	44	950	1,195	56,168
6.1	FRH-505	Stable Bar	0-10	83	740	1,346	43,665
6.1	FRH-506	Stable Bar	10-20	41	3,189	1,248	71,523
6.1	FRH-507	Stable Bar	20-30	83	2,834	538	153,547
6.1	FRH-508	Stable Bar	30-40	85	2,627	302	164,979
5.8	FRH-509	Active Bar	0-10	42	1,004	1,024	64,257
5.8	FRH-510	Active Bar	10-20	47	1,023	1,181	70,924
5.8	FRH-511	Active Bar	20-30	64	672	810	56,069
5.8	FRH-512	Active Bar	30-40	58	1,150	1,854	38,062
4.25	FRH-513	Stable Bar	0-10	56	957	398	80,061
4.25	FRH-514	Stable Bar	10-20	39	1,132	742	102,137
4.25	FRH-515	Stable Bar	20-30	43	747	483	98,093
4.25	FRH-516	Stable Bar	30-40	45	1,003	503	95,145
4.25	FRH-517	Stable Bar	40-50	47	1,260	613	85,869
4.25	FRH-518	Stable Bar	50-60	56	1,153	536	96,193
4.25	FRH-519	Stable Bar	60-70	65	1,896	599	99,663
3.15	FRH-520	Stable Bar	0-10	19	2,399	824	92,163
3.15	FRH-521	Stable Bar	10-20	14	2,069	907	82,375
3.15	FRH-522	Stable Bar	20-30	7	2,280	848	90,331
1.68	FRH-525	Active Bar	0-10	52	1,213	413	101,188
1.68	FRH-526	Active Bar	10-20	40	1,115	538	82,847
1.68	FRH-527	Active Bar	20-30	63	1,248	405	91,776
1.68	FRH-528	Active Bar	30-40	78	1,163	485	82,914
1.68	FRH-529	Active Bar	40-50	63	1,856	888	90,311

Appendix D-2 continued. FRC bar core sediment sampling.

R-km	Sample ID	Dep. Type	Depth (cm)	Fract <2 (%)	Pb (ppm)	Zn (ppm)	Ca (ppm)
1.68	FRH-530	Active Bar	50-60	40	1,333	374	124,076
1.3	FRH-531	Stable Bar	0-10	20	1,915	516	70,475
1.3	FRH-532	Stable Bar	10-20	26	2,752	494	95,534
1.3	FRH-533	Stable Bar	20-30	43	4,443	649	124,952
1.3	FRH-534	Stable Bar	30-40	41	3,937	705	115,712

Appendix D-3. Bar core cross-section for R-km 7.2

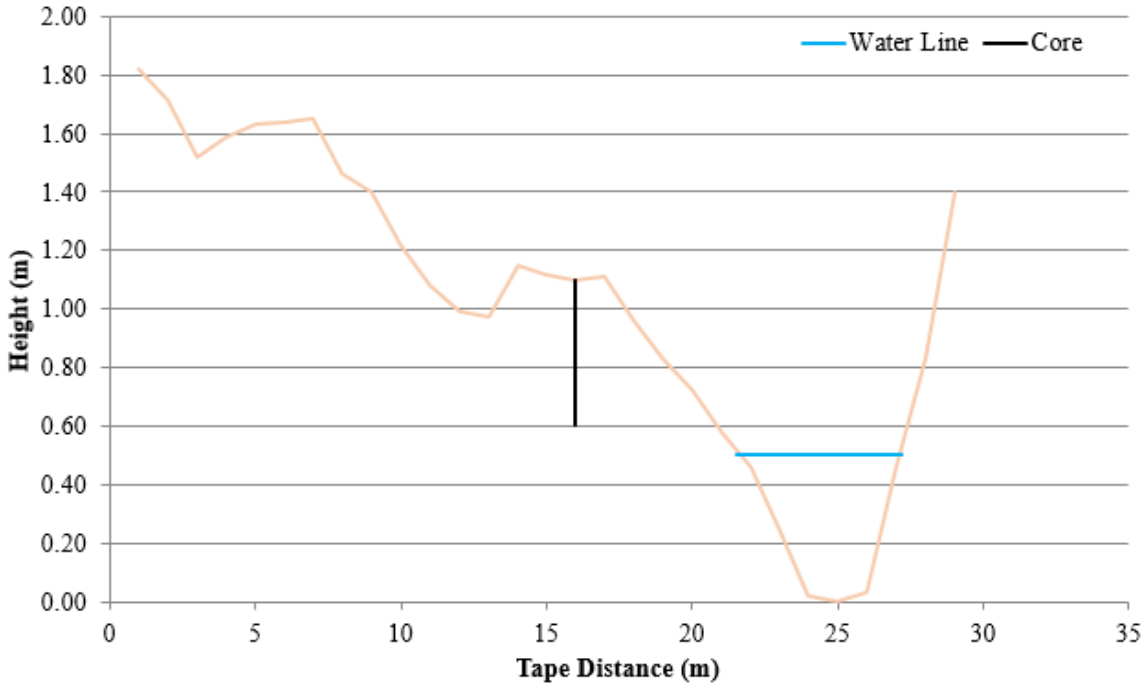

		Metals (ppm)		
Depth (cm)	Percent <2 mm	Pb	Zn	Ca
0-10	33.66	496	881	29,659
10-20	30.53	860	1,148	48,294
20-30	23.48	638	1,178	37,637
30-40	33.13	546	904	46,196
40-50	44.05	950	1,195	56,168
Average	32.97	698	1,061	43,591
Standard Deviation	7.41	198	155	10,206
CV%	22.46	28	15	23

Appendix D-4. Bar core cross-section for R-km 6.0

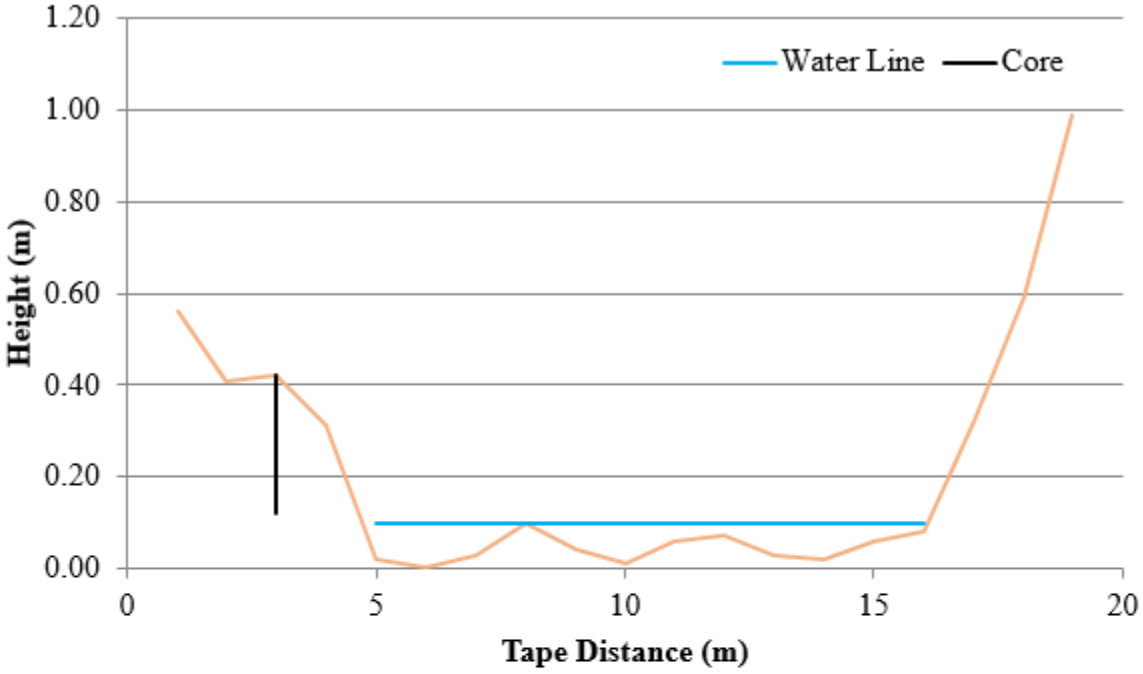

		Metals (ppm)		
Depth (cm)	Percent <2 mm	Pb	Zn	Ca
0-10	83.23	740	1,346	43,665
10-20	41.09	3,189	1,248	71,523
20-30	83.39	2,834	538	153,547
30-40	84.67	2,627	302	164,979
Average	73.09	2,347	858	108,429
Standard Deviation	21.35	1,097	517	59,972
CV%	29.21	47	60	55

Appendix D-5. Bar core cross-section for R-km 5.8

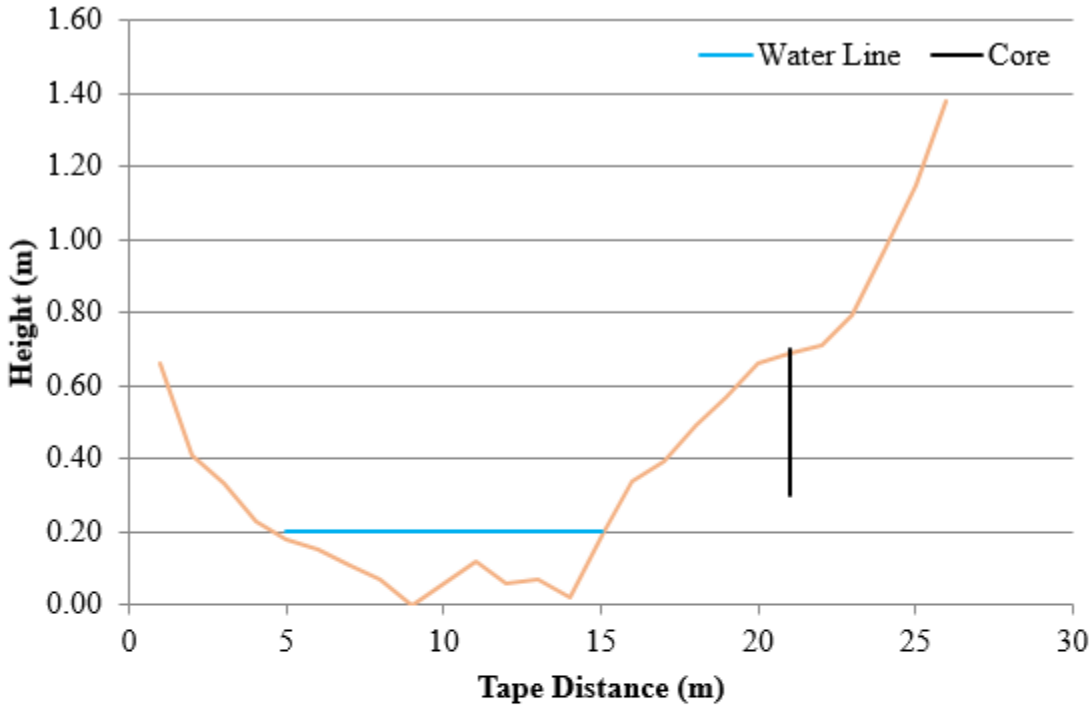

		Metals (ppm)		
Depth (cm)	Percent <2 mm	Pb	Zn	Ca
0-10	42.01	1,004	1,024	64,257
10-20	47.38	1,023	1,181	70,924
20-30	63.59	672	810	56,069
30-40	57.83	1,150	1,854	38,062
Average	52.70	962	1,217	57,328
Standard Deviation	9.79	204	451	14,208
CV%	18.58	21	37	25

Appendix D-6. Bar core cross-section for R-km 4.25

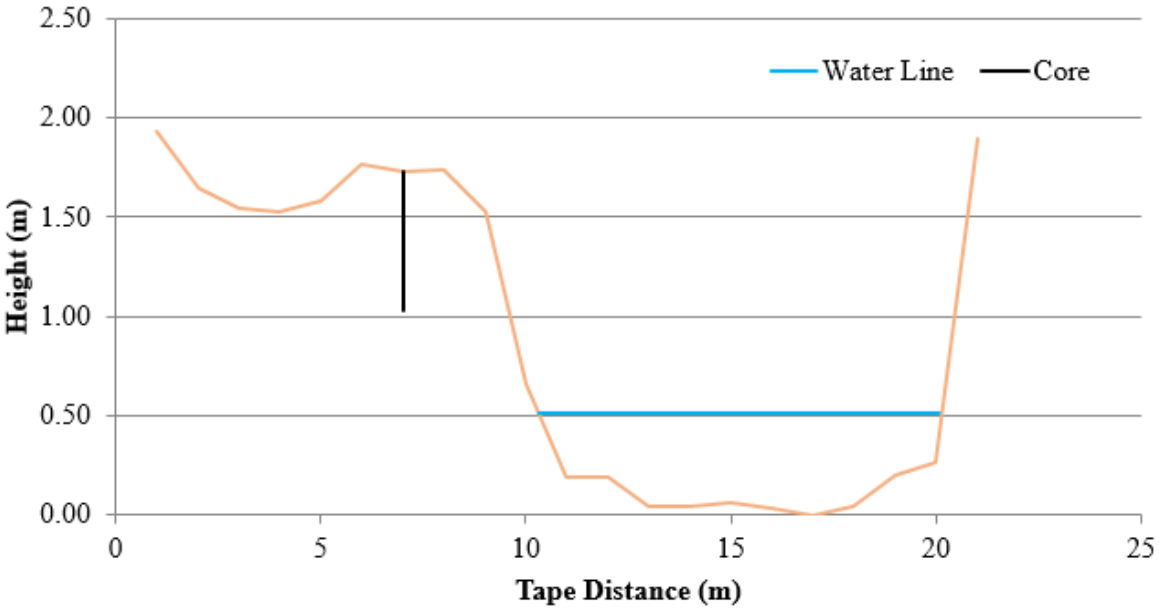

		Metals (ppm)		
Depth (cm)	Percent <2 mm	Pb	Zn	Ca
0-10	56.02	957	398	80,061
10-20	39.09	1,132	742	102,137
20-30	42.90	747	483	98,093
30-40	44.61	1,003	503	95,145
40-50	46.99	1,260	613	85,869
50-60	55.69	1,153	536	96,193
60-70	64.96	1,896	599	99,663
Average	50.04	1,164	553	93,880
Standard Deviation	9.13	363	110	7,973
CV%	18.24	31	20	8

Appendix D-7. Bar core cross-section for R-km 1.68

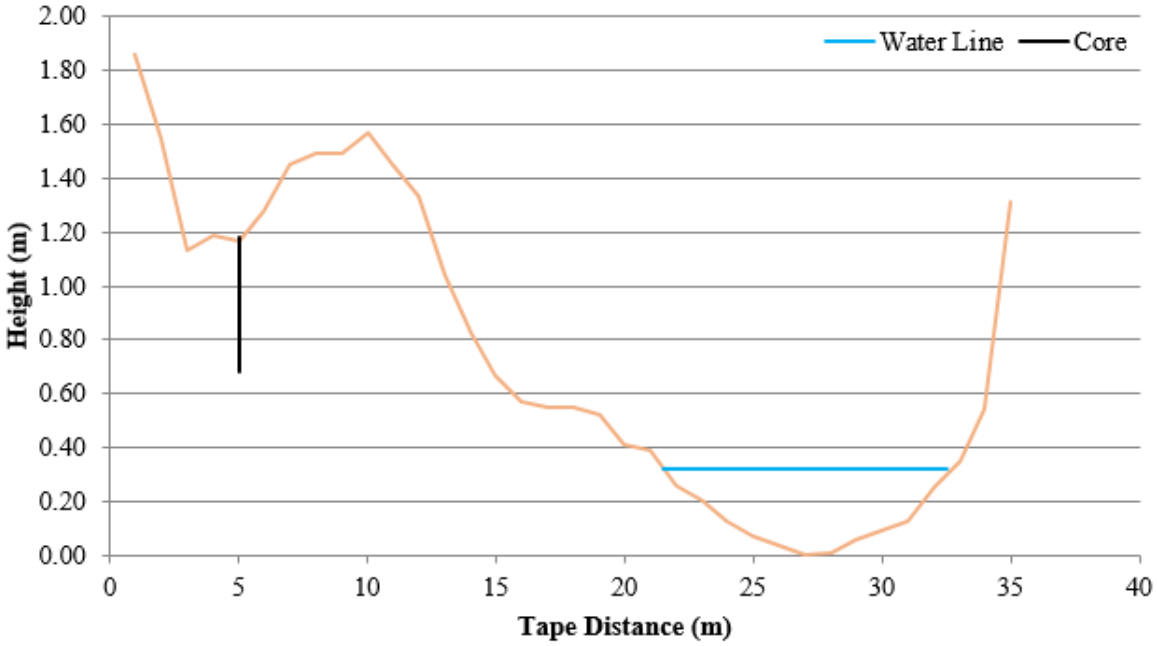

		Metals (ppm)		
Depth (cm)	Percent <2 mm	Pb	Zn	Ca
0-10	52.29	1,213	413	101,188
10-20	39.85	1,115	538	82,847
20-30	62.82	1,248	405	91,776
30-40	77.69	1,163	485	82,914
40-50	63.41	1,856	888	90,311
50-60	40.00	1,333	374	124,076
Average	56.01	1,321	517	95,519
Standard Deviation	14.85	272	191	15,545
CV%	26.51	21	37	16

Appendix D-8. Bar core cross-section for R-km 1.3

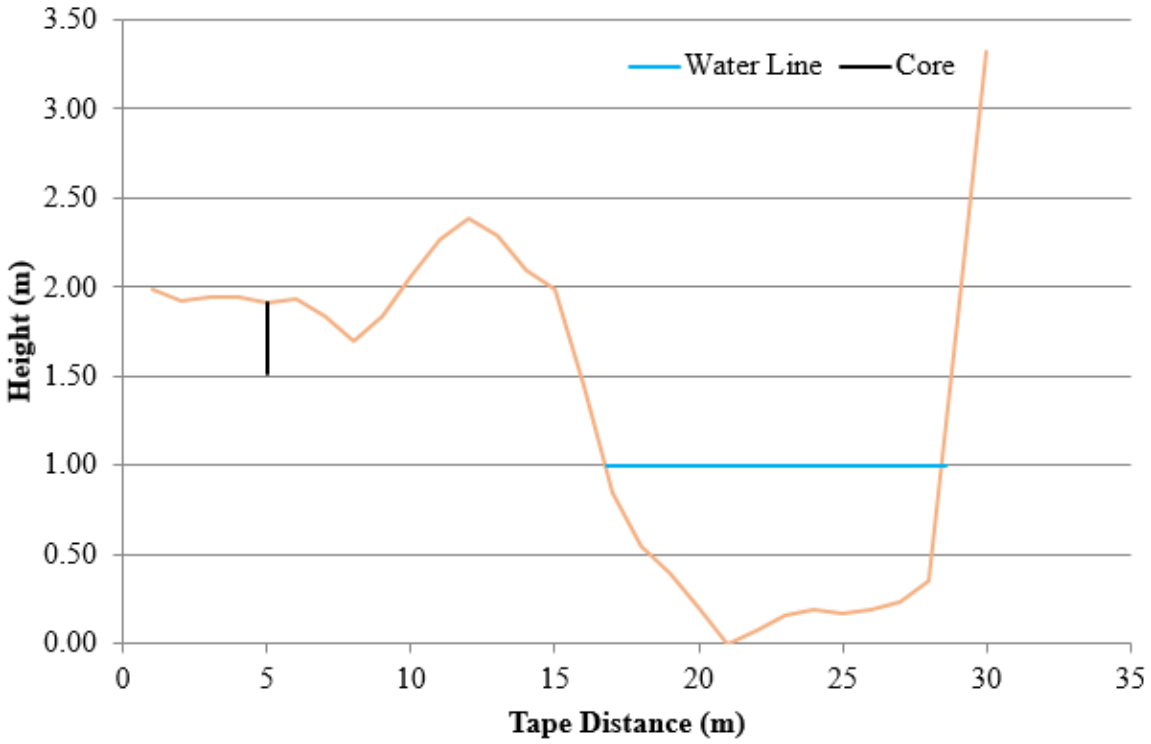

		Metals (ppm)		
Depth (cm)	Percent <2 mm	Pb	Zn	Ca
0-10	20.45	1,915	516	70,475
10-20	26.32	2,752	494	95,534
20-30	42.59	4,443	649	124,952
30-40	41.11	3,937	705	115,712
Average	32.62	3,262	591	101,668
Standard Deviation	10.95	1,144	102	24,153
CV%	33.56	35	17	24

Appendix D-9. Upstream Sediment Samples

R-km	Sample ID	Dep. Type	Frac. <2 (%)	Pb (ppm)	Zn (ppm)	Ca (ppm)
9.1	FRH-550	Active Bar	21.72	544	113	32,112
9.1	FRH-551	Active Bar	27.67	773	44	47,222
9.125	FRH-552	Pool/Glide	31.36	106	51	51,888
9.25	FRH-553	Pool/Glide	20.52	73	64	16,961
9.3	FRH-554	Pool/Glide	25.44	62	42	23,451
9.4	FRH-555	Pool/Glide	20.04	55	48	12,645
10.3	FRH-556	Pool/Glide	23.30	54	41	13,275
10.35	FRH-557	Active Bar	84.58	34	23	5,177
10.43	FRH-558	Active Bar	21.94	265	191	21,542
10.49	FRH-559	Pool/Glide	22.61	37	32	8,798
10.53	FRH-560	Pool/Glide	24.52	39	24	7,984
12.7	FRH-561	Pool/Glide	27.22	44	42	32,234
12.75	FRH-562	Pool/Glide	43.26	44	28	19,858
12.85	FRH-563	Active Bar	30.42	32	33	14,390
12.9	FRH-564	Active Bar	18.60	ND	20	9,580
12.92	FRH-565	Pool/Glide	39.22	50	47	7,230

Appendix D-10. Summary of XRF accuracy and precision for all sediment sampling

	Pb	Zn	Ca
Accuracy Rel% Dif Average (%)	-0.22	-5.54	-6.48
Accuracy Standard Dev Average (ppm)	65.31	56.73	518.26
Precision Rel % Dif Average (%)	6.03	6.81	12.26

Appendix D-11. Geometric metal concentrations and arithmetic percent < 2 mm sediment by segment

Segment	Deposit	n	Pb (Log10) Average	Pb (Log10) St. Dev.	Pb (Log10) Cv%	Zn (Log10) Average	Zn (Log10) St. Dev.	Zn (Log10) Cv%	Ca (Log10) Average	Ca (Log10) St. Dev.	Ca (Log10) Cv%	% <2 mm Average	% <2 mm St. Dev.	% <2 mm Cv%
1	Active	2	2.81	0.61	21.86	2.35	0.84	35.77	4.72	0.29	6.09	73.59	32.53	44.20
	Bed	3	2.37	0.40	17.07	1.93	0.25	12.80	4.36	0.14	3.32	18.69	8.31	44.44
	Shadow	2	2.00	0.06	3.20	1.79	0.19	10.91	4.17	0.06	1.51	73.64	29.69	40.32
	Stable	3	2.29	0.14	6.20	1.89	0.16	8.56	4.20	0.03	0.75	69.95	14.03	20.06
2	Active	0										55.84		
	Bed	4	2.79	0.28	10.05	3.56	1.27	35.56	4.61	0.24	5.30	35.62	16.78	47.10
	Shadow	1	2.03			1.79			4.20			76.55		
	Stable	1	2.44			2.04			4.18			76.92		
3	Active	1	n/a			2.90			5.06			38.08		
	Bed	7	2.68	0.37	13.90	3.34	0.34	10.02	4.51	0.27	5.97	32.25	17.96	55.71
	Shadow	1	2.44			2.78			4.42			77.83		
	Stable	2	2.86	0.29	10.14	3.46	0.69	20.09	4.57	0.15	3.28	84.36	15.60	18.49
4	Active	3	2.84	0.07	2.55	2.95	0.05	1.77	4.82	0.06	1.31	69.61	34.85	50.06
	Bed	1	2.95			2.97			4.97			73.73	18.37	24.91
	Shadow	1	2.65			2.94			4.65			82.98		
	Stable	0										71.09		
5	Active	2	3.09	0.14	4.44	3.04	0.16	5.17	4.76	0.07	1.43	83.05	5.90	7.10
	Bed	4	3.11	0.29	9.28	3.27	0.25	7.53	4.83	0.08	1.62	33.85	18.37	54.26
	Shadow	2	3.01	0.36	11.89	2.96	0.04	1.34	4.81	0.09	1.88	49.53	19.39	39.14
	Stable	1	3.34			3.25			4.64			57.82		
6	Active	2	3.25	0.37	11.48	3.15	0.05	1.46	4.89	0.12	2.37	28.81	3.35	11.64
	Bed	8	3.13	0.12	3.75	2.93	0.21	7.25	4.98	0.06	1.18	42.33	17.44	41.20
	Shadow	4	3.41	0.17	4.97	2.96	0.18	6.19	4.89	0.19	3.97	75.43	23.43	31.06
	Stable	0										58.70		

Appendix D-11 continued. Geometric metal concentrations and arithmetic percent < 2 mm sediment by segment

Segment	Deposit	n	Pb (Log10) Average	Pb (Log10) St. Dev.	Pb (Log10) Cv%	Zn (Log10) Average	Zn (Log10) St. Dev.	Zn (Log10) Cv%	Ca (Log10) Average	Ca (Log10) St. Dev.	Ca (Log10) Cv%	% <2 mm Average	% <2 mm St. Dev.	% <2 mm Cv%
7	Active	0										55.77		
	Bed	4	3.27	0.17	5.23	2.74	0.29	10.40	4.90	0.40	8.10	38.10	11.45	30.06
	Shadow	0										66.59		
	Stable	3	3.52	0.13	3.77	3.10	0.34	10.93	4.98	0.14	2.79	59.58	25.31	42.48
8	Active	2	3.13	0.21	6.71	2.69	0.04	1.44	4.97	0.01	0.21	82.73	19.73	23.85
	Bed	6	3.31	0.23	6.79	2.84	0.12	4.33	5.05	0.03	0.55	48.29	16.10	33.35
	Shadow	1	3.71			2.97			5.08			57.74		
	Stable	1	3.20			2.60			4.92			95.44		
9	Active	2	2.91	0.20	7.05	2.47	0.11	4.59	4.85	0.09	1.85	66.59	5.99	9.00
	Bed	3	2.94	0.45	15.37	2.66	0.25	9.58	4.71	0.47	9.96	34.25	8.69	25.37
	Shadow	1	3.16			3.05			4.88			28.08		
	Stable	3	3.12	0.40	12.82	2.71	0.48	17.85	4.81	0.37	7.68	77.85	6.15	7.90
10	Active	4	3.18	0.06	1.78	2.77	0.07	2.68	4.95	0.10	2.10	35.02	5.92	16.90
	Bed	4	3.05	0.11	3.54	2.60	0.09	3.52	5.02	0.04	0.82	32.94	5.86	17.79
	Shadow	1	3.01			2.81			5.00			62.67		
	Stable	0												
11	Active	1	2.95			2.34			5.07			51.16		
	Bed	5	3.13	0.10	3.21	2.84	0.07	2.58	4.88	0.22	4.54	32.47	11.81	36.36
	Shadow	0												
	Stable	0												

Appendix D-12. Arithmetic metal concentrations by segment

Segment	R-km		n	Pb Average Arithmetic	Zn Average Arithmetic	Ca Average Arithmetic
1	9.2	Active	2	648	225	52,882
		Bed	3	232	86	22,701
		Shadow	2	99	61	14,704
		Stable	3	196	78	15,736
2	8.15	Active	0	670	505	83,312
		Bed	4	619	3,658	40,478
		Shadow	1	108	62	15,764
		Stable	1	279	111	14,997
3	7.55	Active	1	670	785	113,742
		Bed	7	480	2,204	32,081
		Shadow	1	276	605	26,215
		Stable	2	725	2,867	37,452
4	6.25	Active	3	692	901	66,474
		Bed	1	889	943	93,406
		Shadow	1	449	876	44,767
		Stable	0	1,458	2,321	40,675
5	5.75	Active	2	1,244	1,088	57,679
		Bed	4	1,287	1,877	67,499
		Shadow	2	1,019	907	64,367
		Stable	1	2,190	1,775	43,898
6	5.05	Active	2	1,781	1,400	77,696
		Bed	8	1,362	854	95,124
		Shadow	4	2,571	909	77,728
		Stable	0	2,757	1,520	69,691

Appendix D-12. Arithmetic metal concentrations by segment

Segment	R-km		n	Pb Average Arithmetic	Zn Average Arithmetic	Ca Average Arithmetic
7	3.6	Active	0	1,558	942	85,467
		Bed	4	1,878	553	80,023
		Shadow	0	3,839	922	98,586
		Stable	3	3,324	1,264	95,484
8	3.05	Active	2	1,336	484	93,239
		Bed	6	2,056	699	111,560
		Shadow	1	5,106	935	119,444
		Stable	1	1,592	399	82,851
9	2.15	Active	2	805	292	71,055
		Bed	3	880	454	51,678
		Shadow	1	1,429	1,130	76,611
		Stable	3	1,325	516	64,870
10	1.25	Active	4	1,530	586	89,831
		Bed	4	1,113	402	105,835
		Shadow	1	1,033	648	100,549
		Stable	0			
11	0.5	Active	1	895	221	118,170
		Bed	5	1,360	690	75,784
		Shadow	0			
	0	Stable	0			

Appendix E-1. Pb metal storage data

	Pb Storage (kg)				Metal Storage	
Segment	Channel Bed	Active Bar	Stable Bar Total	Stable Bar Fines Only	Total (kg)	Unit (kg / 100 m)
1	301	6,767	6,355	549	13,423	1,278
2	864	1,550	994	158	3,408	568
3	1,100	4,278	6,255	2,754	11,633	895
4	350	690	5,279	1,913	6,318	1,264
5	1,923	7,937	5,080	2,036	14,940	2,134
6	4,368	3,025	4,770	3,699	12,164	839
7	2,630	2,510	4,504	2,813	9,644	1,753
8	4,877	7,511	16,821	8,557	29,209	3,245
9	1,772	11,684	6,942	2,077	20,398	2,266
10	2,298	4,131	192	30	6,621	883
11	1,343	3,930	0	0	5,273	1,055
Average:	1,984	4,910	5,199	2,235		
Sum:	21,828	54,012	57,192	24,585	133,031	

Appendix E-2. Zn metal storage data

	Zn Storage (kg)				Metal Storage	
Segment	Channel Bed	Active Bar	Stable Bar Total	Stable Bar Fines Only	Total (kg)	Unit (kg / 100 m)
1	111	2,351	2,234	217	4,696	447
2	5,111	1,168	693	63	6,973	1,162
3	5,057	5,015	14,989	10,885	25,061	1,928
4	371	898	7,427	3,045	8,696	1,739
5	2,804	6,942	4,312	1,649	14,059	2,008
6	2,738	2,377	2,880	2,039	7,996	551
7	774	1,517	2,092	1,070	4,383	797
8	1,658	2,725	5,143	2,145	9,526	1,058
9	914	4,234	2,571	808	7,719	858
10	831	1,582	74	12	2,488	332
11	682	971	0	0	1,653	331
Average:	1,914	2,707	3,856	1,994		
Sum:	21,052	29,781	42,415	21,932	93,248	

Appendix E-3. Ca metal storage data

	Ca Storage (kg)				Metal Storage	
Segment	Channel Bed	Active Bar	Stable Bar Total	Stable Bar Fines Only	Total (kg)	Unit (kg / 100 m)
1	29,378	552,435	517,920	43,989	1,099,733	104,736
2	56,552	192,688	112,475	8,532	361,715	60,286
3	73,605	726,271	736,507	142,184	1,536,383	118,183
4	36,766	66,224	376,648	53,360	479,638	95,928
5	100,843	368,126	181,993	40,807	650,962	92,995
6	304,987	131,957	140,221	93,496	577,166	39,805
7	112,062	137,645	173,527	80,811	423,234	76,952
8	264,674	524,389	1,022,304	445,414	1,811,366	201,263
9	104,027	1,030,974	531,002	101,629	1,666,003	185,111
10	218,637	242,557	10,992	1,465	472,187	62,958
11	74,884	519,075	0	0	593,959	118,792
Average:	125,129	408,395	345,781	91,972		
Sum:	1,376,415	4,492,342	3,803,590	1,011,687	9,672,347	

Appendix F. Photo Log

Sediment sampling at Elvins/Rivermines tributary at R-km 7.6

Sediment sampling at R-km 7.5.

Channel profile set up at R-km 7.3

Channel profile data collection with active bar on right.

Straight channel with bed substrate at R-km 6.35, above Shaw Branch.

Bar deposits and bed substrate at R-km 6.15, near Main Street, Park Hills.

Active bar deposits and steep channel banks at R-km 5.8.

Straight channel with near the National Pile at R-km 5.05.

Ralph Hill and Dr. Robert T. Pavlowsky in front of National Pile at R-km 4.8.

Sharp right-hand bend with large active bar deposits at R-km 4.1.

Straight bedrock reach under St. Joe Parkway at R-km 3.57.

Stable bar head on left side above entrance of Koen Creek at R-km 3.1.

Active bar feature at R-km 2.8, after US-67 bridge.

Exposed cutbank with historic channel bed deposits and residuum at R-km 1.7.

Active bar deposit above Cedar Falls Road at R-km 1.25.

Exposed bedrock benches on right bank at R-km 0.85.

Fine-grained channel bed sediment at R-km 0.35.

Active bar tail sediment grading at R-km 0.34.

Channel profile data collection team at FRC and Big River Confluence at R-km 0. Left to right: Laura Speir, Allison Keppel, Felix Corrodi, and Ralph Hill.

Bar core sampling at R-km 6.0.

Bar core collection team at National Pile at R-km 4.65. Left to right: Megan Hente, Dr. Dan Hanes, Dr. Aaron Pearson, Matthew Thies, and Nickolas Bradley.

Stable bar core sampling at R-km 4.25.

Upstream active bar sediment sampling at R-km 9.1 at Harris Branch.

Upstream sediment sampling with Lisa Andes at R-km 10.35.